SIMULATION OF CONVECTION EFFECTS ON DENDRITIC GROWTH

Gustav Amberg and Robert Tönhardt

Department of Mechanics, KTH, S-100 44 Stockholm, Sweden

In real solidification processes, convection in the melt is usually difficult to avoid. This convection may often have a strong influence on the solidification rate and also the mode of solidification. We have recently used 2D phase field simulations to study the growth of a small nucleus to a dendrite in an undercooled melt, in the presence of convection in the melt[1,2]. The solution of the equations for viscous flow has been added to a solution of the phase field equations according to Karma and Rappel[3]. An adaptive finite element method is used which allows a large computational domain, so that a single dendrite in an effectively unbounded region can be studied.

As a generic case for growth from solid boundaries, the nucleus is in one case assumed to be attached to a solid wall, and a shear flow parallell to the wall is assumed in the melt. The interaction between the melt flow and the growing dendrite results in a changed growth rate and morphology.

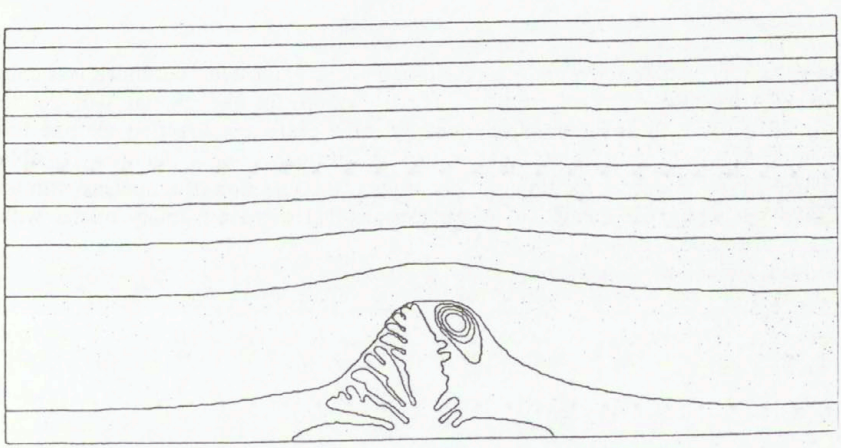

Figure 1

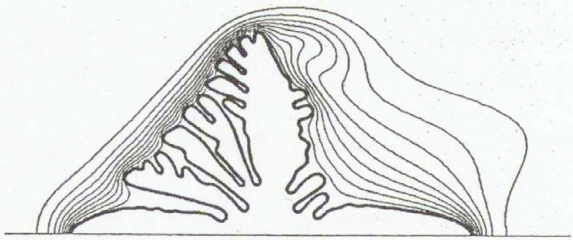

Figure 2

Figure 1 shows a dendrite that has grown into an undercooled high Prandtl number melt. The flow in the melt is a shear flow from left to right, with zero melt velocity at the solid lower wall. Streamlines of the flow are shown above the dendrite. The fluid flow is displaced by the dendrite, and a small clockwise circulating eddy is visible at the rear. The dendrite is seen to be tilting slightly from the direction of preferred growth which is assumed to be perpendicular to the wall. It is very evident that sidebranches are promoted on the upstream side, and suppressed more or less completely on the downstream side. Figure 2 show the corresponding isotherms. It is seen that the isotherms are compressed on the leading side, giving rise to enhanced heat transfer there, i.e. cooling, which will then promote the growth of sidebranches. On the downstream side however, the isotherms reveal a wake with much lower temperature gradients, and thus a reduced solidification rate. Only just below the eddy, where fresh cold melt is convected towards the main stem, two small secondary arms are present.

The simulation shown above shows some tilting of the main stem, but much less than might be expected from experiments. The anisotropy of the crystal will act to maintain the growth direction approximately in the preferred direction, despite the difference in heat transfer at the up- and downstream sides. Another possible mechanism for producing the tilting of dendrites is the selection of a nucleus with an optimal initial crystal orientation, if we assume that there are many nuclei with random orientations present initially.

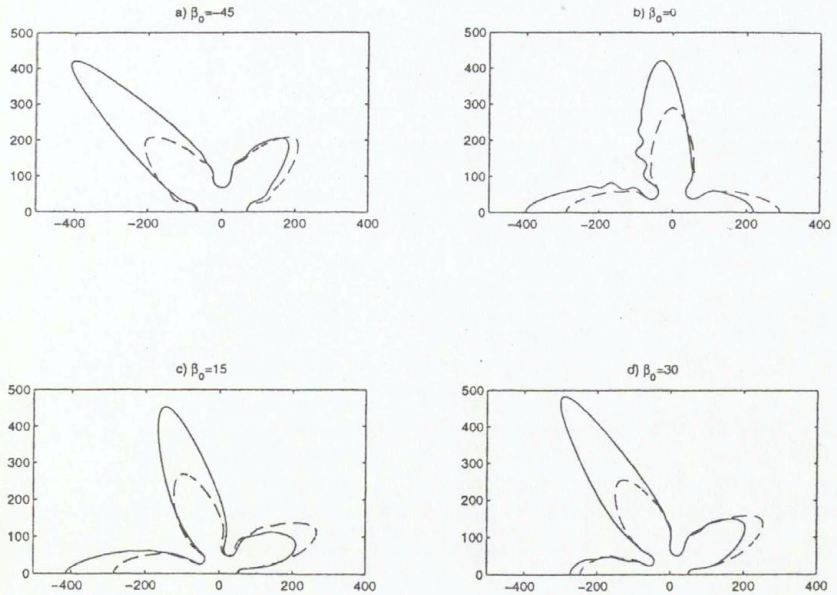

Figure 3

Figure 3 shows a set of simulated dendrites which have grown from nuclei that have different preferred growth directions. The solid contours are simulated with convection, while the dashed contours are obtained for the same conditions, but without convection. It is seen that the dendrite in d) has reached the largest distance from the wall. If we conjecture that this would eventually outgrow neighbouring dendrites with other orientations, then the tilt angle we would observe in an experiment would be around 30 degrees, as in figure 3d. Note that the dendrite in b) which has a preferred direction which is perpendicular to the wall as in figs 1 and 2, has only changed its growth direction slightly.

We have also studied natural convection around a nucleus held in an undercooled melt. This will be discussed briefly in the presentation.

[1] R. Tönhardt, Doctoral Thesis, Dec 1998, Department of Mechanics, Royal Inst. of Tech., Stockholm, Sweden.

[2] R. Tönhardt and G. Amberg, *J. Crystal Growth*, **194** (1998), pp 406-425.

[3] Karma, A. and Rappel W.J. *Phys. Rev. E*, **53** (1996), pp R3017-3020.

NUMERICAL APPROACHES TO SOLVING THE DIRECT AND INVERSE PROBLEMS OF ELECTROMAGNETOELASTICITY

A.V. Avdeev[1], O.N. Soboleva[1], V.I. Priimenko[2]

[1]Institute of Computational Mathematics and Mathematical Geophysics
Siberian Branch of the Russia Academy of Sciences (SB RAS)
Lavrent'ev prosp. 6, 630090 Novosibirsk, Russia.
[2]Sobolev Institute of Mathematics,Siberian Branch of the Russia Academy of Sciences (SB RAS)
prosp. Koptyuga 4, 630090 Novosibirsk, Russia.
&
North Fluminense State University – LENEP/UENF, Rodovia Amaral Peixoto
164 km Imboacica 27.973-030, Macae, RJ, Brazil

INTRODUCTION

It is known that when a conductive wire frame is moving in a constant magnetic field, an electric current and a variable magnetic field are generated in the frame.
Similar phenomena can be observed when a seismic wave propagates in the Earth's constant magnetic field. The seismic wave, with its leading and trailing wave fronts, is analogous to a wire frame. A conductive medium between the leading and trailing wave vibrates in the Earth's constant magnetic field, which brings about local geomagnetic variations. Local geomagnetic variations propagating simultaneously with the seismic wave diffusing into the medium are called seismomagnetic waves. These waves contain information about both electromagnetic and elastic parameters of a medium.
The electromagnetic wave rides the "back" of the seismic wave, that is, the induced electromagnetic wave is "frozen" into the seismic wave and propagates either with P- or with S- seismic wave velocity, depending on the type of waves. The dominant frequency and the velocity of the induced seismomagnetic wave is equal to the frequency and velocity of the seismic wave.
The phenomenon of the seismomagnetic effect caused by an explosion in an elastic medium is described as a simultaneous solution of the self-consistent system of elastic equations with the Lorentz force and quasi-stationary Maxwell's equations with displacement velocity components.

MATHEMATICAL MODEL

We assume that the model under consideration satisfies the basic hypotheses of continuum mechanics: continuity, Euclidity, and absoluteness of time. The first hypothesis means that an uninterrupted continuum is considered, the second one implies the possibility to introduce a Cartesian frame of reference for all points, and according to the third hypothesis relativistic effects are not taken into account. Moreover, the model is inapplicable in the case of strong magnetic fields. We also assume that electromagnetoelastic waves arise under the action of mechanical perturbations, and that one can neglect the effect of electromagnetic waves on the process of propagation of elastic oscillations and also neglect the displacement currents as compared with conduction currents. Lastly, we will consider the fields of small perturbations.
Now we can write down our equations. The assumption that we consider the fields of small perturbations allows us to consider the linearized statement of the problem when the displacement

vector $\mathcal{U}$, the vector of the electric field intensity $\mathcal{E}$, and the vector of the magnetic field intensity $\mathcal{H}$ can be represented in the form

$$(\mathcal{U}, \mathcal{E}, \mathcal{H}) = (0, 0, \mathbf{H}^0) + (\mathbf{u}, \mathbf{E}, \mathbf{H})$$

where $(0, 0, \mathbf{H}^0)$ is the value related to the unperturbed state of the medium ($\mathbf{H}^0 = (H_1^0, H_2^0, H_3^0)$ is a constant vector); and the vectors $\mathbf{u} = (u_1, u_2, u_3)$ (displacement of the points of the medium from the reference configuration), $\mathbf{E} = (E_1, E_2, E_3)$ (intensity of the electric field), and $\mathbf{H} = (H_1, H_2, H_3)$ (intensity of the magnetic field) correspond to small perturbations of the elastic and electromagnetic fields. Besides, in view of our assumptions one can consider that the process of elastic waves propagation is governed by the usual system of differential equations of the theory of elasticity:

$$\rho \frac{\partial^2 u_i}{\partial t^2} = \sum_{j=1}^{3} \frac{\partial T_{ij}(\mathbf{u})}{\partial x_j}, \quad i = 1, 2, 3, \tag{1}$$

where the stress tensor $T_{ij}(\mathbf{u})$ is defined in terms of the components u_i of the displacement vector and in the case of an isotropic magnetoelastic medium has the form

$$T_{ij}(\mathbf{u}) = \kappa \left(\frac{\partial u_i}{\partial x_j} + \frac{\partial u_j}{\partial x_i} \right) + \delta_{ij} \lambda \operatorname{div} \mathbf{u}, \quad i, j = 1, 2, 3. \tag{2}$$

Here ρ, λ, κ denote the density of the medium and the Lamé coefficients respectively, and δ_{ij} is the Kronecker symbol.

The propagation of electromagnetic waves through an elastic conductive medium is described in our case by the following set of equations:

$$\operatorname{rot} \mathbf{H} = \mathbf{J}, \qquad \frac{\partial \mathbf{B}}{\partial t} = -\operatorname{rot} \mathbf{E}, \qquad \operatorname{div} \mathbf{B} = 0 \tag{3}$$

where, in virtue of our assumptions, the constitutive relations are written as

$$\mathbf{B} = \mu(\mathbf{H}^0 + \mathbf{H}), \qquad \mathbf{J} = \sigma \left(\mathbf{E} - \mu \frac{\partial \mathbf{u}}{\partial t} \times \mathbf{H}^0 \right). \tag{4}$$

Here μ is the magnetic permeability, and σ is the conductivity of the medium. Such are, in general outline, the differential equations describing the process of interaction of electromagnetic and elastic waves in our case.

Now we proceed to the statement of the direct problem for differential equations (1)–(4). Consider the rectangular Cartesian frame of reference $(x_1, x_2, x_3) = \mathbf{x}$. Let the plane $x_3 = 0$ be the interface of two media of the types "air" ($x_3 < 0$) and "conductive ground" ($x_3 > 0$). Electromagnetic and elastic characteristics of the ground are described by piecewise constant functions with break planes parallel to the plane $x_3 = 0$. Let us introduce the notation

$$[f]_\Gamma = f|_{\Gamma+} - f|_{\Gamma-},$$

i. e., the symbol $[f]_\Gamma$ denotes the jump of the function f on the oriented surface Γ in the direction from the inner to the outer side of Γ. We assume that elastic oscillations arise under the action of a force source concentrated at the origin of coordinates

$$T_{k3}(\mathbf{u})|_{x_3=0} = \delta_{k3} f(t)\, \delta(x_1, x_2), \quad k = 1, 2, 3, \tag{5}$$

where $\delta(\cdot)$ is the generalized Dirac delta.

As concerns the force source and initial data, we assume that the function $f(t)$ and the electromagnetoelastic field are absent before the moment $t = 0$, i. e.,

$$(f, \mathbf{u}, \mathbf{E}, \mathbf{H})|_{t<0} \equiv 0. \tag{6}$$

To single out the unique solution to the direct problem, one has to require the fulfilment of the radiation condition at infinity:

$$\lim_{|\mathbf{x}|\to\infty} (\mathbf{E}, \mathbf{H}) = 0. \tag{7}$$

Moreover, on the planes where the coefficients of the problem have breaks we require the fulfilment of standard consistency conditions

$$[u_m] = [E_k] = [H_k] = [T_{m3}(\mathbf{u})] = 0, \quad k = 1, 2, \quad m = 1, 2, 3. \tag{8}$$

Thus, the direct problem consists in finding the vector functions $\mathbf{u}$, $\mathbf{E}$, $\mathbf{H}$ satisfying equations (1)–(8) providing that we know the elastic and electromagnetic characteristics of the medium and the constant vector $\mathbf{H}^0$ characterizing the magnetic field of the Earth.

Our main task will consist in showing the possibility of the simultaneous determination of electromagnetic and elastic characteristics of the medium from the system (1)–(8) basing on some additional information on the components of the vector functions $\mathbf{u}$, $\mathbf{H}$.

To carry out numerical experiments a software package is written on the language Watcom C++ with enhanced graphical interface.

Results of numerical experiments will be given to illustrate the efficiency of the proposed methods.

ACKNOWLEDGEMENT

THIS work was supported by the Russia Foundation for Basic Research under grant No. 98-05-65280.

NUMERICAL SIMULATION OF A SEMICONDUCTOR FLOATING ZONE

Eberhard Bänsch* & Burkhard Höhn**
*Zentrum f. Technomath., FB 3, Universität Bremen, Postfach 330440, D-28334 Bremen, Germany
**Inst. f. Ang. Math., Universität Freiburg, Hermann–Herder Str. 10, D-79104 Freiburg, Germany

Summary In this article we present numerical results concerning the simulation of semiconductor melts with free capillary surfaces, particularly silicon crystal growth by the floating zone method. Considering the solid/liquid interface as fixed the simulation requires the computation of the moving capillary surface of the melting zone. The mathematical model is a coupled system which consists of a heat equation and the Navier-Stokes equations in the melt with a Marangoni boundary condition. We describe an efficient numerical method for solving this problem and give some results for different physical parameters.

INTRODUCTION

Fluctuations of the electrical resistivity due to inhomogeneous dopant distribution are still a serious problem for the industrial processing of doped semiconductor crystals. In the case of silicon floating–zone growth, the main source of these inhomogeneities are time–dependent flows in the liquid phase during the growth process. Hence, for optimizing the growth process, it is of great importance to study the influence of thermocapillary and buoyancy convection on macro– and microsegregation[1-5].

Due to the opaqueness of semiconductor melts, experimental fluid flow observation is extremely difficult and expensive in general. Therefore the numerical simulation of the growth process is an important tool in understanding and predicting the behavior of the system[3].

MATHEMATICAL MODEL

Figure 1 gives a schematic diagram of a floating–zone configuration.

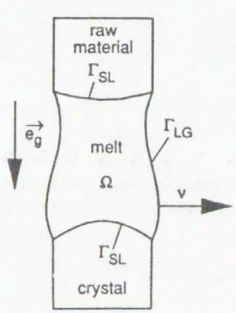

Figure 1. Geometry of a floating zone

The heat and mass transfer in the liquid zone $\Omega = \Omega(t) \subseteq I\!R^d$ $(d = 2, 3)$ is governed by a coupled system of partial differential equations for the flow velocity $u(\cdot, t) : \Omega(t) \to I\!R^d$, the pressure $p(\cdot, t) : \Omega(t) \to I\!R$ and the temperature $T(\cdot, t) : \Omega(t) \to I\!R$, namely the Navier-Stokes equations and the heat equation in Boussinesq approximation. The interfaces Γ_{SL} and Γ_{LG} are free boundaries, the first one being subject to a Stefan condition, the latter one determined by a balance of capillary forces versus

normal stresses of the flow. We simplify the problem by focusing on the free boundary conditions on Γ_{LG} and prescribing a given solid–liquid interface Γ_{SL} where we impose a homogeneous Dirichlet boundary condition for u and T ($T = 0$ the dimensionless melting temperature). Furthermore on the free liquid–gas interface Γ_{LG} the temperature is prescribed by a given parabolic profile T_D. The complete system in dimensionless form reads as follows:

$$\partial_t u + u \cdot \nabla u - \frac{1}{Re} \triangle u + \nabla p = -\frac{Ra}{Re^2\, Pr} T \vec{e}_g \qquad \text{in } \Omega(t), \quad (1)$$

$$\nabla \cdot u = 0 \qquad \text{in } \Omega(t), \quad (2)$$

$$\partial_t T + u \cdot \nabla T - \frac{1}{Re\, Pr} \triangle T = 0 \qquad \text{in } \Omega(t), \quad (3)$$

$$T = 0 \qquad \text{on } \Gamma_{SL}, \quad (4)$$

$$u = 0 \qquad \text{on } \Gamma_{SL}, \quad (5)$$

$$T = T_D \qquad \text{on } \Gamma_{LG}(t), \quad (6)$$

$$\nu \cdot \sigma \nu = \frac{1}{Re\, Ca} H + \frac{Bo}{Re\, Ca} \vec{e}_g \cdot x \qquad \text{on } \Gamma_{LG}(t), \quad (7)$$

$$\tau \cdot \sigma \nu = -\frac{Ma}{Re^2\, Pr} \nabla T \cdot \tau \qquad \text{on } \Gamma_{LG}(t), \quad (8)$$

$$u \cdot \nu = V_\Gamma \qquad \text{on } \Gamma_{LG}(t), \quad (9)$$

with $\sigma := \left(\frac{1}{Re} D(u)_{ij} - p\,\delta_{ij}\right)_{i,j=1}^{d}$ the stress tensor, $D(u) := \left(\partial_{x_i} u_j + \partial_{x_j} u_i\right)_{i,j=1}^{d}$ the deformation tensor, κ the sum of the principal curvatures, the unit outer normal vector ν, an arbitrary tangential vector τ and the normal velocity V_Γ of the free boundary Γ_{LG}.
The system has to be closed by initial conditions for u, T and Ω. Note that in the continuous case we have conservation of volume since the velocity u is divergence free.

The dimensionless numbers occurring in the above equations are the Reynolds number $Re = \frac{\rho U L}{\eta}$, the Prandtl number $Pr = \frac{\eta}{\rho k}$, the Rayleigh number $Ra = \frac{g \rho \beta \delta T L^3}{k \eta}$, the capillary number $Ca = \frac{\eta U}{\gamma}$, the Marangoni number $Ma = -\frac{(\partial \gamma / \partial T) \delta T L}{k \eta}$ and the Bond number $Bo = \frac{\rho g L^2}{\gamma}$, with a characteristic velocity U, a characteristic length L, a characteristic temperature difference δT, the density ρ, the surface tension γ, the thermal coefficient $\partial \gamma / \partial T$ of surface tension, the thermal diffusivity k, the dynamic viscosity η and the gravitational acceleration g.

Even if all data are rotationally symmetric or two dimensional according to the physical setup, the solution may be expected to be 3D and also time–dependent due to symmetry breaking. Thus, it is necessary to define a numerical scheme for the time–dependent case and which works also in 3 space dimensions.

NUMERICAL APPROXIMATION

Discretizing equations (1)–(3), the free boundary conditions cause several problems, in particular the treatment of the curvature terms and in finding a stable and efficient time discretization.

To resolve these problems we use a variational formulation, where the free boundary conditions are transformed to a boundary integral part of the bilinear forms[6]. To this end we write the momentum part of the Stokes equations (analogously for the Navier–Stokes equations) in the strong form, multiply

by a solenoidal test function φ and integrate by parts. We get

$$\int_\Omega \{-\frac{1}{Re}\triangle u + \nabla p\} \cdot \varphi \;=\; \frac{1}{2Re}\int_\Omega D(u) : D(\varphi) - \int_\Omega p\nabla\cdot\varphi - \int_{\Gamma_{LG}} \nu\cdot\sigma\varphi.$$

Taking into account the boundary conditions on Γ_{LG} and making use of the identity

$$\underline{\triangle}\mathrm{id}_{\Gamma_{LG}} = \underline{\nabla}\cdot\underline{\nabla}\mathrm{id}_{\Gamma_{LG}} = \kappa\,\nu, \tag{10}$$

where $\underline{\triangle}$ denotes the Laplace Beltrami operator on Γ_{LG} and $\underline{\nabla}$ the tangential derivatives, yields

$$\int_\Omega \{-\frac{1}{Re}\triangle u + \nabla p\} \cdot \varphi \;=\; \frac{1}{2Re}\int_\Omega D(u) : D(\varphi) - \int_\Omega p\,\nabla\cdot\varphi + \frac{1}{ReCa}\int_{\Gamma_{LG}} \underline{\nabla}\mathrm{id}_{\Gamma_{LG}}\cdot\underline{\nabla}\varphi \tag{11}$$

$$+\frac{Ma}{Re^2Pr}\sum_{i=1}^{d-1}\int_{\Gamma_{LG}} \nabla T\cdot\tau_i\varphi\cdot\tau_i - \frac{Bo}{ReCa}\int_{\Gamma_{LG}} \mathrm{id}_{\Gamma_{LG}}\cdot\vec{e}_g\varphi\cdot\nu \tag{12}$$

Time discretization

To discretize in time a semi–implicit coupling of the unknowns for temperature T, geometry Ω and the flow variables u, p is used. More precisely, giving the values at the discrete time instant t_{k-1} we compute

Step 1: T^k by solving (3) on Ω^{k-1} with u^{k-1}

Step 2: u^k, p^k by solving (1)–(2) with boundary conditions (7, 8) on Ω^{k-1} and using T^k on the right hand side

Step 3: Γ_{LG}^k by $\Gamma_{LG}^k := \Gamma_{LG}^{k-1} + (t_k - t_{k-1})\; u^k\cdot\nu\;\nu$

In **Step 2** the boundary conditions (7, 8) are incorporated into the variational formulation according to (11). The curvature terms are treated in a semi–implicit way:

$$\int_{\Gamma_{LG}^{k-1}} \underline{\nabla}\mathrm{id}_{\Gamma_{LG}^k}\cdot\underline{\nabla}\varphi \;=\; \int_{\Gamma_{LG}^{k-1}} \underline{\nabla}\mathrm{id}_{\Gamma_{LG}^{k-1}}\cdot\underline{\nabla}\varphi + (t_k - t_{k-1})\int_{\Gamma_{LG}^{k-1}} \underline{\nabla}u^k\cdot\underline{\nabla}\varphi,$$

thus decoupling the flow computation from the determination of the geometry. This leads to a stable and efficient treatment of the free boundary conditions[6].

The computation of u^k, p^k is based on the fractional step θ–scheme in a variant as an operator splitting, which decouples two major numerical difficulties, the solenoidal condition and the nonlinearity[6-7].

Spatial discretization

To discretize in space piecewise quadratic, globally continuous elements for u and T and piecewise linear, globally continuous elements for p are used on a tetrahedral grid.

NUMERICAL RESULTS

The following example shows the influence of the hydrostatic pressure on the shape of a floating zone with aspect ratio $h/d = 1.5$. Here $g_E = 9.81 m\,s^{-2}$ denotes the gravitational acceleration on earth. We consider pure Marangoni convection without buoyancy convection, i.e. $Ra = 0$. The other

dimensionless parameters are: $Re = 50$, $Pr = 2$, $Ma = 150$, $Ca = 0.016$, $Bo = 0.18 * |g|$ with $g \in \{0, 1.0 * g_E, 2.0 * g_E\}$. Figure 2 shows the velocity field together with the temperature distribution in the melt and Figure 3 the corresponding triangulation of the domain Ω.

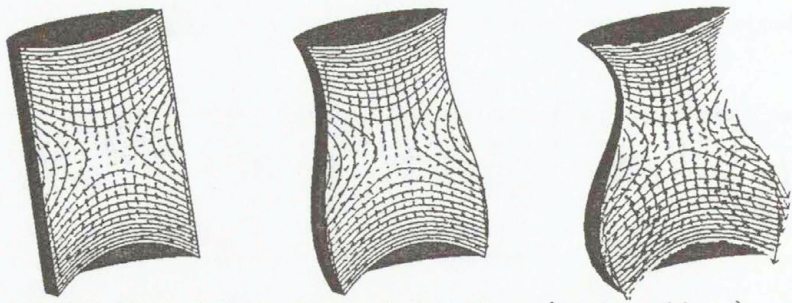

Figure 2. Velocity field and temperature distribution for $g \in \{0,\ 1.0 * g_E,\ 2.0 * g_E\}$

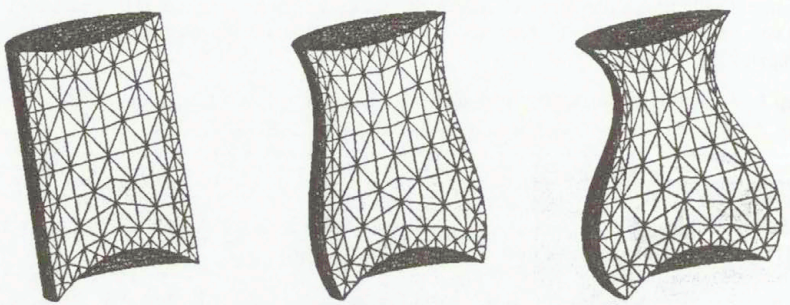

Figure 3. Triangulation for $g \in \{0,\ 1.0 * g_E,\ 2.0 * g_E\}$

REFERENCES

1. Cuvelier C., Driessen J.M.:, Thermocapillary free boundaries in crystal growth. *J. Fluid mech.* **169**, pp 1–26, 1986.
2. Dold P., Cröll A., Benz K.W.: Floating–zone growth of silicon in magnetic fields, Part I: Weak static axial fields. *J. Crystal Growth* **183**, pp 545–553, 1998.
3. Kaiser T., Benz K.W.: Floating–zone growth of silicon in magnetic fields, Part III: Numerical simulation. *J. Crystal Growth* **191**, pp 365–376, 1998.
4. Müller G., Ostrogorsky A.: Convection in Melt Growth. in *Handbook of Crystal Growth 2B*, D. T. J. Hurle, eds., Elsevier Science Publishers, North-Holland, pp 709-819, 1994.
5. Schwabe D.: Surface–Tension–Driven Flow in Crystal Growth Melts. in *Crystal Growth, Properties and Applications* **11**, Springer, Berlin, 1988.
6. Bänsch E.: Numerical methods for the instationary Navier–Stokes equations with a free capillary surface. *Habilitation thesis*, Univ. Freiburg, 1998.
7. Bristeau M.O., Glowinski R., Periaux J.: Numerical methods for the Navier–Stokes equations. Application to the simulation of compressible and incompressible flows. *Computer Physics Report* **6**, pp 73–188, 1987.

FEM ANALYSIS OF ALLOY SOLIDIFICATION USING THE ANISOTROPIC POROUS MEDIUM MODEL OF THE MUSHY ZONE

Jerzy Banaszek, Piotr Furmański

Institute of Heat Engineering, Warsaw University of Technology, Poland

Semi-implicit FEM scheme is used for two dimensional computer simulation of binary alloy solidification controlled by buoyancy forces and conduction. The computational algorithm is based on the combination of:

(1) the projection method to uncouple velocity and pressure calculations for incompressible fluid,
(2) the backward Euler and explicit Adams-Bashforth schemes to effectively integrate diffusion and advection in time, and
(3) an enthalpy-porosity approach to account for the latent heat effect on a fixed finite element grid.

The focus of this paper is on the analysis of the impact that the anisotropy of both the permeability and heat conductivity can have on the flow structure and temperature field in the mushy zone. Example calculations are given for an aqueous ammonium chloride solution, which has well-established thermophysical properties and solidifies in manner typical of many metallic alloys.

THE PROBLEM OF AUTHENTICITY OF INITIAL AND THERMAL BOUNDARY CONDITIONS IN THE CODE VALIDATION ANALYSIS

Jerzy Banaszek & Marek Rebow

Institute of Heat Engineering, Warsaw University of Technology, Poland

If a computer simulation is to have a major impact on the design of engineering hardware or to be a desirable supplement to an experimental study of complex phenomena, we first have to be convinced that this simulation has a satisfactory level of confidence. Such analysis consists of two procedures: verification and validation. The former one is the process that demonstrates the ability of a numerical model and its computer program to solve specific set of governing equations. It establishes the level of accuracy and sensitivity of the results to parameters appearing in the discrete formulation through purely numerical experiments. This procedure is based on both grid refinement study and comparison of the results with other available solutions of some benchmark problems. The verification procedure, although indispensable, is not sufficient to establish the confidence of numerically obtained predictions. Indeed, for engineers and physicists the most important issue is the degree to which the computer simulation is an accurate representation of reality, i.e.: the degree to which inevitable simplifications of physical and mathematical models reflect reality. This is established through the code validation procedure where calculations are extensively compared with trustworthy detailed experimental measurements.

In complex phenomena of coupled fluid flow/heat transfer with the solid-liquid isothermal/non-isothermal phase transition an experimental study is very often difficult and prohibitively expensive, particularly for materials with high fusion temperatures (e.g. metallic alloys). Therefore, in such cases the computer code validation procedure is rather performed through comparing the calculations with experimental data for some substitute media, which solidify or melt in the way similar to the materials of interest but in much lower temperatures. For example, in the case of isothermal phase change, melting of gallium [1] or freezing of pure water [2,3] in the differentially heated cavity is studied experimentally, whereas an aqueous ammonium chloride solution [4] is used to mimic the metallic alloy solidification occurring in the range of solidus-liquidus temperatures.

The freezing process of pure water, driven by natural convection in fluid and conduction in both phases, is often used as an experimental benchmark [2,3,5], which is a challenging test for a computer simulation of the solid liquid phase transition. Indeed, water is a fluid that does not obey the Boussinesq approximation of the linear buoyancy force-temperature relation because water density at low temperatures is a non-linear function of temperature. Water density anomaly creates a complex flow pattern that contains two different circulation regions - the hot clockwise vortex and the cold counter-clockwise one. Moreover, experimental investigations of fluid flow and heat transfer processes in the solidifying water are relatively easy to arrange in a small laboratory scale. The up-to-date field acquisition technique, where Thermochromic Liquid Crystal suspended in water as seeding along with the Digital Particle Image Velocimetry and Thermometry can be used here to get detailed, transient, local two-dimensional velocity and temperature fields [2,3,5]. Such experimental findings are commonly acknowledged as exact and reliable enough to be a reference standard for comparison with numerical results [2,3].

However, when water freezes in a small cavity (typically used in experiments), high sensitivity of flow structure and, thus, of the temperature field, to thermal boundary conditions is observed. Moreover, at early times of the process the effect of water super-cooling occurs in the cavity [3,5]. It significantly changes the early-time flow structure and temperature field, and retards the regular ice formation. Therefore, it is reasonable to expect that the calculations can also be affected by some ambiguity of the assumed heat transfer coefficients and by the accuracy of numerical modeling of the real boundary conditions (those that occur during experimental investigations).

To elucidate the problem, the experimental findings reported in [2,3,5], are compared with the results of computer simulation of natural convection of pure water in a square cavity at low but positive temperatures and during the freezing process.

The computationally efficient numerical model has been developed [5] through the combination of the projection method [6], semi-implicit time marching scheme [6,7] and the enthalpy-porosity approach [8] along with equal-order or unequal-order finite element space discretization [9]. This computer code has been used to calculate the natural convection and solidification of pure water inside the cavity and heat conduction in the cavity walls as the conjugate circumstance for diverse thermal boundary conditions imposed on external surfaces of the cavity.

Detailed comparison of the calculated local flow pattern, temperature field and the temporal front shape and position shows significant impact of the initial and thermal boundary conditions on the velocity and temperature distribution in the cavity. Thus, the problem of the authenticity of these conditions is crucial when the above-discussed experimental benchmark is used in the detailed code validation analysis. Special care is needed for precise modeling of realistic boundary and initial conditions to avoid some ad hoc, but not necessary fully correct, conclusions concerning the accuracy and the scope of validity of the computer simulation.

REFERENCES

1 Gau and R. Viskanta, Melting and Solidification of a Pure Metal on a Vertical Wall, *J. Heat Transfer*, vol.108, pp. 174-181, 1986.

2 T. A. Kowalewski, Experimental Validation of Numerical Codes in Thermally Driven Flows. CHT-97: *Advances in Computational Heat Transfer*, eds. G. Vahl Davis and E. Leonardi, pp.1-16, Begell House Inc.,N.Y., 1998.

3 T. A. Kowalewski, A. Cybulski and M. Rebow, Particle Image Velocimetry and Thermometry in Freezing Water, *Proceedings of 8th International Symposium on Flow Visualization*, Sorrento, 1998.

4 W. D. Bennon and F. P. Incropera, Numerical Analysis of Binary Solid-Liquid Phase Change Using a Continuum Model, *Numerical Heat Transfer*, vol.13, pp.277-296, 1988.

5 J. Banaszek, Y. Jaluria, T. A. Kowalewski., M. Rebow, Semi-Implicit FEM Analysis of Natural Convection in Freezing Water, accepted for publication, *Numerical Heat Transfer*, 1999.

6 P. M. Gresho, On the Theory of Semi-Implicit Projection Methods for Viscous Incompressible Flow and Its Implementation via a Finite Element Method That Also Introduces a Nearly Consistent Mass Matrix. Part 1: Theory, *Numerical Heat Transfer*, Part A, vol.29, pp. 49-63, 1996.

7 B.Ramaswamy, T.C. Jue and J.E. Akin, Semi-Implicit and Explicit Finite Element Schemes for Coupled Fluid/Thermal Problems. *Int. J. Num. Meth. Eng.*, vol.34, pp.675-692, 1992.

8 D. Brent, and V. R. Voller, Enthalpy-Porosity Technique for Modeling Convection-Diffusion Phase Change: Application to the Melting of a Pure Metal, *Numerical Heat Transfer*, vol.13, pp.297-318, 1988.

9 O. C. Zienkiewicz and R. L. Taylor, *Finite Element Method*. Fourth Edition, McGraw-Hill Company, London, 1989.

A GENERALIZATION OF THE NAVIER-STOKES EQUATIONS TO TWO-PHASE FLOWS

Thomas Blesgen

Fakultät für Mathematik u. Inf., Universität Leipzig, Augustusplatz 10/11, D-04109 Leipzig, Germany

Summary A modified Allen-Cahn equation is combined with the compressible Navier-Stokes system. After a physically motivated modification of the stress-tensor, for the resulting equations the second law of thermodynamics is valid. The model can be used to describe the forming of gas phases in a flowing liquid.

INTRODUCTION

In the present text, a modified Allen-Cahn equation[1], is combined with the Navier-Stokes system. The resulting model has some simplifications, but is a first step to describe the behaviour of gas phases in a flowing liquid. The model allows phases to grow or shrink due to changes of temperature and density in the fluid and incorporates their transport with the current. For related works we refer to a combination of the Cahn-Hilliard model with the Navier-Stokes equations[2], the general variational approach of the energy[3], and to the models[4,5].

NOTATIONS AND THERMODYNAMIC RELATIONSHIPS

Let $\Omega \subset \mathbb{R}^d$, $1 \leq d \leq 3$ be a bounded domain with Lipschitz boundary. For $0 < D \leq \infty$ let $\Omega_D := \Omega \times (0, D)$ and $\varrho : \Omega_D \to \mathbb{R}^+$ denote the (averaged) density of the fluid, $e : \Omega_D \to \mathbb{R}^+$ the internal energy, $v : \Omega_D \to \mathbb{R}^d$ the velocity field of the fluid. Governed by a phase parameter $\chi : \Omega_D \to [0, 1]$, two phases (e.g. a gas and a liquid phase) may exist in Ω. Let $\sqrt{\delta}$ denote the thickness of transition layers between two phases. Generally, we postulate the potential energy density E_{pot} of the system to be the convex combination of the corresponding values of the two phases, giving rise to the definition

$$E_{\text{pot}} = \chi E_{\text{pot},1} + (1 - \chi) E_{\text{pot},2}. \tag{1}$$

Similar relationships will be assumed for the entropy density S and the Gibbs free energy density G. The internal energy density E is obtained after adding the kinetic energy:

$$E = E_{\text{pot}} + \frac{1}{2} |v|^2.$$

Capital letters generiely denote densities, values corresponding to small letters include a factor ρ or ρ_i. Indices refer to the phase, values without index to the whole system. Hence,

$$\begin{aligned} e_{\text{pot}} &= e_{\text{pot},1} + e_{\text{pot},2} = \varrho_1 E_{\text{pot},1} + \varrho_2 E_{\text{pot},2} \\ &= \varrho(\chi E_{\text{pot},1} + (1 - \chi) E_{\text{pot},2}) = \varrho E_{\text{pot}}, \\ e &= e_{\text{pot}} + \frac{\varrho}{2} |v|^2. \end{aligned} \tag{2}$$

ϱ and χ are solutions of the system of partial differential equations (4) – (7) below and allow us to calculate the specific densities ϱ_1, ϱ_2 of the phases.

Consider the specific volume $V = \frac{1}{\varrho}$. Let V_i be the specific volume of phase i and $\tilde{V}_i$ be the volume phase i is actually occupying in V. Now we define

$$\begin{aligned}
&\psi_i := \tfrac{\tilde{V}_i}{V} && \text{volume fraction of phase } i \text{ in } V,\ 0 \le \psi_i \le 1,\\
&\varrho_i := \tfrac{\psi_i}{V_i} = \tfrac{\tilde{V}_i}{V_i}\,\tfrac{1}{V} && \text{specific density of phase } i,\ 0 \le \rho_i \le \rho,\\
&\chi_i := \tfrac{\varrho_i}{\varrho} = \tfrac{\tilde{V}_i}{V_i} && \text{density quotient = mass of phase } i \text{ in } V,\ 0 \le \chi_i \le 1.
\end{aligned}$$

To guarantee the formation of phases, we subtract the mixing entropy density $\tilde{S}$,

$$\begin{aligned}
\tilde{S} &:= W(\chi) + \frac{\delta}{2}\,|\nabla\chi|^2,\\
W(\chi) &:= \chi \ln\chi + (1-\chi)\ln(1-\chi) - \frac{1}{2}\chi^2,
\end{aligned} \tag{3}$$

from S and set $\tilde{s} := \varrho\tilde{S}$. This represents the entropy density as

$$S = \chi S_1 + (1-\chi)S_2 - W(\chi) - \frac{\delta}{2}\,|\nabla\chi|^2$$

and consequently for the free energy density F and the Helmholtz free energy density G

$$F = \chi F_1 + (1-\chi)F_2 + T\tilde{S}, \quad G = \chi G_1 + (1-\chi)G_2 + T\tilde{S}.$$

MATHEMATICAL FORMULATION

Beside the definitions above, let $\varepsilon > 0$ be a scaling constant for the substantial derivative $d\chi := \partial_t\chi + v\cdot\nabla\chi$ of χ, $T : \Omega_D \to \mathbb{R}^+$ be the temperature and $p : \Omega_D \to \mathbb{R}^+$ the pressure of the fluid. For given velocity field v, let R_I denote the inlet, R_O the outlet of the domain Ω, where $\vec{n}$ is the unit outer normal vector to $\partial\Omega$. R_I and Ω are assumed not to depend on time t.

We modify the stress tensor and set (δ_{ij} be the Kronecker delta)

$$\begin{aligned}
\Gamma_{ij} &:= \tau_{ij} - p\delta_{ij} - \delta\varrho T\partial_i\chi\partial_j\chi,\\
\tau_{ij} &:= \mu(\partial_i v_j + \partial_j v_i) + \nu(\mathrm{div}v)\delta_{ij}
\end{aligned}$$

with viscosity coefficients ν, μ, where $\nu \ge -\frac{2}{3}\mu$ for $d = 3$ and $\nu \ge -\mu$ for $d = 2$.

One can show that the new term $-\delta\rho T\partial_i\chi\partial_j\chi$ is a consequence of adding $\frac{\delta\varrho}{2}\,|\nabla\chi|^2$ to the system entropy.

The thermodynamic driving force of the Allen-Cahn type equation is defined by

$$J(\varrho, T, \chi) := W(\chi) + \frac{1}{T}[\chi G_1(\varrho, T) + (1-\chi)G_2(\varrho, T)].$$

With these definitions, we introduce the following system of equations corresponding to conservation of mass (4), momentum (5) and energy (6):

For given $(\varrho_0, v_0, e_0, \chi_0)$, (v_r, T_r, χ_r) *and* ϱ_l *find the solution* $U = (\varrho, \varrho v, e, \chi)^t$ *of*

$$\partial_t \varrho = -\mathrm{div}(\varrho v), \tag{4}$$

$$\partial_t(\varrho v) = -\mathrm{div}(\varrho v \otimes v + \delta \varrho T \nabla\chi \otimes \nabla\chi) + \mathrm{div}(\tau) - \nabla p, \tag{5}$$

$$\partial_t e = \mathrm{div}(L\nabla T - (e - \Gamma)v), \tag{6}$$

$$\varepsilon\, \partial_t \chi = -\partial_\chi J + \frac{\delta}{\varrho}\mathrm{div}(\varrho \nabla\chi) - \varepsilon v \cdot \nabla\chi \tag{7}$$

in Ω *with the initial values*

$$(\varrho, \varrho v, e, \chi)(\cdot, 0) = (\varrho_0, \varrho_0 v_0, e_0, \chi_0) \qquad \text{in } \Omega$$

and the boundary values

$$\chi = \chi_r, \quad v = v_r, \quad T = T_r \quad \text{on } \partial\Omega$$

and

$$\varrho = \varrho_l \quad \text{on } R_l.$$

As a consequence of a parabolic maximum principle for (7), the logarithmic form of W in (3) guarantees $0 < \chi < 1$ in Ω_∞, if the same is true for the initial data χ_0.

All extrema β of the phase parameter χ satisfy

$$\partial_\chi J(\varrho, T, \beta) = \ln\left(\frac{\beta}{1-\beta}\right) - \beta + \frac{1}{T}(G_1(\varrho, T) - G_2(\varrho, T)) = 0.$$

This identity explains how ρ and T determine over $T^{-1}(G_1 - G_2)(\rho, T)$ the preferred phase (gas or liquid).

The above approach has some simplifications, e.g. that both phases move with the same velocity vector, that no chemical reactions take place, that the temperature of two neighbouring phases is the same, that there is no buoyancy, and that no heat is generated by shearing of boundary layers.

One can show that the entropy of the system obeys the formula

$$\int_\Omega \partial_t s + \int_{\partial\Omega} s v \cdot \vec{n} = \int_\Omega \left[L\frac{|\nabla T|^2}{T^2} + \frac{\tau}{T} : \nabla v + \varepsilon\varrho\,(\partial_t\chi + v \cdot \nabla\chi)^2\right] - \int_{\partial\Omega} \varrho(\partial_t\chi + v\cdot\nabla\chi)\,\delta\nabla\chi\cdot\vec{n} + \int_{\partial\Omega}\frac{L\,\nabla T}{T}\cdot\vec{n}. \tag{8}$$

Now, for a thermodynamically closed system, there is no temperature and entropy flux at $\partial\Omega$. So, by choosing Neumann-boundary data for χ or $\chi \equiv$ const on $\partial\Omega$, all boundary integrals in (8) vanish. $L\frac{|\nabla T|^2}{T^2}$ is a production term due to heat diffusion, $\frac{\tau}{T} : \nabla v$ is the dissipated motion energy that is positive for $\nu \geq -\frac{2}{3}\mu$ $(d = 3)$ or for $\nu \geq -\mu$ $(d = 2)$, as can be shown by principal axis transformation. Hence the second law of thermodynamics is valid. Notice that $\int_\Omega \varepsilon\varrho\,(\partial_t\chi + v\cdot\nabla\chi)^2$ corresponds to the Lyapunov functional of the unmodified Allen-Cahn equation.

CONCLUSION

The model presented here is a first step to incorporate transport mechanisms in the description of phase formation processes where the mass of the phases is no conserved order parameter. It still needs generalizations to be applicable to practical problems. Numerical sample calculations underline the physical meaningness of the approach.

REFERENCES

1. Allen S.M., Cahn J.W.: A microscopic theory for antiphase boundary motion and its application to antiphase domain coarsening. *Acta Metallurgica* **27**, pp 1085-1095, 1979

2. M.E. Gurtin, D. Polignone, J. Viñals J: Two-Phase Binary Fluids and Immiscible Fluids described by an Order Parameter. *Math. Models and Math. in Sci.* **2**.pp 191-211, 1996

3. L. Truskinovsky: Shock induced Transitions and Phase Structures in General Media. *IMA* **52**, pp 185-229 Springer, 1992

4. K.H. Hoffmann, V.N. Starovoikov: Phase-transitions of liquid-liquid type with convection. *Adv. Math. Sci. Appl.* **8** no 1, pp 185-198, 1998

5. A.A. Kostikov: The thermodiffusion Stefan problem in the presense of convection. *Ukr. Math. J.* **44** no 2, pp 236-240 (translation from Russian), 1992

SPREADING WITH BASAL SOLIDIFICATION

Michael Bunk & Peter Ehrhard
Forschungszentrum Karlsruhe, IKE, P.O.Box 3640, D-76021 Karlsruhe, Germany

Summary Based on an underlying lubrication theory we derive an approximation for the velocity and temperature fields and, thus, for the solid/liquid-interface of a spreading melt with poor thermal conductivity. The spreading flow is characterized in terms of Reynolds number Re, Froude number Fr, Prandtl number Pr and an aspect ratio ϵ. For the spreading volume we allow for $V \propto \tau^{\alpha}$. Solutions are found based on similarity transformations or numerical schemes using the method of lines. The influence of solidification on the spreading flow is discussed in terms of the spreading length history which depends on various parameters, as e.g. inflow rate and solidification temperature.

INTRODUCTION

Spreading of melts under the influence of solidification has a wide range of applications in geology and engineering. For example the spreading of a corium melt after a severe core melt down accident can lead to critical conditions for the coolability and the subsequent long-term removal of decay heat. We present an analytically based scheme to investigate the influence of basal solidification onto a spreading flow for liquid melts with poor thermal conductivity. We investigate the plane spreading problem over a horizontal isothermal plate in cartesian coordinates. A sketch of the spreading problem is shown in figure 1.

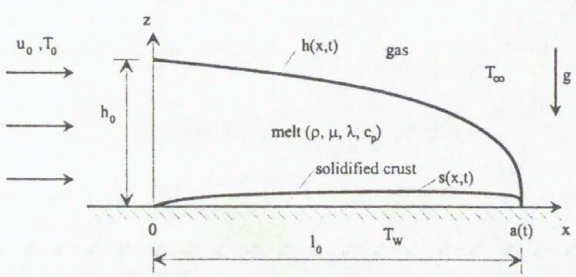

Figure 1. Sketch of the plane spreading problem

THEORY

The basic equations that describe the plane spreading process under the influence of gravity are the conservation equations for mass, momentum and energy[1].

In a dimensionless form using

$$X = \frac{x}{l_0} \quad , \quad Z = \frac{z}{h_0} \quad , \quad U = \frac{u}{u_0} \quad , \quad W = \frac{w}{\epsilon u_0} \quad ,$$

$$P = \frac{p}{(\mu l_0 u_0)/(h_0^2)} \quad , \quad \tau = \frac{t}{l_0/u_0} \quad , \quad \Theta = \frac{T - T_W}{T_0 - T_W} \quad ,$$

we obtain for $\epsilon \ll 1, \epsilon Re \ll 1$

$$\begin{aligned} U_X + W_Z &= 0 \quad , \\ 0 &= -P_X + U_{ZZ} \quad , \\ 0 &= -P_Z - \frac{\epsilon Re}{Fr} \quad , \\ \epsilon RePr(\Theta_\tau + U\Theta_X + W\Theta_Z) &= \Theta_{ZZ} \quad . \end{aligned}$$

The dimensionless groups are defined as

$$\epsilon = \frac{h_0}{l_0} \quad , \quad Re = \frac{u_0 h_0}{\nu} \quad , \quad Fr = \frac{u_0^2}{g h_0} \quad , \quad Pr = \frac{\nu}{\kappa} \quad .$$

For the spreading problem over a solidified crust at the horizontal bottom plate the boundary conditions are

$$\begin{aligned} X = 0, Z: \quad & \Theta = 1 \quad , \\ X, Z = 0: \quad & \Theta = 0 \quad , \\ X, Z = S: \quad & U = W = 0 \quad , \\ & \Theta = \Theta_S, \\ X, Z = H: \quad & W = H_X U + H_\tau \quad , \\ & P = 0 \quad , \\ & U_Z = 0 \quad , \\ & \Theta_Z = 0 \quad . \end{aligned}$$

Effects due to capillarity are negligible for $\mu u_0/\sigma \gg \epsilon^2$. Solidification occurs at a defined temperature, no mushy regime is presumed. The liberation of latent heat is negligible for $\tau \gg \Theta_S^2 (\epsilon RePr)^{1/3} L/(c_p(T_S - T_\infty))$.

BASIC IDEA OF THE MODEL

For melts with a high Prandtl number $Pr \gg 1$ we can expect thin thermal boundary layers and, therefore, thin solidified regions. Thus, solidification should have only a weak influence onto the spreading process. Given thin crusts, we attempt to solve for the flow and temperature field successively to avoid a strong coupling between the velocity and the temperature field. The influence of the bottom crust onto the spreading flow can be captured by successively performing the following steps:

1. First we solve the isothermal spreading problem without solidification[2] on the bottom plate. This gives for the velocities

$$U = \frac{\epsilon Re}{Fr} H_X \left(\frac{Z^2}{2} - HZ \right) \quad , \quad W = \frac{\epsilon Re}{6Fr} Z^2 \left(3H_X^2 + H_{XX}(3H - Z) \right) \quad .$$

The position of the l/g-interface $H(X, \tau)$ results from the evolution equation

$$H_\tau - \frac{\epsilon Re}{3Fr} \left(H^3 H_X \right)_X = 0 \quad \text{with} \quad V = \int_0^{A(\tau)} H(X, \tau)\, dX = C_V \tau^\alpha \quad , \quad H(A, \tau) = 0 \quad .$$

2. Based on the above flow field we solve for the temperature field. We restrict to the quasi-steady problem $\Theta_\tau = 0$, thus, we get a 'worst-case approximation' for the influence of nonisothermal effects on the spreading process. A weighted residual method shows that the thermal boundary layer thickness will be overestimated less than $\approx 20\%$ for the used parameter regime. Using a matched asymptotic representation together with a similarity transformation gives for the temperature

$$\Theta = 1 - \frac{\Gamma(1/3, \varphi^3/3)}{\Gamma(1/3)} \quad , \quad \varphi = \left(\frac{(\epsilon Re)^2 Pr}{3Fr} \frac{(-HH_X)^{3/2} Z^3}{\int_0^X \sqrt{-HH_X}\, dX^*} \right)^{1/3} .$$

3. Given the thermal field, we determine the position of the solid/liquid-interface $S(X,\tau)$. Here we use the condition $\Theta = \Theta_S$, where Θ_S is the dimensionless solidification temperature, to find $S(X,\tau)$. This gives a relationship between the l/g-interface $H(X,\tau)$ and the s/l-interface $S(X,\tau)$

$$S(X,\tau) = \varphi_S (1 - e^{-C_{mS} X / A(\tau)}) \left(\frac{3Fr}{(\epsilon Re)^2 Pr} \frac{\int_0^X \sqrt{-HH_X}\, dX^*}{(-HH_X)^{3/2}} \right)^{1/3} .$$

4. At this point we start an iterative scheme to solve the spreading problem over a solidified crust at the bottom plate. The position of the new l/g-interface $H_i(X,\tau)$ can be calculated from

$$H_{i,\tau} - \frac{\epsilon Re}{3Fr} \left((H_i - S_i)^3 H_{i,X} \right)_X = 0 \quad \text{with} \quad V = \int_0^{A_i(\tau)} H_i(X,\tau)\, dX = C_V \tau^\alpha \,,\; H_i(A_i,\tau) = 0.$$

For the special case $\alpha = 7/4$ solutions can be found using similarity transformations. For arbitrary values of α we use the method of lines to get a numerical solution.

5. In a next step it is necessary to calculate the new temperature field, which includes both, heat convection and conduction in the liquid melt and pure heat conduction within the solidified crust. Furthermore, we assume both thermal conductivity and density to be constant and equal in the liquid and solid phases. For this purpose we use a numerical scheme based on the method of lines.

6. Based on this improved temperature field, we infer an improved crust $S_{i+1}(X,\tau)$ at the solidification isotherm $\Theta = \Theta_S$. From

$$E_i = \frac{S_{i+1}(X,\tau) - S_i(X,\tau)}{S_i(X,\tau)} \quad ,$$

we judge the quality of the model. For the investigated parameter regime we get after 4 Iterations over steps 4.-6. a converged solution with $E_4 < 4\%$.

RESULTS

Figure 2 shows the position of the contact line $A(\tau)$ and the position of the l/g-interface $H(X,\tau)$ for $\epsilon = 0.01, Re = 1, Fr = 0.01, Pr = 10000, C_V = 1, \alpha = 1$. All height profiles show a significant influence of the solidified bottom crust. With increasing solidification temperature

Θ_S, we find an increasing crust thickness. Subsequently, the front propagation slows down due to a reduction of the driving hydrostatic pressure head.

For $\alpha = 7/4$ we get a significant change of the influence of the bottom crust onto the front propagation. For $\alpha < 7/4$ the crust $S(X,\tau)$ is growing faster in time than the position of the l/g-interface $H(X,\tau)$, thus, for $\tau \to \infty$ we can expect a complete freezing of the spreading flow. For $\alpha > 7/4$ we find that $H(X,\tau)$ is growing faster than $S(X,\tau)$. This leads to no limiting conditions regarding the propagation of the front $A(\tau)$.

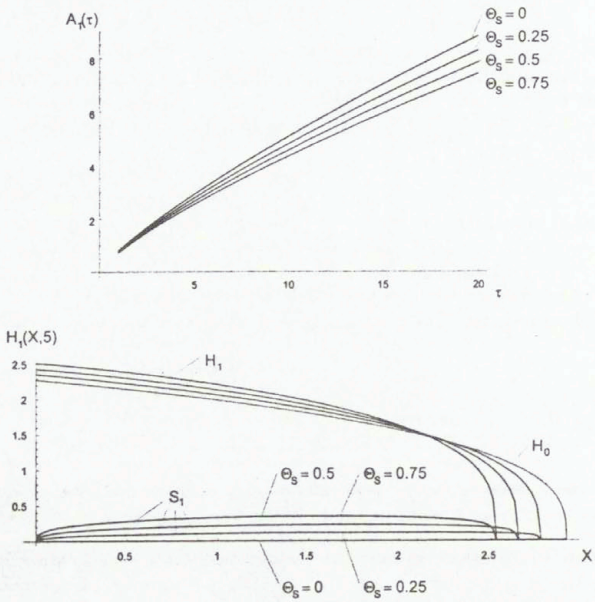

Figure 2. Position of the contact line $A(\tau)$ and the free l/g-interface $H(X,5)$

CONCLUSIONS

The influence of a solidifying crust on the cold bottom plate can be investigated by a mainly analytical approximation. This saves a huge amount of computer power in order to avoid the discretization of the very thin thermal boundary layers for melts with poor thermal conductivity. Due to the quasi-steady approximation we get an upper bound for the influence of nonisothermal effects onto the spreading flow. Thus, for numerical simulations we get a first check of the used discretization, which will strongly influence the effects of the solidifying crust onto the spreading flow.

REFERENCES

1. Schlichting H., Gersten K.: Grenzschicht-Theorie, Springer, 1997.
2. Huppert H.: The propagation of two-dimensional and axisymmetric viscous gravity currents over a rigid horizontal surface. *J. Fluid Mech* **121**, pp 43-58, 1982.

A NUMERICAL METHOD FOR THE RESOLUTION OF TWO-PHASE FLOWS AND APPLICATION TO A VERTICAL HEATED PIPE

F. Coquel[†], E. Godlewski[†], Arun In[†§], B. Perthame[‡] & P. Rascle[§]

[†] LAN, Université P. et M. Curie, 4, place Jussieu, 75252 Paris Cedex 05, France

[‡] DMI, Ecole Normale Supérieure, 45, rue d'Ulm, 75230 Paris Cedex 05, France

[§] EDF/DER/RNE/PhR, 1, avenue du Général De Gaulle, 92141 Clamart Cedex, France.

Summary We consider an equal pressure two-fluid model for two-phase flows with phase change, described by a system of six balance equations with source terms. We present a numerical method to solve this system. Then we use this method to study a low pressure slow water flow in a vertical heated pipe, this problem being the first stage to simulate a Loss Of Coolant Accident (LOCA) in a Pressurized Water Reactor (PWR).

INTRODUCTION

Several codes, as *CATHARE* [1] and *RELAP-5* [2], have provided so far efficient means for the safety analysis and the definition of accident and post-accident operationnal procedures in PWR, in particular during LOCA. But these advanced thermal-hydraulic codes are still quite time-consuming. Moreover, unfortunately, the prediction of the reflooding stage after LOCA apppeared not to be accurate at normal pressure conditions[1]. Thus, new methodologies are being explored in order to reduce computational time and to predict accurately such phenomena.

This presentation is devoted to the method introduced by Coquel *et al.*[3] to solve the two-fluid two-phase flow system. Using a splitting of this system, it reduces significantly the computational time compared to other explicit methods. This method has been recently upgraded by using the so-called *relaxed schemes*[4], which allow to deal with real fluid efficiently[5]. We present briefly the upgraded method, after recalling the two-fluid model. Then we give an application, say, a low pressure slow water flow in a vertical heated pipe.

THE SPLITTING METHOD FOR RESOLUTION OF TWO-PHASE FLOW

The Two-Fluid Two-phase flow model

We consider in this paper an equal pressure two-fluid model. For $k = v,\ l$, (v for vapor, l for liquid), let denote in mean value, α_k, ρ_k, u_k, e_k, h_k, h_{ik}, Γ_k, q_{ik}, M_{ik}^p, M_{wk}, q_{wk}, the volume fraction, the density, the velocity, the specific internal energy, the specific internal enthalpy, the interfacial specific internal enthalpy, the interfacial mass transfer, the interfacial heat flux, the interfacial drag force per unit volume, the wall friction, the wall heat flux for k-phase, p

the common pressure for the two phases, p_i the common interfacial pressure, u_i the interface velocity, and g the gravity. The two-fluid model, we consider in this work, is written

$$\begin{cases} \partial_t \alpha_v \rho_v + \partial_x \alpha_v \rho_v u_v = \Gamma_v, \\ \partial_t \alpha_v \rho_v u_v + \partial_x \alpha_v (\rho_v u_v^2 + p) - p_i \partial_x \alpha_v = \\ \alpha_v \rho_v g + M_{wv} + \Gamma_v u_{iv} + M_{iv}^D, \\ \partial_t \alpha_v \rho_v (e_v + u_v^2/2) + \partial_x \alpha_v \rho_v (h_v + u_v^2/2) u_v + p \partial_t \alpha_v = \\ (\alpha_v \rho_v g + M_{wv}) u_v + \Gamma_v (h_{iv} + u_i^2/2) + M_{iv}^D u_i + q_{iv} + q_{wv}, \end{cases} \tag{1a}$$

$$\begin{cases} \partial_t \alpha_l \rho_l + \partial_x \alpha_l \rho_l u_l = \Gamma_l, \\ \partial_t \alpha_l \rho_l u_l + \partial_x \alpha_l (\rho_l u_l^2 + p) - p_i \partial_x \alpha_l = \\ +\alpha_l \rho_l g + M_{wl} + \Gamma_l u_i + M_{il}^D, \\ \partial_t \alpha_l \rho_l (e_l + u_l^2/2) + \partial_x \alpha_l \rho_l (h_l + u_l^2/2) u_l + p \partial_t \alpha_l = \\ (\alpha_l \rho_l g + M_{wl}) u_l + \Gamma_l (h_{il} + u_i^2/2) + M_{il}^D u_i + q_{il} + q_{wl}, \end{cases} \tag{1b}$$

These systems represent the balance equations for mass, momentum and energy for each phase. We also have the continuity condition

$$\alpha_v + \alpha_l = 1. \tag{2}$$

and the following interfacial transfer conditions

$$\begin{cases} \sum_{k=v,l} \Gamma_k = 0, \\ \sum_{k=v,l} (\Gamma_k u_i + M_{ik}^D) = 0, \\ \sum_{k=v,l} (\Gamma_k (h_{ik} + u_i^2/2) + M_{ik}^D u_i + q_{ik}) = 0. \end{cases} \tag{3}$$

In order to close the problem, the equations of state of the two phase, and closure laws for the transfer terms must be given. These systems are obtained by averaging local instantaneous conservation equations and neglecting second order correlations[6].

The splitting method

In order to solve the two-fluid system, we use the splitting technique [3–6]. Let us recall the main features of this technique. Being given the variables at t^n, we proceed as follows.

During a first step we solve the two following systems, one for each phase k,

$$\begin{cases} \partial_t m_k + \partial_x m_k u_k = \Gamma_k, \\ \partial_t m_k u_k + \partial_x (m_k u_k^2 + \tilde{p}_k) = p_i \partial_x \alpha_k + m_k g + M_{wk} + \Gamma_k u_i + M_{ik}^D, \\ \partial_t E_k + \partial_x (E_k + \tilde{p}_k) u_k = \\ \quad (m_k g + M_{wk}) u_k + \Gamma_k (h_{ik} + u_i^2/2) + M_{ik}^D u_i + q_{ik} + q_{wk}, \end{cases} \tag{4}$$

where we have denoted $m_k = \alpha_k \rho_k$, and $\tilde{p}_k = \alpha_k p$. The second members are treated explicitely, so the resolutions of the two systems are decoupled. Thus, we just solve two hydrodynamical systems, one for each phase, and we add the values of the source terms at t^n. At the end of this step the pressures of the two phases are different, as the two-phases evolved independantly.

During the second step, we restore the equality of pressure, by solving for $k = v,\ l$

$$\begin{cases} d_t m_k = 0, \\ d_t m_k u_k = 0, \\ d_t E_k = -p\partial_t \alpha_k \text{ pour } k = v, l. \end{cases} \tag{5}$$

We refer the reader to the references[3–6] for details. Until then this method has been discretized using first-order finite-volume schemes. For the first step, if we consider two phases for which the equations of state are tabulated as for the following numerical test, the relaxed schemes are particularly interesting in terms of accuracy and efficiency. They enable to reduce the first step to the resolution of two Euler systems for polytropic gases. This scheme is an alternative to others methods for the resolution of the two-fluid model (see Toumi[7] or Städke and Holtbecker[8] for instance).

APPLICATION : A VERTICAL HEATED PIPE

We consider now a vertical boiling pipe that we study using the two-fluid model and the scheme we introduced in the previous section. This test is a simplified modelization of the reflooding process after a LOCA in a PWR. It illustrates the ability of the splitting method to treat rather complex multiphase flows.

The heated pipe is 3 meter long, with a section of 1 m^2, in a uniform gravity field. The spatial mesh size is $h = 0.1$ meter. Liquid water enters at the bottom of the tube at constant mass flux of $100 kg.s^{-1}$ and constant specific internal enthalpy equal to $h_{sat}(1.08\ bar)$. The pressure at the outlet is 1 bar. The first 0.5 meter and the last 0.5 meter of the pipe are not heated. As the liquid enters goes up the pipe, it boils. At the steady state, the vapor fraction increases along the pipe, and the pressure is slightly convex where some liquid remains (at the bottom of the pipe) and almost constant where there is few liquid. Fig. 1 show the volumic vapor fraction and the pressure along the tube, at the steady state, obtained with the splitting method and a mesh size of 0.1 *cm*. These results are in agreement with the physical expectation. For such a mesh size, there are important errors on the mixture mass flow. Refinement allows to correct these errors but increases the computational time. In the future some experiment data concerning this test should be obtained at the *PERICLES* test facility[1–9] in *CEA*, Grenoble.

CONCLUSION

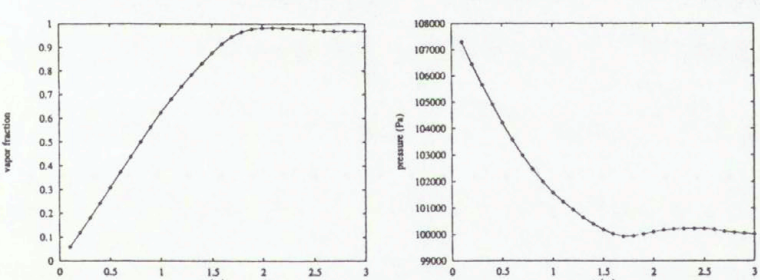

Figure 1: volumic vapor fraction and pressure

On this simplified reflooding problem, at low pressure condition and low speed, the results obtained with the splitting method are quite satisfactory. In the future, these results should be compared with the ones of other codes and with experimental data. The splitting method and the relaxed scheme have been used for other two-phase flows as sedimentation problem, Edward's pipe blowdown and Ransom's water faucet[10-11] and it has been recently extended to nozzle flows. Some developments concerning the treatment of the boundary conditions and the source terms are under progress.

REFERENCES

1. F. Barre, M Bernard, *The CATHARE code strategy*, Nucl. Engrg. & Des., 124 (1990), pp. 257-284.

2. V.H. Ransom et al. *RELAP5/MOD2 Code Manual*, Idaho National Laboratory, NUREG/CR-4312, EGG-2396.

3. F. Coquel, K. El Amine, E. Godlewski, B. Perthame, and P. Rascle, *A Numerical Method Using Upwind schemes for the Resolution of Two-Phase Flows*, J. Comp. Phys., 136 (1997), pp. 272-288.

4. F. Coquel, B. Perthame, *Relaxation of energy and approximate Riemann solvers for general pressure laws in fluid dynamics equations*, SIAM J. Numer. Anal., 35 (1998), pp 2223-2249.

5. A. In, *Numerical Evaluation of an Energy Relaxation Method for Inviscid Fluids*, to appear in SIAM J. Sci Comput.

6. A. In, *PhD Thesis*, Université Pierre et Marie Curie, Paris, France, to appear.

7. I. Toumi, *An Upwind Numerical Method for Two-Fluid Two-phase Flow Models*, Nucl. Engrg. & Des., 1996.

8. H. Städtke, R. Holtbecker, *Numerical Simulation of Multi-Dimensional Two-Phase Flow Based on Hyperbolic Flow Equations*, submitted to the 30th Meeting of the European Two-phase Flow Group, Piacenza, 6-8 June 1994, Italy.

9. D. Bestion, *personal communication*, 1999.

10. F. Coquel, E. Godlewski, A. In, B. Perthame, P. Rascle, *Influence of the Riemann solver over the splitting method for the resolution of two-phase Flows*, Sixteenth International Conference on Numerical Methods in Fluid Dynamics, Lectures Notes in Physics 515, Springer-Verlag.

11. F. Coquel, E. Godlewski, A. In, B. Perthame, P. Rascle, *An energy relaxation method for inviscid real fluids and Application to two phase flows*, ICFD Conference on Numerical Methods for Fluid Dynamics, Numerical Methods for Fluid Dynamics VI, M. J. Baines Ed., ICFD, Oxford, 1998.

NUMERICAL SIMULATION OF FRONTAL POLYMERIZATION

Thierry Dumont

CNRS & Université Lyon 1, F-69621 Villeurbanne Cedex, France.

Summary Frontal polymerization has been studied for many years experimentally and theoretically. Mathematical analysis has been devoted to the study of the stability of the front which separates the two phases, in the presence of thermal convection [1]. We present here an approach for a numerical simulation of this problem.

MATHEMATICAL MODEL

We consider an exothermic reaction between two reagents; C is the concentration of one of them ($0 \leq C \leq 1$), T is the temperature. The reaction rate is given by $W(C,T) = k(1-C)\ e^{-E/RT}$, where E is the activation energy, R the ideal gas constant and k the pre-exponential factor. We make the assumption that the density is constant, and we use Boussinesq approximation for the fluid. We can write the following equations :

$$\left\{ \begin{array}{rcl} \partial_t u + (u.\nabla)\, u - \nu \Delta u + \frac{1}{\rho} \nabla p & = & k_0\, \vec{g}\, (T - T_0) \\ \nabla . u & = & 0. \end{array} \right. \tag{1}$$

$$\begin{array}{rcl} \partial_t T + (u.\nabla)\, T - \kappa\, \Delta T & = & k_1\, W(C,T) \\ \partial_t C + (u.\nabla)\, C & = & k_2\, W(C,T). \end{array} \tag{2}$$

ν is the kinematic viscosity of the fluid, $\vec{g}$ is the gravitational acceleration, κ the coefficient of thermal diffusivity. k_0, k_1 and k_2 are positive constants.

Polymerization is taken into account in a very simplified way : when $C \geq C_0$, we have a phase change from liquid to solid. Real domains for this reaction are typically cylindrical tubes, but we restrict our simulations to a 2 dimensional quadrilateral domain Ω.

At time $t = 0$, we have $u = 0$, $T = T_0$, $C = 0$ everywhere in Ω. For boundary conditions, we take (see Figure 1) $u = 0$ on $\partial\Omega$, $\partial T/\partial n = 0$ on the "large" walls (2,4), $T = T_0$ on the wall (3), and $T = T_1$ on the wall (1), with $T_1 > T_0$. The reaction and, with a good choice of parameters and of the orientation of Ω a front of polymerization, propagate from wall (1) to the right.

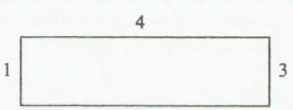

Fig. 1 : Ω.

NUMERICAL METHODS

Our simulations are based on two techniques associated with a spatial discretisation by the finite element method :

1. splitting of the system of equations with 2nd order characteristics ;
2. a fictitious domain method.

Splitting by the characteristics method : (based on the method of Boukir, Maday & Métivet) [2]. This method is based on an approximated 2nd order backward differentiation formula. Denote U^n, T^n and C^n the approximations of U, T and C at time $t_n = n\,\Delta t$. Define $U_c^{n+1} = 2\,U^n - U^{n-1}$; we compute a first order approximation $X_x^{n+1}(t)$ of the curves :

$$\begin{cases} \dfrac{dX_x^{n+1}}{dt} & = U_c^{n+1}(X_x^{n+1}(t)), \\ X_x^{n+1}(t_{n+1}) & = x. \quad t \in (t_{n-1}, t_{n+1}). \end{cases}$$

For the temperature, with :

$$f_c(x) = 2\,k_1 W(C^n(x), T^n(x)) - k_1 W(C^{n-1}(x), T^{n-1}(x)),$$

we compute :

$$\hat{T}(x) = \quad T^n(\tilde{X}_x^{n-1}(t_n)) \quad + \int_{t^n}^{t^{n+1}} f_c(\tilde{X}_x^{n+1}(s))ds, \tag{3}$$

$$\hat{\hat{T}}(x) = \quad T^{n-1}(\tilde{X}_x^{n+1}(t_{n-1}) \quad + \int_{t^{n-1}}^{t^{n+1}} f_c(\tilde{X}_x^{n+1}(s))ds, \tag{4}$$

and $\hat{C}(x)$, $\hat{\hat{C}}(x)$ by the same method. (the integrals are approximated by a quadrature formula like trapeze rule).
Then we calculate T^{n+1} satisfying boundary conditions and solution of :

$$\frac{3\,T^{n+1} - 4\,\hat{T} + \hat{\hat{T}}}{2\,\Delta t} - \kappa\,\Delta T^{n+1} = 0, \tag{5}$$

and C^{n+1} solution of :

$$\frac{3\,C^{n+1} - 4\,\hat{C} + \hat{\hat{C}}}{2\,\Delta t} = 0, \tag{6}$$

(note that we treat the 2nd member with the convective term).

When we compute $\hat{T}$, $\hat{C}$ (and $\hat{\hat{T}}$, $\hat{\hat{C}}$) in (3) (and (4)), we obtain independent nonlinear algebraic systems of 2 equations for every quadrature point of the finite element discretisation. The same method can be applied to Navier-Stokes equations.
One step of our algorithm, from t_n to t_{n+1}, is :

1. compute $\hat{T}$, $\hat{C}$, $\hat{\hat{T}}$, $\hat{\hat{C}}$, then T^{n+1} and C^{n+1} as in (5), (6);

2. compute $\hat{U}$ and $\hat{\hat{U}}$ as in (3), (4), (but with $f_c = 0$) and U^{n+1}, verifying boundary conditions and solution of the generalized Stokes problem :

$$\frac{3\,U^{n+1} - 4\,\hat{U} + \hat{\hat{U}}}{2\,\Delta t} - \nu\,\Delta U^{n+1} = k_0\,\vec{g}\,(T^{n+1} - T_0), \quad \nabla . U^{n+1} = 0. \tag{7}$$

We obtain a fully decoupled scheme.

Fictitious domain method : we impose to the velocity of the fluid to be approximately zero in the polymerized zone $\Omega_1 = \{x;\ C(x) \geq C_0\}$ ($\Omega = \Omega_0 \cup \Omega_1$). To obtain this, we use the method of N.S. Bakhvalov [3] :
Consider the generalized Stokes problem :

$$\alpha u - \nabla.(\eta Du) + \nabla p = f,\ \ \nabla.\, u = 0,\ \ u_{\partial\Omega} = 0. \tag{8}$$

Set $\varepsilon << 1$ a penalization parameter and choose :

$$\alpha(x) = \alpha_0, \eta(x) = \eta_0,\quad \forall x \in \Omega_0,$$

$$\alpha(x) = \alpha_0/\varepsilon, \eta(x) = \eta_0/\varepsilon\quad \forall x \in \Omega_1.$$

Let S_ε be the Stokes operator defined in (8) and $S_1(u,p)$ the constant coefficient Stokes operator (i.e. with $\varepsilon = 1$).
On the subspace :

$$V = \{v \in H_0^1(\Omega);\ \ \nabla.v = 0;\quad \int_{\Omega_1} \alpha_0 \nabla(v-u)\nabla\phi + \eta_0(v-u)\phi = 0 \\ \forall \phi \in H^1(\Omega_0),\ \ \nabla.\phi = 0,\ \ \phi_{\partial\Omega_1} = 0.\}$$

S_ε and S_1 are spectraly equivalent. Choosing as departure point for conjugate gradient iterations a solution of $S_1(u_0, p_0) = f$ and S_1 as preconditioner, the iterates remain in V and we obtain a rate of convergence which depends only of the domain Ω_1.

The modification of our splitting method is obvious : once we have computed T^{n+1} and C^{n+1}, we obtain the set Ω_1 and solve (7), imposing $U^{n+1} \simeq 0$ on Ω_1 by the fictitious domain method.

References

1. Bowden, Garbey, Ilyashenko, Polman, Solovyov, Taik, Volpert. *Effect of Convection on Propagating Front with a Solid Product: Comparison of Theory and Experiments.* The J. of Phys. Chemistry B, vol. 101, (4),1996, pages 678-686.

2. Boukir, Maday & Métivet. *A high order characteristics method for Navier Stokes equations.* Comp. Meth. in Appl. Mech. & Eng.,1993.

3. Bakhvalov *Solution of the Stokes nonstationary problems by the fictitious domain method.* Russ. J. Numer. Anal. Math. Modeling, Vol.10 no 3 (1995).

IDENTIFICATION OF A MOVING SOLID/LIQUID INTERFACE

A. El Badia

Compiegne University of Technology
Division of applied Mathematics, B.P. 529
F-60205 Compiegne cedex, France
e-mail: abdellatif.elbadia@utc.fr

Summary The moving solid/liquid interface of a melting solid in one dimensional case is identified from temperature and flux measurements performed on the solid part only. An algorithm is used, based on the least square approach using conjugate gradient method and sensitivity equation. A comparison with the numerical results obtained in [4] is given.

INTRODUCTION AND STATEMENT OF THE PROBLEM

Introduction

Identification problem of the solid/liquid interface in a phase change process,such as casting, crystal growth and welding is a subject of great interest to industry.The interface is often unknown and its determination by direct measurements is impracticable. An alternative method to determine the interface consists of using the model which connects the parameters and the sizes governing the transfers of heat and mass in the phases to the position of the interface. But the coupled physical phenomena occurring in the liquid (natural convection, thermal conduction, surface effects,...) are often partially unknown and cannot be easily modeled. To overcome this problem only the model in the solid part which is accessible to measurements, is used.
Among phase change problems, two inverses cases can arise: the control problem or the identification one. Several studies have been devoted to the control problem ([9], [2], [3], [1]). But, fewer results are available for the identification problem, considered especially in ([10], [4], [5], [6], [7], [8]). The latter studies have used a sequential algorithm to solve the identification problem from discrete measurements, collected at the fixed part.
In this study, we propose a new algorithm to solve the identification problem in one phase one-dimensional Stefan problem. In the last sectionh, we present a brief comparison with the results obtained in [4].

Statement of the problem

Let us consider the one phase Stefan problem, in one space dimensional which is a particular moving boundary problem: the isothermal interface between the solid phase and the liquid phase is driven by the diffusive heat two connected phases. The only modeled part is the solid one. The interface solid/liquid is characterized by a positive function σ of class C^1, defined in $[0, T]$ with values in $]0, 1[$.
The solid part :

$$I_s(t) = \{x/\sigma(t) < x < 1\}$$

is governed by the heat equation:

$$\theta_t - \theta_{xx} = 0 \text{ in }]\sigma(t), 1[\times(0,T), \tag{1}$$

satisfying the initial condition

$$\theta(x,0) = 0 \text{ in }]\sigma(0), 1[, \tag{2}$$

the boundary condition

$$\theta(1,t) = u(t) \text{ in } (0,T), \tag{3}$$

and the interface condition

$$\theta(\sigma(t),t) = T_f \text{ in } (0,T), \tag{4}$$

where the function u and the constant T_f, respectively the temperature and the melting point, are assumed to be known. Without loss of generality, we will suppose that $T_f = 0$.

If the interface σ is given, one can calculate the flow $\theta_x(1,t)$ and thus to define the observation operator,

$$C(\sigma) = \theta_x(1,t).$$

That is the direct problem. The inverse problem we are concerned with, is as follows :

Inverse problem
Given the observation ϕ, can we find a function σ such that:

$$C(\sigma) = \phi\,? \tag{5}$$

RESOLUTION METHOD

Criterion

The identification of the parameter σ is a nonlinear problem that is solved by the minimization of a penalized least square criterion J cf.(6). The minimization is performed with conjugate gradient method, which requires the calculation of the gradient $\dfrac{\partial J}{\partial \sigma}$ of J with respect to σ. The calculation of the latter, is done by the equation of sensitivity state, compared to σ and its adjoint state. The regularization parameter ϵ is chosen according to required precision and stability.

$$J(\sigma) = \frac{1}{2}\int_0^T (C(\sigma)(t) - \phi(t))^2 dt + \frac{\epsilon}{2}\int_0^T \sigma^2 dt \tag{6}$$

Equation of sensitivity

This section aims to calculate the directional derivative of the operator C at the point σ in the direction h, defined by :

$$C'(\sigma).h = \lim_{\lambda \to 0} \frac{C(\sigma + \lambda h) - C(\sigma)}{\lambda} \tag{7}$$

that is given in the following theorem

Theorem 1 *Let θ be the solution of the problem* (1) − (4).
Let ψ be the solution of the problem:

$$\psi_t - \psi_{xx} = \frac{2h}{1-\sigma}\theta_{xx} + \left(\frac{h}{1-\sigma}\right)'[\beta\theta + (1-x)\theta_x] \text{ in }]\sigma(t), 1[\times]0, T[, \quad (8)$$

$$\psi(x,0) = 0 \text{ in }]\sigma(0), 1[, \quad (9)$$

$$\psi(\sigma(t), t) = 0 \text{ in }]0, T[, \quad (10)$$

$$\beta\psi(1,t) + (1-\beta)\psi_x(1,t) = \frac{h}{1-\sigma}u(t) \text{ in }]0, T[, \quad (11)$$

then

$$C'(\sigma).h = (1-\beta)\psi(1,t) + \beta\psi_x(1,t) \quad (12)$$

where β is a constant such that

$\beta = 1$ *for the Dirichlet condition*
$\beta = 0$ *for the Neumann condition*

Adjoint State

The aim of this section is to express the directional derivative $J'(\sigma).h$ of the criterion J at point σ in the direction h, by means of the state associated to the system ((8) − (11)).

By direct calculation, one obtains:

$$J'(\sigma).h = \int_0^T (C(\sigma) - \phi(t))\, C'(\sigma).h dt + \epsilon \int_0^T \sigma\, h dt \quad (13)$$

and in a classical way, one defines the state associated, p by the equation

$$-p_t - p_{xx} = 0, \text{ in } \quad]\sigma(t), 1[\times(0,T), \quad (14)$$

satisfying the final condition

$$p(x,T) = 0, \text{ in } \quad]\sigma(0), 1[, \quad (15)$$

the boundary condition

$$p(1,t) = C(\sigma)(t) - \phi(t), \text{ in } \quad (0,T), \quad (16)$$

and the interface condition

$$p(\sigma(t), t) = 0, \text{ in } \quad (0,T). \quad (17)$$

Let f be the function defined by

$$f(x,h,\sigma,\theta) = \frac{2h}{1-\sigma}\theta_{xx} + \left(\frac{h}{1-\sigma}\right)'[\beta\theta + (1-x)\theta_x] \text{ in } \quad]\sigma(t), 1[\times]0, T[, \quad (18)$$

Then the expression of the directional derivative $J'(\sigma).h$ is given by the following proposal

Property 1

$$J'(\sigma).h = \int_0^T \frac{h}{1-\sigma}\, u(t)\, p_x(1,t)\, dt + \epsilon \int_0^T \sigma\, h dt - \int_0^T \int_{\sigma(t)}^1 f(h,\sigma,\theta)\, p(x,t)\, dx\, dt.$$

Similarly, when the Neumann boundary condition is considered in the problem ((1)-(4)), the expression of gradient becomes:

$$J'(\sigma).h = \int_0^T \frac{h}{1-\sigma}\, u(t)\, p(1,t)\, dt + \epsilon \int_0^T \sigma\, h dt + \int_0^T \int_{\sigma(t)}^1 f(x,h,\sigma,\theta)\, p(x,t)\, dx\, dt,$$

where

$$f(x,h,\sigma,\theta) = \frac{2h}{1-\sigma}\theta_{xx} - (1-x)\left(\frac{h}{1-\sigma}\right)'\theta_x \quad \text{and} \quad C(\sigma) = \theta(1,t).$$

It follows that,

$$J'(\sigma).h = -\int_0^T \int_{\sigma(t)}^1 \frac{h}{1-\sigma}\left((1-x)\,[\theta_x\, p]_{|t} - 2\,\theta_{xx}\, p\right) dt\, dx$$

$$- \int_{\sigma(0)}^1 (1-x)\,\frac{h(0)}{1-\sigma(0)}\,\theta_x(x,0)\, p(x,0) = dx + \int_0^T \frac{h}{1-\sigma}\, u(t)\, p(1,t)\, dt + \epsilon \int_0^T \sigma\, h dt.$$

APPLICATION

Test case: Neumann solution for Stefan problem[13]

We Consider a 1D slab ($0 \le x \le 1$). The one-dimensional slab is initially at zero dimensionless temperature and the analytical Neumann solution (19) for the heat equation is considered.

$$\theta(x,t) = \frac{1}{erfc(\lambda\sqrt{\kappa^*})} erfc(\frac{x}{2\sqrt{t}}),\ t > 0, \tag{19}$$

where λ is solution to

$$k^* \frac{e^{-\lambda^2}}{erfc(\lambda)} - \sqrt{\kappa^*}\frac{e^{-\kappa^*\lambda^2}}{erfc(\lambda\sqrt{\kappa^*})} = \frac{\sqrt{\pi}\kappa^*\lambda}{Ste}.$$

The corresponding phase interface position is given by

$$\hat{\sigma}(t) = 2\lambda\sqrt{\kappa^* t},$$

and the time-dependent boundary condition, temperature and flow, at $x = 1$ are given by:

$$u(t) = \theta(1,t) = \frac{1}{erfc(\lambda\sqrt{\kappa^*})} erfc(\frac{1}{2\sqrt{t}}),$$

$$\phi(t) = -\theta_x(1,t) = -\frac{1}{\sqrt{\pi t}}\frac{1}{erfc(\lambda\sqrt{\kappa^*})} e^{-\frac{1}{4t}},$$

where

$$\begin{cases} erfc(x) = \dfrac{2}{\pi}\displaystyle\int_x^\infty e^{-t^2}dt, \\ k^* = \dfrac{k_{liq}}{k_{sol}}, \quad \text{relative conductivity,} \\ \kappa^* = \dfrac{\kappa_{liq}}{\kappa_{sol}}, \quad \text{relative diffusivity,} \\ Ste = C_{sol}\dfrac{\theta_f^{dim} - \theta_i^{dim}}{L}, \quad \text{Stefan number,} \\ \text{where} \begin{cases} C_{sol} = \text{solid heat-storage capacity,} \\ \theta_f^{dim} = \text{dimensionless final temperature,} \\ \theta_i^{dim} = \text{dimensionless initial temperature,} \\ L = \text{latent heat of fusion.} \end{cases} \end{cases}$$

The temperature θ and the flow ϕ are calculated for ice/water with

$$\begin{cases} Ste = .00316, \\ k^* = .272, \\ \kappa^* = .125, \\ \lambda = .158. \end{cases}$$

Algorithm of minimization

The minimization of J is done by the Matlab finite dimensional optimization subroutine " con str ". This subroutine uses a sequential quadratic programming method. In this method, a quadratic method programming subproblem is solved at each iteration. An estimate of the Hessian of the Lagrangian is updated at each iteration using the BFGS formula [11]-[12]. The subroutine " constr" requires :

1. an initial function (σ_{init}) for our problem
2. the discretized function J
3. the discretized gradient ∇J of J

For the determination of J (at each step of the optimization algorithm) we have to solve one parabolic problem (1)-(4). This will be done by a finite differences methode. Similary, one has to solve parabolic problem (14)-(17) to obtain ∇J.

References

[1] R. Reemtsen and A. Kirsch (1984). A method for the numerical solution of the one-dimensional inverse Stefan problem, Numer. Math., 45, 253-273.

[2] P. Jochum (1980). The inverse Stefan problem as a problem of nonlinear approximation theory, J. Approx., 30, 81-98.

[3] P. Jochum (1982) The numerical solution of the inverse Stefan problem, Numer. Math., 34, 411-429.

[4] Afshine Afshari (1990). Identification de l'évolution d'un front de fusion/solidification par la résolution de l'équation inverse de la chaleur dans le domaine solide. Thèse, Univercité de Paris-Sud centre d'Orsay.

[5] A. Afshari and C. Bénard and C. Duhamel and B. Guerrier (1989). On-line identification of the state of the surface of a material undergoing thermal processing, 5th IFAC symposium on control of distributed systems, Perpignan (France), 209-213.

[6] A. Afshari and C. Bénard and C. Duhamel and B. Guerrier (1991). Problème inverse : suivi de l'évolution de la position d'un front de fusion à l'aide de mesure sur la phase solide. Journée S.F.T. Modélisation en thermique industrielle.

[7] C. Bénard and A. Afshari (1991). Front tracking for the control of solid-liquid phase change process, 7th Int conf. on numerical methods in thermal problem, Stanford 7, 1, 186-198.

Inverse method in phase change problems, Eurotherm, seminar 6, Delft (the Netherlands).

[8] X. Wang and M.M. Rosset-Louërat and C. Bénard (1992). Inverse problem : identification of a melting front in the 2D case, Int. Series of Num. Math., 107, 99-110.

[9] D. Colton and R.Reemtsen (1984). The solution of inverse Stefan problem in two space variables, SIAM J. Appl. Math., 5, 996-1013.

[10] M.A. Katz and R.Reemtsen(1984). An inverse finite elememt technique to determine the change of phase interface location in one dimensional melting problem, Num. Heat transfer, vol.7, pp.269-283

[11] C.G. Broyden(1970). The convegence of a class of Ddouble-rank Minimization Algorithm, J. Int. Math. app. Vol 6, pp 76-90

[12] D.F. Shanno (1970). Conditioning of Quasi-Newton Methods for function minimization, Maths. of Comp., Vol 24, pp 647-656

[13] H.S. Carslaw and J.C. Jaeger (1959). Conduction of heat in solids, Oxford University Press.

2D NUMERICAL SIMULATION OF GAS - LIQUID TYPE PHASE TRANSITION FOR MOLECULES IN CERAMICS

Vilnis Frishfelds*, Ilmars Madzhulis*, Janis Rimshans**
*Faculty of Physics and Mathematics ,University of Latvia, Zellu 8, LV-1002,Riga,Latvia
**Institute of Mathematics and Computer Sciences, University of Latvia , LV-1459,Rainja Boulevard 29, Riga ,Latvia

Summary Based on microscopic kinetic equations, a mathematical model is considered for the time-dependent diffusion process of self-interacting metal vapour in a fireproof material in a strongly inhomogeneos temperature field. Due to the self-interaction of metal vapour phase transition (condensation) appears. The developed conservative, monotonous and absolutely stable difference scheme is based on a special exponential substitution for the concentration of molecules. The results of non- steady state 2D numerical experiments are presented.

Mathematical model and differential equations

We have studied metal vapour penetration in ceramics. It is considered that this process can be described as the motion of molecules in a porous medium . By using *approach*[1] from the microscopic model, a diffusion equation is proposed. One-dimensional *calculations*[2] show the stochastic nature of phase transition. The actual problem is presented by calculations in a more realistic two - dimensional geometry.

The expression for a microscopic flow of particles, taking into account the nearest neighboring sites, is obtained in *work*[3]. The next simplification is possible if we assume that the size of pores is much smaller than the mean free path of ideal gas at the same concentration of particles and the length of particle jumping is greater than the distance of the interacting particles.

Then, expressions for flow $f_+(x+a/2,y_j)$ in a positive direction, and flow $f_-(x+a/2,y_j)$ in a negative direction at a fixed point y_j may be *written*[4] :

$$f_\pm(x+a/2,y_j)=\Omega_0 C(x+a/2\mp a/2,y_j)(1-C(x+a/2\pm a/2,y_j)\times$$

$$\times\exp\left[\frac{\varepsilon}{K}\left(\frac{C(x+a/2\pm a/2,y_j)}{T(x+a/2\pm a/2,y_j)}-\frac{C(x+a/2\mp a/2,y_j))}{T(x+a/2\mp a/2,y_j))}\right)\right], \qquad (1)$$

where: Ω_0 -the collision frequency, $C(x.y)$ - the concentration of molecules , normalized so that it can reach its values within the range $[0,1]$, $T(x,y)$ - temperature , ε - the energy of the bond between two neighboring molecules, K - the Boltzmann constant .

Then the flow $J_x(x+a/2,y_j)$ of the particles in direction x can be expressed as :

$$J_x(x+a/2,y_j)=f_+(x+a/2,y_j)-f_-\left(x+a/2,y_j\right) .$$

After linearization (1) for J_x we have obtained:

$$J_x=-\Omega_0 a\cdot ch\left(\gamma_{x+a,y}\right)\frac{\partial C}{\partial x}+2\Omega_0 C(1-C)sh\left(\gamma_{x+a,y}\right),\gamma_{x+a,y}=\frac{\varepsilon}{K}\left(\frac{C(x+a,y)}{T(x+a,y)}-\frac{C(x,y)}{T(x,y)}\right)$$

The expression for J_y can be written in a similar way by appropriate substitution.

For a full flow we have obtained : $\vec{J} = J_x\vec{i} + J_y\vec{j}$.

With the known macroscopic expression for a full flow the diffusion (flow continuity) equation is written :

$$\frac{\partial C}{\partial t} = - \ div\vec{J} . \tag{2}$$

In the proposed model the macroscopic flow is created by temperature gradients which play the role of an external force. As the first approximation in this work, we consider that the temperature of molecules is the same as the frame temperature. The temperature conduction equation can be written in the traditional form:

$$\frac{\partial T}{\partial t} = D\nabla \cdot (\nabla T) + Q \ , \tag{3}$$

where D - the diffusion coefficient , Q - the thermal source. It is considered that the source of the metal vapour is located at the boundary points $\Omega_S = (x = 0 \ , 0 \le y \le y_L)$, and the cooler is disposed at the end of structure $\Omega_C = (x = x_L \ , 0 \le y \le y_L)$. At these boundary lines the temperature is kept constant and equal $T_S = T_C = 300K$. On the other boundary lines the temperature derivatives are equal to zero. Equation (3) is solved in a traditional way by using the central difference scheme. The steady- state of temperature distribution is shown in Fig. 1.

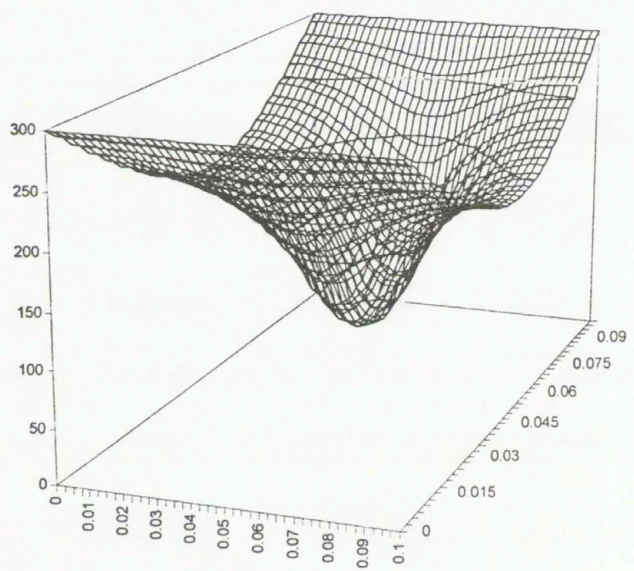

Fig. 1. Steady-state temperature distribution

As it shown in Fig. 1, a strongly nonhomogeneous temperature distribution arises only in the region near the cooler. This means that the flows of molecules in the main part of the examined structure are near to zero and the thermal equilibrium conditions are approximately fulfilled.

Difference scheme for diffusion equation

In the one dimensional case conservative, monotonous and absolutely stable exponential difference *scheme*[2] is elaborated. In this work the *method*[2] is extended to a two-dimensional case.

Let us introduce the nonuniform space grid with steps h_i $(i = 1,2,\ldots, M_1)$ and r_j $(j = 1,2,\ldots, M_2)$ and substitute the concentration $C(x,y)$ by $W(x,y)$ in such a way:

$$C(x,y) = W(x,y)\exp\left\{\int_{x_0}^{x} dx \frac{2(1-C)}{a} th(\gamma_{x+a,y})\right\}, \qquad (4)$$

where x_0 is an arbitrary real number which, in the final form, does not affect the coefficients of the difference scheme. Substitution (4) is intended for flow J_x approximation. A similar substitution is used for J_y approximation, only if integration is provided a direction y and function $\gamma_{x+a,y}$ is changed to $\gamma_{x,y+a}$. Using the balance method and the previous substitutions for $C(x,y)$, the difference scheme for equation (2) is written:

$$\frac{C_{i,j}^{l+1} - C_{i,j}^{l}}{\tau} = -\left\{\frac{(J_x)_{i+1/2,j} - (J_x)_{i-1/2,j}}{h_i^*} + \frac{(J_y)_{i,j+1/2} - (J_Y)_{i,j-1/2}}{r_j^*}\right\}, \qquad (5)$$

where : τ – the time step , l – the time step index , $h_i^* = (h_i + h_{i+1})/2$, $r_j^* = (r_j + r_{j+1})/2$.

For the grid flows $(J_x)_{i+1/2,j}$ and $(J_y)_{i,j+1/2}$ we have :

$$(J)_{k+1/2,m} = -\frac{\Omega_0 a}{h_{k+1}} \cdot ch\left(\frac{\varepsilon}{K}\left(\frac{C_{k+1,m}}{T_{k+1,m}} - \frac{C_{k,m}}{T_{k,m}}\right)\frac{a}{h_{k+1}}\right)\cdot\left(\frac{\beta_{k+1/2,m}\exp(-\beta_{k+1/2,m})}{\left(1-\exp(-\beta_{k+1/2,m})\right)}C_{k+1,m} - \right.$$

$$\left. - \frac{\beta_{k+1/2,m}}{\left(1-\exp(-\beta_{k+1/2,m})\right)}C_{k,m}\right), \qquad (6)$$

$$\beta_{k+1/2,m} = \frac{2\varepsilon}{K}(1-C)_{k+1/2,m}\left(\frac{C_{k+1,m}}{T_{k+1,m}} - \frac{C_{k,m}}{T_{k,m}}\right).$$

On the boundary lines Ω_S and Ω_C the concentration C is changed in the time moment $t = 0$ to a constant value from segment [0,1] . On other boundary lines the derivatives of the molecule concentrations are kept at zero. The initial distribution of C in the whole structure is constant, and equal to zero. As it is proved in the one-dimensional case and shown by numerical calculations, difference scheme (5) is also conservative, monotonous and absolutely stable.

Results of calculations

For numerical calculations equation (5) was written in a half-implicit way without a linearization

procedure . The linear system of equations was solved by the *ILUCGS* [5] method. Calculations are provided for the case when the concentrations on the boundary lines Ω_S and Ω_C are smaller than the critical one, when C distribution reaches homogeneous concentrations which are equal to the boundary concentration, and for the case when they exceed the critical concentration $C^* \cong 0.2$. In Fig. 2 steady-state distribution of the molecule concentration is presented where $C_S = C_C = 0.3$.

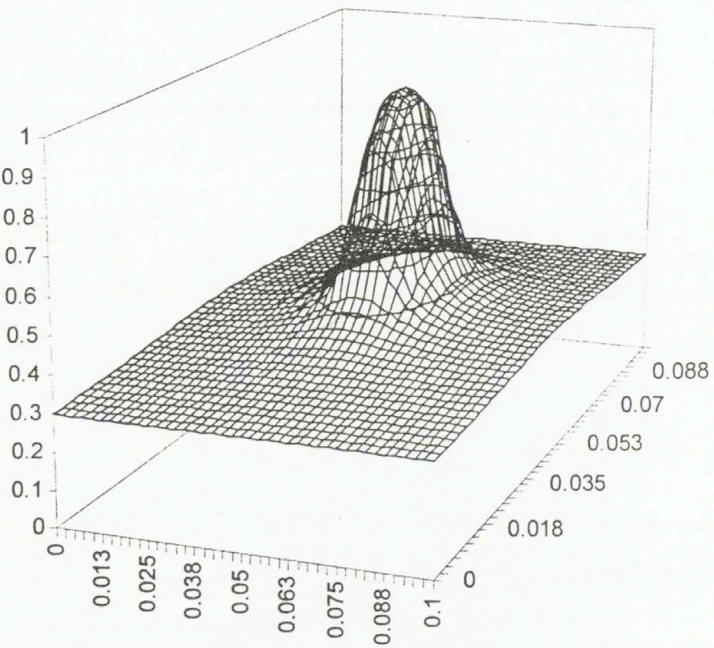

Fig. 2 . Steady-state distribution of concentration

As can be seen from numerical calculations, in the kinetics process the molecules are separated into two regions, and in a steady-state (Fig. 2) the gas - liquid type system is developed.

REFERENCES

1. Nicolis G., Prigogine I.: Exploring Complexity. W.H. Freeman & company, NY 1989.
2. Frishfelds V., Madzhulis I., Rimshans J.: Difference Scheme for Dynamic Simulation Describing Stochastic Kinetics of Molecules in Ceramics. *Mathematical Modelling and Analysis*, Lithuania, Vilnius "Technika" **3**, pp 93-97, 1998.
3. Suzuki M., Kubo P.: Dynamics of the Ising Model Near the Critical Point. *J. Phys. Soc. Japan* **24**, N 1, pp 50-60, 1968.
4. Medvid A., Madzhulis I., Kaupuzs J., Blums J.: Buried Layer Formation in Silicon by Laser Radiation. *Journ. Appl. Physics* **79**, N 12, pp 23-26, 1996.
5. Heijer C. : Preconditioned Iterative Methods for Nonsymmetric Linear Systems. *Proceedings of ITC on Simulation of Semiconductor Devices and Processes*, pp 267-285 , Pineridge Press. Swansea 1984

MATHEMATICAL MODELING OF TRANSPORT PHENOMENA DURING SOLIDIFICATION OF BINARY SYSTEMS USING THE ENSEMBLE AVERAGING APPROACH

Piotr Furmański
Warsaw University of Technology, ul. Nowowiejska 25, 00-665 Warsaw, Poland, e-mail: pfurm@itc.pw.edu.pl

Solidification problems play an important role in material processing (like casting of steel, non-ferrous alloys, metal-matrix composites),the ground freezing technique, in phase change materials used in thermal energy storage systems, etc. In most of these processes multicomponent solutions are present. These multicomponent solutions undergo solidification over a range of temperatures which causes a solid-liquid mixture to be formed. The solid-liquid zone, where solidification takes place and known as a mushy region, consists of solid and liquid phases of varying proportions and often makes a substantial part of the whole system. Within the mushy region proportions of solid and liquid vary in time and space. Moreover, the phase-change phenomenon is assisted by transport phenomena occurring in the individual phases and the mutual interactions between solid and liquid are present.

Complex microstructure of the mushy region is the main reason for carrying out the analysis on the macroscopic scale, the scale much greater than dimensions of dendrites or equiaxed crystals formed during the solidification. Thus, before any numerical implementation, a problem of macroscopic modeling of heat and mass transfer phenomena in the mushy region should be addressed. The macroscopic equations describing the process of solidification are usually introduced via a volume averaging approach. It is however known, from theory of heterogeneous materials, that the volume averaging has many limitations. Its drawbacks lie in problems of finding proper representative elementary volume for averaging, accounting for the macroscopic variation of the microstructure and its statistical character, proper formulation of the constitutive relations describing macroscopic transport phenomena, accounting for thermodynamic relations existing at the solid-liquid interface, etc.

A different approach to describe solidification process in the mushy region, based on an ensemble averaging, is proposed in the paper. The ensemble averaging approach is taken from theory of random fields and stochastic processes where it proved to be useful in finding solution of many problems that appear both in description and understanding of the transport phenomena. This approach was followed to derive conservation equations and the basic constitutive relations appearing in the macroscopic description of the solidification phenomena occurring in the mushy region.

HIGH-AZIMUTHAL NUMBER AXISYMMETRY-BREAKING CONVECTIVE INSTABILITIES IN AXISYMMETRIC FREEZING OF ICE

Alexander Yu. Gelfgat*, Pinhas Z. Bar-Yoseph*, Alexander Solan* and Tomasz A. Kowalewski**

*Computational Mechanics Laboratory, Faculty of Mechanical Engineering, Technion – Israel Institute of Technology, Haifa 32000, Israel

**Polish Academy of Sciences IPPT PAN, Swietokrzyska 21, PL 00-049, Warszawa, Poland

Summary The experimentally observed non-axisymmetric structure of ice frozen under axisymmetric thermal boundary conditions is assumed to be a result of the three-dimensional instability of an axisymmetric natural convection flow. The latter is investigated numerically using a global spectral Galerkin method. The linear stability problem separates for different azimuthal modes such that the problem reduces to a sequence of 2D-like problems. The numerical results are successfully compared with an experiment on natural convection of water in a vertical cylinder, which shows an axisymmetry-breaking instability with a high azimuthal wavenumber.

INTRODUCTION

This work is devoted to a theoretical explanation of an effect observed during the study of freezing of ice in an axisymmetric container [1]. The solidification front observed on the ice had an asymmetric, circumferentially periodic surface shape. Likewise, measurements of the temperature field also showed a periodic structure.

It was assumed that the effect is due to an axisymmetry-breaking instability of the convective flow of water. Detailed numerical analysis of the stability of the basic axisymmetric flow with respect to all possible three-dimensional perturbations showed that the instability sets in with a relatively high azimuthal wavenumber k, which varies between 7 and 10. The corresponding pattern of the most unstable three-dimensional perturbation of the temperature is similar to the experimentally observed temperature distribution. It is shown that the calculated instability is caused by the Rayleigh-Bénard mechanism which leads to the appearance of a system of convective rolls distributed along the azimuthal direction inside a relatively thin convective layer.

EXPERIMENTAL SETUP AND RESULTS

A sketch of the experimental setup is shown in Fig.1a. A cylinder (37.1 mm inner diameter by 41 mm inner height) filled with water was immersed in a thermostatic water bath held at a hot temperature and was closed on its top by a metal plate held at a cold temperature. The walls of the cylinder (side and bottom) were made of 2.1mm thick glass. Experiments were carried out at bath temperatures in the range θ_{hot} = 10°C - 25°C and top plate temperature cold, ranging from slightly below the bath temperature, viz., θ_{cold} = 20°C, down to below the freezing point, viz., θ_{cold} = -10°C. The temperature distributions at various cross-sections were measured optically by a suspension of liquid crystals. In all situations the thermal stratification resulted in a free convective flow, and for below-freezing lid temperature an ice front formed and grew downward from the top (Fig.1b). At a certain characteristic temperature difference the growing ice forms a star-like structure shown in Fig.1b. This shape of the growing ice is most likely a reflection of the azimuthal distribution of the temperature below the cold cover.

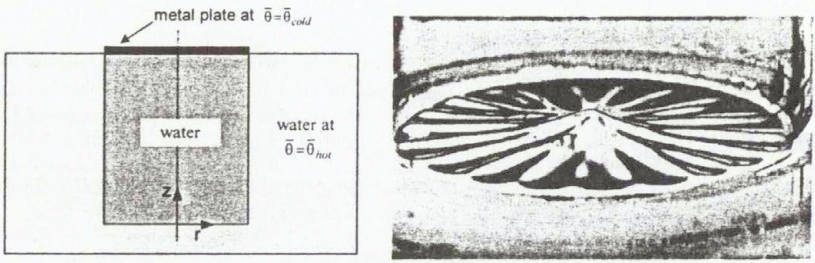

Fig.1. (a) Experimental setup; (b) Star-like structures on the freezing ice.

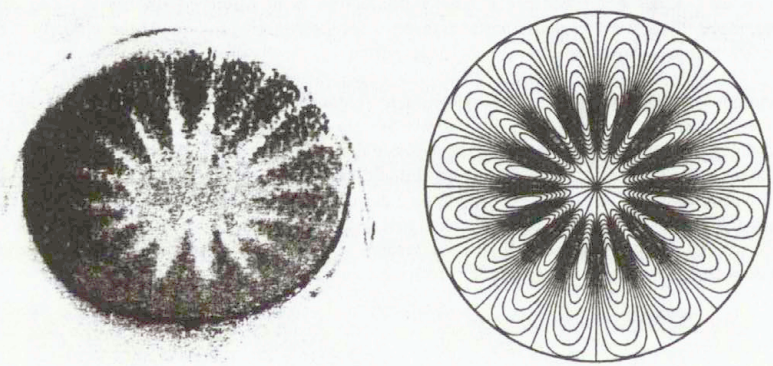

Fig.2. (a) Photograph of temperature field taken at the horizontal cross-section z=0.95H, $Gr \approx 2.5\times10^4$ (from [1]); (b) Isolines of perturbation of temperature at the cross-section $z = 0.95A$ (from[2]).

The azimuthally-periodic shape of the ice surface can be a reflection of the temperature below the cold lid. In fact, a photograph of the temperature field in the liquid water, taken slightly below the cover shows a similar azimuthal distribution of the temperature (Fig.2a). Since the system is completely axisymmetric, such a non-axisymmetric temperature distribution can result as an instability of the axisymmetric convective flow. Therefore, the main purpose of the study was to find out under which conditions such instability can set in.

FORMULATION OF THE PROBLEM

We consider a three-dimensional system of Boussinesq equations

$$\frac{\partial \mathbf{v}}{\partial t} + (\mathbf{v}\cdot\nabla)\mathbf{v} = -\nabla p + \Delta \mathbf{v} + Gr\theta \mathbf{e}_z, \qquad \nabla\cdot\mathbf{v} = 0, \qquad \frac{\partial \theta}{\partial t} + (\mathbf{v}\cdot\nabla)\theta = \frac{1}{Pr}\Delta\theta \tag{1,2,3}$$

with no-slip boundary conditions for velocity and prescribed axisymmetric temperature profiles at the boundaries. To find the distribution of the temperature at the container walls we perform a preliminary calculation, which takes into account the finite thickness of the walls [2]. The basic steady flow is axisymmetric. The stability of this flow with respect to all possible three-dimensional perturbations is studied.

Since any possible perturbation is 2π-periodic, it can be expressed in the Fourier series

$$\{\mathbf{v}, p, \theta\} = \sum_{k=-\infty}^{k=\infty} \{\mathbf{v}_k(r,z,t), p_k(r,z,t), \theta_k(r,z,t)\} exp(ik\varphi) \tag{4}$$

The liner stability problem separates for each Fourier mode such that the 3D stability problem reduces to a set of 2D-like problems (see [2] for details). These problems are treated using the global Galerkin method, formulated in [3] for axisymmetric flows. As a result we obtain the critical Grashof number $Gr_{cr}(k)$ for each azimuthal wavenumber k. The minimum of Gr_{cr} over the whole spectrum of k gives the critical Grashof number for the onset of three-dimensional flow with k-fold azimuthal symmetry.

The calculated values of the critical Grashof number Gr_{cr} for different azimuthal wavenumbers k are reported in [2]. It is shown that, independently of the boundary condition at the wall, the minimal values of the critical Grashof numbers correspond to $k = 7$, 8 and 9 and are located close to $Gr = 10^4$. An example of isolines of the perturbation of the temperature at the horizontal cross-section $z = 0.95A$ (corresponding to the location where the photograph shown in Fig.2a was taken) is shown in Fig.2b. The pattern of the perturbation in this cross-section contains 8 maxima and 8 minima and looks similar to the experimental pattern of isotherms (Fig.2a). However, there is no complete agreement with the experiment, because the dark areas in Fig.2a correspond to the minima of the temperature. Therefore one should expect the existence of 16÷18 maxima and minima in the perturbation of the temperature.

The disagreement of the experimental and numerical results can be explained if one compares the Grashof number corresponding to Fig.2a ($Gr \approx 2.5\times10^4$) with the calculated critical Grashof number ($Gr_{cr} \approx 10^4$). The experimental study was carried out at more than 100% supercriticality, where non-linear interaction of the dominant modes of the perturbation cannon be neglected. Thus, the 17 minima of the temperature, seen in Fig.2a, can be a result of non-linear interaction of modes with $k = 8$ and 9, or $k = 7$ and 10, whose critical Grashof numbers have close values. On the other hand, modes with $k = 16\div18$ also become unstable at $Gr \approx 2.5\times10^4$, and can become dominant at certain conditions.

A comparison of the dominant perturbation with the distribution of the temperature in the mean axisymmetric flow (Figs.3a and b) allows us to make some conclusions about the nature of the

instability. It is seen that an unstably stratified fluid layer is always located near the upper cold plate. The depth of the layer depends on the thermal conditions at the upper edge of the cylinder. The maximal absolute values of the perturbation of the temperature also are located near the upper plate inside the unstably stratified layer. This allows us to suppose that the observed instability is caused by a Rayleigh-Benard mechanism in the unstably stratified fluid layer.

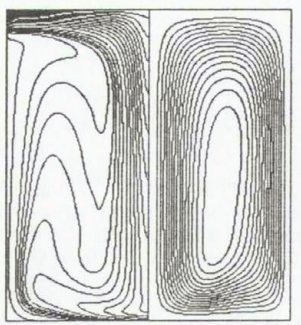

(a)

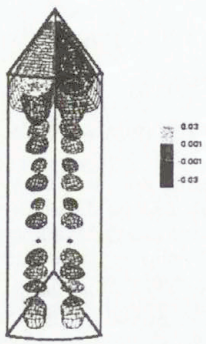

(b)

Fig.3.(a) Streamlines and isotherms of the axisymmetric flow at $Bi = 20$, $Pr = 8$, $Gr = 6770$;
(b) The corresponding three-dimensional perturbation of the temperature corresponding to $k = 9$.

CONCLUDING REMARKS

Similarly to other problems with combined convection and solidification, the described study provides an example of the decisive influence of convective flow on the resulting shape of the solidification front. The numerical approach used here allowed us to obtain the correct pattern of the three-dimensional perturbation without solution of the full 3D problem. We intend to apply this approach to other practically important problems of crystal growth.

ACKNOWLEDGMENT. This work was supported by the Israel Science Foundation under Grant 110/96, by the Center for Absorption in Science, Israel Ministry of Immigrant Absorption (to A.Gelfgat) and by the Y.Winograd Chair of Fluid Mechanics and Heat Transfer.

REFERENCES

1. Kowalewski T. A., Cybulski A.: Konwekcja Naturalna z Przemiana Fazowa (Natural Convection with Phase Change) (in Polish). *IPPT PAN Report 8/97*, Warsaw,1997.
2. Gelfgat A.Yu., Bar-Yoseph P.Z., Solan A., Kowalewski T.A.: An Axisymmetry-Breaking Instabilities of Axially Symmetric Natural Convection, *Int. J. Transport Phenomena* (to appear).
3. Gelfgat A.Yu., Bar-Yoseph, P.Z. and Solan A., Stability of Confined Swirling Flow with and Without Vortex Breakdown, *Journal of Fluid Mechanics*, Vol. 311, pp.1-36,1996.

NUMERICAL AND PHYSICAL MODELLING OF THE EFFECT OF DIFFERENT CONFIGURATIONS OF ROTATING MAGNETIC FIELDS ON HYDRODYNAMICS AND CRYSTALLIZATION FRONT IN A CYLINDRICAL VOLUME

Yu. M. Gelfgat

Institute of Physics, University of Latvia, 32 Miera Str., Salaspils-1, LV-2169, Latvia

Summary. The work presents the results of the numerical and experimental study of the influence of various configurations and combinations of rotating magnetic fields on the melt flows and the shape of the crystallization front in a cylindrical volume filled with an electrically conducting melt. The obtained data give evidence that the above mentioned versions of electromagnetic influence on the solidifying melt is an effective tool allowing active controlling of the characteristics of motion, heat and mass transfer.

The report presents the results of numerical and experimental investigations of hydrodynamic flows and their influence of on the shape of the crystallization front in cases, when an electrically conducting vessel is exposed to the impact of different rotating magnetic fields (RMF). This problem is of a considerable interest with regard to the development of active methods for controlling the characteristics of heat and mass transfer in solidifying melts in order to implement optimal conditions for crystallization in the technologies for the production of metals, alloys, semiconductor single crystals, composites, etc.

The paper considers different versions of the axially symmetric system "RMF inductor – melt-filled vessel" application, including some combinations of several RMF, which allow to significantly enhance their efficiency and make wider the range of RMF possible application. In particular, we investigated the situations, when:

- the length of the RMF inductor or that of the cylinder was unlimited;
- the length of the RMF inductor and that of the cylinder were limited;
- the inductor was arranged asymmetrically about the central plane of the cylinder over its height;
- the cylinder was enveloped by two short inductors inducting counter-rotating magnetic fields (the arrangement of these inductors along the cylinder's axis was arbitrary);
- the cylinder was enveloped by a system of inductors, one of which generates a quasi-uniform RMF, another one – an opposite non-uniform RMF (its distribution along the cylinder's radius was arbitrary).

The calculation procedure is the following: first the distribution of electric and magnetic fields in the working volume is defined, then – the distribution of electromagnetic forces. The found distribution of electromagnetic forces as an outside force is substituted into the set of hydrodynamic

equations, then the characteristics of azimuthal and meridional flows in the liquid volume are found out. Additionally, to solve the non-isothermal problem and to define the influence of RMF on the shape of the crystallization front, the equation of convective heat transfer is solved together with the crystallization heat of a solidifying melt.

An original method, which allows calculations with account for:
- finite dimensions of the inductor and the cylinder;
- the influence of frontal parts of the RMF inductor coils;
- the non-uniform distribution of magnetic induction over the cylinder's radius,

is used to calculate complicated enough distributions of electromagnetic fields and forces for the above said unusual situations. The calculations are performed following the standard procedure by the method of finite differences. A calculation grid with a non-uniform pitch is applied, if necessary.

The numerical results obtained for the distribution of electromagnetic forces, azimuthal velocities and meridional flow evidence that:
- A definite flow velocity pattern - primary azimuthal rotation and secondary meridional flows as two toroidal vortices – is driven in the melt at symmetrical arrangement of RMF inductors about the axis and the edges of the cylindrical volume with a melt and at any ratios of the diameters and lengths of the inductor and the cylinder. Herewith, the flow of the liquid in the meridional vortices at the cylinder's edges is directed from its walls to the vessel's axis, but in the central plane – from the center to the periphery.
- If the symmetry in the system "RMF inductor - melt-filled cylinder" is kept, any change of their diameter/length ratio is equivalent to increasing or decreasing of the current in the inductor's coils.
- It is possible to alter the pattern of meridional flows (not changing the flow direction) by breaking the symmetry in the system "RMF inductor - melt-filled cylinder", e.g., asymmetrical arrangement of the inductor about the cylinder's height.
- If influence the cylindrical melt-filled volume by two counter-rotating magnetic fields arranged one above another along the cylinder's height, one can alter as the velocity pattern of driven meridional flows as the direction of liquid in these flows near the cylinder's edges as well.
- A combination of two RMF having an extremely non-uniform distribution of electromagnetic forces along the radius of the cylindrical volume provides an opportunity to obtain zones with different values of azimuthal and meridional velocities in the melt. In particular, it is possible to drive a strong motion of liquid in the central zone of the vessel and to brake the flow near its solid walls or to obtain an opposite result: a strong flow near the solid walls and its absence in the central zone of the cylinder.

The results of similar calculations for non-isothermal versions of the discussed problems and the obtained distributions of isotherms in the cylindrical volume reveal the influence of different uniform, non-uniform and combined RMF on the shape of the crystallization front. These results give evidence that:
- the rotating magnetic fields can be an effective tool to control the shape of the crystallization front varying it from concave into the melt to flat and then to convex into the melt;
- when analyzing the influence of RMF on the heat transfer in the melt and on the interface shape, the presence of thermogravity flows in the melt should be considered even if these flows are not so strong;

- the variation range of heat characteristics in the melt and, relatively, the influence of the shape of the crystallization front becomes much wider, when asymmetric and combined RMF are imposed;
- the influence of different RMF on the interface shape in the solidifying melt should be analyzed considering the temperature distribution in the already solidified part of the cylindrical volume.

Special experiments have been carried out to verify the numerical methods and the obtained theoretical results. The distributions of azimuthal velocities were studied on the models with eutectic alloy InGaSn (melting temperature 10.6 °C). A conductive anemometer with its own magnetic field induced by a small steady magnet (∅ 2-3 mm) measured the velocities. In the course of measurements the conductive anemometer shifted along the axis and the radius of the cylindrical vessel filled with a liquid metal and enveloped by different systems of RMF inductors.

The experimental results obtained illustrating the distribution of azimuthal velocities were compared to the corresponding calculations performed for similar versions of RMF influence. The comparison of the numerical and experimental data has revealed their satisfactory qualitative and quantitative correlation.

The influence of different RMF on the interface shape was studied experimentally on molten tin. To mark the shape of the crystallization front, small amounts of Antimony were added the molten tin. After the sample solidified, it was cut along its longitudinal axis, and the shape of the interface at the moment of crystallization could be seen clearly indicated.

The analysis of the obtained experimental and corresponding numerical data show that the shape of the crystallization front changes under the influence of different RMF. At the optimal for definite situation parameters of electromagnetic impact the primary curved phase interface can be transformed to flat. Yet, the optimal values of the RMF characteristics vary in a rather narrow range and must be defined together with the heat characteristics in the melt and in the solidified part of the sample.

The conducted investigations allow to state that the RMF and especially their combinations can be an effective tool to control the heat and mass transfer characteristics in the solidifying melt. This also provides a possibility to intensify the convective transfer of motion, heat and mass for two regimes: for increased level of pulsations of velocity and, relatively, temperature and concentration and for sharply attenuated pulsating velocities with the increased integrated values of stirring flow velocities.

NUMERICAL SIMULATION OF THE SINGLE CRYSTAL GROWTH PROCESS

V.P. Ginkin
SSC IPPE, Bondarenko sq.1, Obninsk, Kaluga region, 249020, Russia.

There are many papers on the numerical simulation of the single crystal growth process (see, for example, [1] and all the references presented there). At the same time, there is no established notion to single out the most efficient approach or algorithm for solving this problem now. An approach developed at the Institute of Physics and Power Engineering in Obninsk is described in the paper. The approach was originally proposed within the framework of a 2D conductive-radiative heat transfer problem in [2] and was further developed in [3]-[5].

The essential features of the process simulated are its nonstationary character and the presence of phase changes. Therefore, considering the heat transfer problem, one has to solve the Stefan problem. Different approaches for solving the problem are known presently [6], each of them having its advantages and disadvantages. We develop the enthalpy approach under which the nonstationary heat transfer equation is formulated and solved in variables of enthalpy. This approach provides a stable and efficient numerical algorithm for solving the Stefan problem.

To describe the radiation heat transfer, the method of angular coefficients is used. The main difficulties here are caused by calculation of the angular coefficient matrix for irregular forms of the radiation surfaces including heat shields situated inside of cavities. The conductive heat and mass transfer is described by the Navier-Stockes equations under the Boussinesq approximation. Our approach presupposes that the Boussinesq equations are solved in the natural variables by the control volume method according to the Patankar scheme. The equations are previously transformed to exclude the convective terms and to bring them into the divergence form by a method proposed in [7].

The system of equations in enthalpy for calculational meshes in each connected combination of zones with the boundary conditions prescribed is linearized by the Newton method. The system of linear equations is solved by the conjugate direction method with preconditioning by the incomplete factorization method. The algorithm described was realized in 2D (r,z)-geometry for calculating the process of crystallization of germanium conducted by the noncrucible melting method on a device "Zona-1" under the null gravity conditions. A demonstration calculation of the process was performed. Previously, a similar calculation was performed without taking into account the influence of convection [5]. The described technique for calculating heat transfer in crystals growing from the melt has the following distinctive features:

1) heterogeneity of the domain;
2) the presence of radiation;
3) the presence of convective heat-mass transfer;
4) nonlinearity of properties, i.e. dependence of the thermophysical parameters on enthalpy;
5) nonstationarity stipulated by the time dependence of the heat generation source and the domain geometry configuration;
6) taking into account the heat of phase change;
7) validity of the model for 3D calculations;
8) possibility to increase the complexity of the model (e.g. by introduction of control magnetic field and vibration impact).

The calculational stability of the technique proposed is provided by the use of enthalpy variables in solving the heat transfer equation, by the use of natural variables and the Patankar scheme in calculation of velocities and pressures, by the use of the Newton iteration process to solve the nonlinear system, and by the use of balanced monotonic neutral finite-difference schemes to discretize the space variable and the implicit scheme to discretize the time variable.

A high efficiency of the technique is basically provided through the use of a special organization of calculations and through performing the inner iterations by the conjugate direction method with preconditioning of initial operators by the incomplete factorization method.

REFERENCES

1. Polezhaev V.I., Bune A.V., Verezub N.A., Glushko G.S., Gryaznov V.L., Dubovik K.G., Nikitin S.A., Prostomolotov A.I., Fedoseev A.I., Cherkasov S.G. *Matematicheskoe modelirovanie konvektivnogo teplomassoobmena na osnove uravnenii Navie-Stoksa.* M., Nauka, 1987, 271c.
2. Ginkin V.P., Zinin A.I., Balakin I.P. *The Method a Global Calculation of Heat Transfer in Numerical Simulation of Crystal Growth.* The Third International Seminar on Simulation of Devices and Technologies: Abstract. Obninsk, 1994, p.85.
3. Artemyev V.K., Ginkin V.P., Gusev N.V., Zinin A.I., Ozernyh I.L. *Chislennoe modelirovanie protsessov teploperenosa pri vyrashivanii kristallov metodom Bridzhmena.* III-i Minskii mezhdunarodny forum "Teplomassoobmen MMF-96": tezisy dokladov, Minsk, 1996, pp.3-6.
4. Artemyev V.K., Ginkin V.P., Ozernyh I.L. *Numerical Study of Convection Flow Influence on Dopant Distribution for Bridgman and Floating Zone Methods Under Microgravity.* The Fifth International Conference on Simulation of Devices and Technologies - ICSDT'96: Abstract. Obninsk, 1996, p.126-127.
5. Ginkin V.P., Artemyev V.K., Gusev N.V., Luhanova T.M., Ozernyh I.L., Shishulin V.P., Sviridenko I.P. *Numerical Simulation of Crystal Growth by Floating Zone Methods.* International Symposium on Advances in Computational Heat Transfer. Cesme, Izmir, Turkey, 1997.
6. Vabshievich P.N. *Chislennye metody resheniya zadach so svobodnoi granitsei.* Moskva, izd-vo MGU, 1987, 164p.
7. Buleev N.I., Timukhin G.I. *O sostavlenii raznostnykh uravnenii gidrodinamiki vyazkoi neszhimaemoi zhidkosti. Chislennye metody mekhaniki sploshnoi sredy.* SO RAN, т.3, №4, 1972, c.19-26.
8. Patankar S.V., Spalding D.B. *A Calculation Procedure for Heat, Mass and Momentum Transfer in Three- Dimensional Parabolic Flows.* J. Heat Mass Transfer. Vol.15, p.1787-1806. Pergamon Press 1972.

SOLIDIFICATION OF A PARAFFIN WITHIN A TALL ENCLOSURE

Józef Gościk
Bialystok University of Technology, Wiejska 45C, PL 15-351 Bialystok, Poland

Summary Experimental results are presented for solidification of a paraffin (cytoparaffin 52-54) within a vertical perpendicular container made of aluminium. The container is cooled at the all around sidewalls as well as from the bottom and is open at the top so the upper surface of the phase change material is bounded by thermally insulating air gap. The focus in the paper is on influence of the volume contraction on shape and geometry of the shrinkage cavity being formed during solidification. Especially, for Stefan number $0.068 < Ste < 0.745$ and superheating parameter $S_H = 0.178$, results of the series experimental runs confirmed that the shrinkage cavity is creating around axis of symmetry and is strongly dependent on cooling intensity.

INTRODUCTION

Apart from of significant achievements in the mathematical modelling of the solidification process there is still a lot of different aspects to be studied and explained. No doubt that one of them is effect of the convective flow on the solidification process intensity. More in details speaking, we still needed to explain broadly different mechanisms of the solidification kinetics referring to different levels – the microscopic as well as macroscopic. This is very important even for single component systems where the convective transfer affects solidification in many ways especially at the vicinity of the liquid – solid interface. The particular phenomena – whiskerlike (dendritic) growth into the flowing liquid phase or liquid region at the rest, influences of the convective flow induced by external forcing or internal thermal gradients (buoyancy). The flow is associated also for most of the substances with reduction in volume because of density differences. In engineering approaches the volume contraction upon solidification has been rarely included into the modelling and analysis because of two reasons. By the first of them – the flow induced by the suction at the phase change interface does not be too much intensive (being compared for example to intensity of the natural convective flow) to consider for practical purposes. The second reason seems to be connected with complexity of the phenomena. However, there are situations that show that during solidification processes the volume contraction or in another words the shrinkage formation is so important that should be taken into account.

In the presented paper it is shown that the volume contraction can play significant role upon solidification from point of view of design and analysis latent heat (solid↔liquid) thermal energy storage devices. This is very important particularly when the shrinkage cavities arising close to the heating walls can increase drastically the resistance for heat transfer. The series experimental runs are presented that confirm important influence of the difference. The most spectacular is to present a shape and geometry of the shrinkage cavity forming during solidification of a cytoparaffin 52-54 as a phase change material within a tall rectangular container.

EXPERIMENTS

It should be mentioned that the demonstrated samples were not prepared especially for phenomena considered. They were registered when experimentally tried to obtain homogenous solid core of material in form of the perpendicular block.

A paraffin of technical quality, (less than 0.7% oil impurities) has been chosen as the phase change material, because of its very promising properties for heat storing in the latent storage equipment.

Due to limited access to the material properties series of measurements determining temperature and energy effect of the phase change preceded principal experimental works. The measurements were carried out using differential scanning calorimeter (the measurements were independently performed on two different DSC's). It has been found from the measurements that the cytoparaffin does have phase change temperature $\Delta\theta^*$ ranged within 52÷54 °C and phase change energy effect $\Delta h^* = 155$ kJ/kg. Based on the results the material analysed can be qualified as a raffinated paraffin, which remain thermophysical properties can be taken from commonly available literature. Consequently, thermal properties given by Bardon et.al.[1] have been used in further considerations, e.g.: thermal conductivity [W/m·deg] of solid λ_1 = 0.270 and liquid λ_2 = 0.163; specific heat [kJ/kg·deg] of solid c_1 = 3.5 and liquid c_2 = 2.3; density [kg/m^3] of solid ρ_1 = 956.0 and liquid ρ_2 = 818.0.

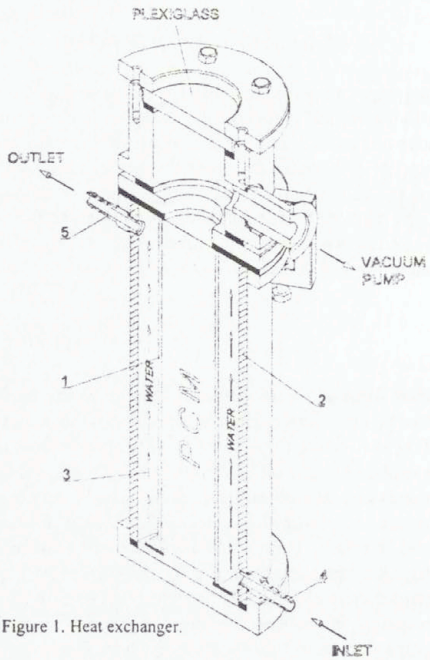

Figure 1. Heat exchanger.

Heat transfer apparatus

The experimental study of the solidification process has been performed in a special designed device[2], which is schematically shown in the Figure 1. In particulars, the device is a kind of small shell-and-tube heat exchanger forming on the tube side of a perpendicular container (1) for paraffin which is 240 mm height, width 45 mm and depth 45 mm (aspect ratio defined as height/width A ≅ 6.0). The container is immersed in cylinder (2) of 80 mm inner diameter. On the shell side of the exchanger there is some space (3) between container and external cylinder. It forms the water channel, which through the nozzle (4) and (5) is connected to water circulating system supplied by two thermostatic baths. In this way the initially temperature was carefully controlled and adjusted at the desired level of temperature above the fusion temperature of paraffin.

Experimental procedure

Before starting the experiment, the constant temperature bath was stabilised to a particular temperature slightly above the fusion point. Then the container was filled with liquid paraffin taking care to insure minimum air traps inside. Then, the paraffin filling the heat exchanger was allowed to remain at a desired temperature (here mostly at $\theta_o = \theta_H = 65^oC$) for five hours before the solidification started. At the same time, the temperature of the cooling water was stabilised in the second constant temperature bath. Then as a start for each solidification experiments was the switching between circulation loops – heated at the temperature $\theta_H > \theta^*$ and cooled at the temperature $\theta_C < \theta^*$. For each experimental run the same time period for solidification lasted five hours.

The experimental device has been designed with special emphasis on convenient disassembling, particularly on easy acces to withdraw the container filled up by the solidified core of the paraffin. Owing to such design the container could be easily withdraw after each experimental run from the heat exchanger and then by temporarily heated in the bath at temperature above the fusion point to draw the solidified core out of the container. Afterwards, the solidified core by cutting layer–by–layer of the material and removing it out to disclose plane of symmetry of the perpendicular block was prepared to shoot photographs. Outlined shape of the shrinkage cavity was recorded after preparatory stage which consists of: firstly - covering all of the exposed surface by matt paint, secondly – removing dried, thin layer of the paint only from the surface all over of the plane of symmetry. In this way at the region where volume contracts and which is concave with respect to the cutting plane, the paint still left clearly demonstrating shape the shrinkage cavity.

RESULTS AND CONCLUDING REMARKS

In general, assuming that the thermophysical properties are constant but may be different for liquid and solid phases, the problem under consideration is governed by following dimensionless parameters: the Rayleigh number Ra, Prandtl number Pr, Stefan number Ste ($=c_1\cdot(\bar{\theta}^*-\theta_C)/\Delta h^*$, where $\bar{\theta}^*$ stands for average of the phase change temperature), superheating parameter S_H ($=c_2\cdot(\theta_H-\bar{\theta}^*)/\Delta h^*$), the container aspect ratio A as well as property ratios $\hat{a} = a_1/a_2$, $\hat{\lambda} = \lambda_1/\lambda_2$, $\hat{\rho} = \rho_1/\rho_2$, where subsequently subscript 1 refers to solid and subscript 2 refers to liquid. A number of solidification experiments has been performed, but all of the reported experimental runs were made for the same level of superheating $S_H = 0.178$, which corresponds initial temperature $\theta_o = \theta_H = 65^\circ C$.

The results are presented in Figure 2 - with the emphasis on the final state. The solid core and shrinkage cavity are represented as a distinct shadowed regions. Original pictures were grabbed as colour ones (in a format of 24 bit RGB) and than without any manipulation transformed to the monochromatic picture (in a format 8 bit unsigned). The first trials of solidification were carried out keeping the cooling temperature at 20 °C. Further results, obtained according the same procedure with increasing temperature of the cooling water θ_C from 20°C to 45°C by 5°C showed insignificant effect on shape and form of the shrinkage cavity which was similar to that at Fig. 2a. As far as 45°C of the cooling temperature the samples were prepared increasing the θ_C by 1°C. At $\theta_C = 48^\circ C$ the shrinkage cavity changed its shape to be in form as in Fig. 2b. Further increasing of the cooling temperature and thus decreasing of the cooling rate resulted in also decreasing in the depth of the shrinkage cavity (see in Fig. 2c). Fig. 2d corresponds to $\theta_C = 50^\circ C$ than very close to lower limit of the temperature phase change region.

The results collected showed that the density difference essentially affects geometry of the solid core especially at regions around axis of symmetry. The conclusion based on the study is self-evident. When the problem of mathematical modelling as well as materials are as considered in the study the volume contraction should be taken into account. It is also clear that engineering design of a real heat storing unit should asserts such the working conditions in practice to carry out the destoring cycle with reasonable low cooling intensity. Finally, it is also worth to emphasise that the results presented refer to fully 3D conditions very close corresponding to solidification process occurring in practice. Such the feature undoubtedly distinguish the work presented when compared to the others published which were concerned with the solidification in somewhat analogous configurations, for example experiments performed by Ho and Viskanta[3] and numerical simulations by Kim and Ro[4], where the results for open rectangular containers with aspect ratios A = 0.5 and 1.0 are presented. However, the objects investigated were specially adjusted to the experimental technique requirements, i.e.

visualisation of the process evolution bearing the main assumption that the third dimension (depth) has no influence on the process considered.

Fig. 2a) θ_C=45°C, Ste = 0.181, S_H = 0.178;

Fig. 2b) θ_C=48°C, Ste = 0.113, S_H = 0.178;

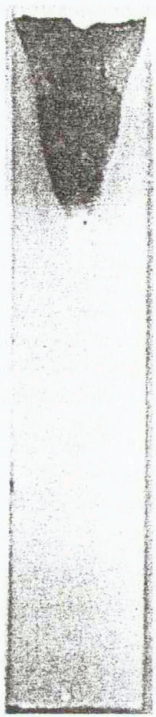

Fig. 2c) θ_C=49°C, Ste = 0.090, S_H = 0.178;

Fig. 2d) θ_C=50°C, Ste = 0.0678, S_H = 0.178.

REFERENCES

1. Bardon J.P., Vrignaud E., Delaunay D. Etude experimentale de la fusion et de la solidification periodique d une plaque paraffine, Rev. Gen. Therm., Fr., No. 212-213, 1979, pp. 501-510.
2. Gościk J., Jarmocik A. Design of a device for solidification paraffin in a form of perpendicular blocks. Version 1. Bialystok University of Technology. Internal report KTiMP PB Nr 4/97 (in Polish)
3. Ho C.J., Viskanta R. Experimental study of solidification heat transfer in an open rectangular cavity. Journal of Heat Transfer, Vol. 105, No. 3, 1983, pp. 671-673.
4. Kim C.-J., Ro S.T. Shrinkage formation during the solidification process in an open rectangular cavity. Journal of Heat Transfer, Vol. 115, No. 4, 1993, pp. 1078-1081.

This work has been done under the research contract KBN No 8 T10B 005 11

STRESS PROBLEMS IN LIQUID BRIDGE THERMOCAPILLARY CONVECTION: A NUMERICAL APPROACH.

Guillaume Kasperski & Gérard Labrosse

LIMSI-CNRS, UPR 3251, Université Paris-Sud XI, BP 133, 91402 Orsay Cedex France

Axisymmetric thermocapillary convection is computed in a liquid bridge, held between two cylindrical isothermal rods and laterally heated. Geometrical simplifications lead to a rectangular computational domain. Flow fields and spatial derivatives are estimated by a Chebyshev collocation method and the conservation equations are solved by a projection-diffusion algorithm. To avoid mathematical singularities on the axial velocity boundary conditions, the thermocapillary stress is weighted by a regularising function, which cancels at the junctions of the free surface and the solid rods. The shape of this function, particularly the characteristic length scale of the filtering, can be controlled by the experimentalist and may depend on the temperature profile at the free surface.

The role of the Prandtl number, characteristic of the considered fluid, on the flow regimes has been studied for a particular, smooth, filtering of the thermocapillary stress. Increasing the control parameter of the convection, the Marangoni number, high-Pr flows keep a diffusive nature, as low-Pr flows become rapidly convective. They respectively undergo hydrothermal and hydrodynamical transitions to unsteadiness. The discussion will be lead on the role of the filter shape, on which thermally convective flows seem to be very dependent, leading to expensive computationnal investigations. The results could be partly relevant for fluid phenomena occurring in floating zone crystal growth processes.

CONTRIBUTION TO OPTIMIZATION OF CONTINUOUS CASTING OF STEEL SEMIPRODUCTS

František Kavička*, Karel Stránský *, Josef Štětina*, Pavel Ramík*, Bohumil Sekanina*, Věra Dobrovská**, Jana Dobrovská**

* *Technical University, FME, Technická 2, 616 69 Brno, Czech Republic*

** *Technical University-VŠB, Tř. 17. Listopadu, 708 33 Ostrava, Czech Republic*

Summary This process can be described by the Fourier or the Fourier-Kirchhoff equations, which can not be solved exactly. An original three-dimensional (3D) numerical model (the first of the two) of a CCM temperature field had been assembled. This model is able to simulate the temperature field of a CCM as a whole, or any of its parts. Simultaneously, together with the numerical computation, the experimental research and measuring have to take place not only to be confronted with the numerical model, but also to make it more accurate in the course of the process.
The second original numerical model for dendritic segregation of elements assesses critical points of blanks from the viewpoint of their increased susceptibility to crack and fissure. In order to apply this model, it is necessary to analyze the heterogeneity of samples of the constituent elements (Mn, Si and others) and impurities (P, S and others) in characteristic places of the solidifying blank. The numerical model, based on measurement results obtained by an electron micro-probe, generates distribution curves showing the dendritic segregation of the analyzed element, together with the distribution coefficients of the elements between the liquid and solid states. Both models will be used for optimization of concasting technology.

A NUMERICAL MODEL OF THE TEMPERATURE FIELD

We are presenting the first results of a numerical solution. Final program will have the following properties: it will solve non-stationary temperature field of continuously casted blanks and of a crystallizer as a non-linear task, it will simulate CCM as a whole or any of its parts, it will solve current thermo-kinetic problems in general and in details.

The tree-dimensional unsteady temperature field of a blank passing through a device for continuous casting (through the zones of primary, secondary, and tertiary cooling) in a direction of a z axis by a rate is described by the Fourier-Kirchhoff equation (1). The equation must be adapted in such a way so that it would describe the temperature field of the blank in its all three phases: in a melt, in a cooling interval, and in a solid phase. Therefore the specific volume enthalpy dependent on temperature is introduced, $i_v = c_v T$ [J.m^{-3}]. The specific volume heat capacity c_v and conductivity k are the function of temperature, too. Figure gives an example of a cross-section through the crystallizer - the zone of primary cooling.

$$c_v\left(\frac{\partial T}{\partial t} + w_z \frac{\partial T}{\partial z}\right) = \frac{\partial}{\partial x}\left(k\frac{\partial T}{\partial x}\right) + \frac{\partial}{\partial y}\left(k\frac{\partial T}{\partial x}\right) + \frac{\partial T}{\partial z}\left(k\frac{\partial T}{\partial z}\right) \qquad (1)$$

The functional relationship $i_v = f(T)$ must be determined for the given material of the blank. If the calculation node is on the boundary of the system and the environs or on the interface of the

individual system bodies, then the respective unitary heat conductivity must characterise the limit condition. The limit condition on the interface of the blank - the crystallizer depends on the thermophysical properties and on the state of parting powder and on the space form too, and on the interface of the crystallizer - the steel frame it depends on the both surface treatment quality. In the limit condition on the upper and the lower base of the crystallizer, on the frame wall, and on the blank surfaces after its exit from the crystallizer the influence of the convection (natural or forced under the nozzles) and the influence of radiation are included. The effect of the cooling tubes passing through the crystallizer wall is simulated in the model by the so called heat drop. But the analysis of the limit conditions definition is not a matter of this article. After running on the steady state the derivative of the temperature or enthalpy according to time in the equations and is zero. The thermophysical properties of the steel blank, of the copper crystallizer, and of the steel frame were available.

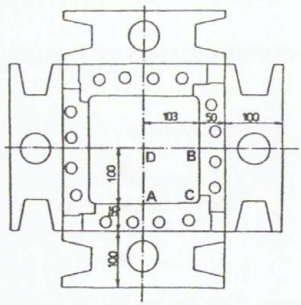

Figure 1. The cross-section through the crystallizer for radial pouring of continuous casting of 200x200 mm

The choice of the solution limit conditions was adapted to this experimental information, and namely in several precisionings. Figure shows e.g. the temperature field of the blank, of the crystallizer, and of the frame in a cross section led in a half of the crystallizer height. To this temperature field corresponds the mean value of heat transfer from the blank to the working wall of the crystallizer.

The calculated temperature field of the basic variant is real and it served to the analysis of the influence of the blank shift rate as a comparative variant. It was found out that the temperature fields of another variants of the rate choice are convenient for technical practice if the coefficient of heat transfer are proportionate to the change of the rates. In addition the same condition were analysed by calculation with the difference that in the first and in the second section the spraying is not applied so that h_N (natural) will characterise the natural heat transfer from the blank surface (including convection and radiation, too) in accord with the limit condition in the tertiary cooling zone after exit from the zone of secondary cooling for each variant. The spraying on the opposite walls of the blank is the same, therefore the temperature field is symmetrical by a diagonal of the cross section and it is sufficient to solve the one quadrant of the system only.

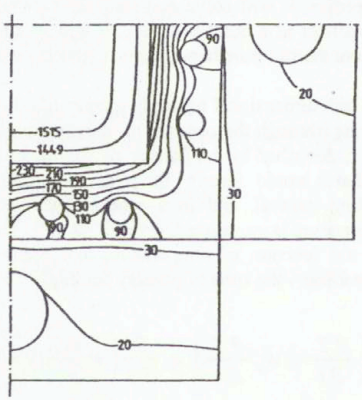

Figure 2. The calculated temperature field in the blank, the crystallizer and in the frame in a cross-section led

Comparison of the calculated temperature fields of individual variants of the limit conditions choice mutually and with the basic variant can be demonstrated by the isotherms course in the cross and longitudinal sections through the blank and by the source of

temperature curves of the characteristic corner points A, B, C, and D of the cross section in dependence on the depth under the melt level in the crystallizer.

DENDRITIC SEGREGATION OF ELEMENTS

In the course of continuously cast steel solidification in a crystalizer, some chemical heterogeneities originate, i.e. the chemical heterogeneity of individual elements, as these elements both constitutive and attendant as well as additions, segregate [1]. This liquation, or also segregation, is realized in microvolumes, so we speak about a microsegregation, which is a term identical to that of a dendrite segregation of steel, as the steels solidify always in a dendrite way. But under specific conditions of crystallization, the differences in chemical composition in macrovolumes also take place, so we can speak by analogy about a macrosegregation. The study of a microsegregation, i.e. of a dendritic segregation in the main, and a chemical heterogeneity of elements connected with it, is a base needed for the knowledge and explanation of differences in the chemical composition of steel both microscopic and macroscopic size.

At the same work an original method of the quantitative evaluation of chemical heterogeneity through their distribution curves of a dendritic segregation as well as an original determination method of effective distribution coefficients of these elements has been applied. To determine a chemical heterogeneity of continuously cast carbon steel slab, a slab of 1530x250 mm size was poured in VÍTKOVICE Metallurgical Works. The chemical composition in wt.% of the slab steel from which the samples for the measurement of a chemical heterogeneity has been taken off, is following: 0,11 C, 0,49 Mn, 0,27 Si, 0,019 P, 0,009 S, 0,07 Cr, 0,04 Ni, 0,01 Mo, 0,01 V and 0,01 Ti. The samples for the determination of a chemical heterogeneity and structure were taken from the slab off based on the scheme in the figure.

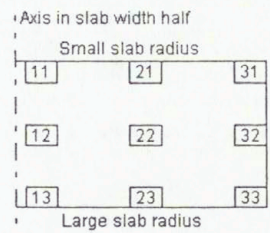

Figure 3. Scheme of taking slab samples off and their marking

From the samples figure the special metallographic samples have been prepared and the line segment of 1 mm length has been selected for the measurement in every metallographic sample then. To determine a concentration distribution of elements, an microanalytical complex JEOL JXA 8600/KEVEX Delta V Sesame has been applied by means of energy-dispersed point X-ray microanalysis method. The concentration of Al, Si, P, S, Ti, Cr, Mn and Fe was measured in the selected line segment in 101 points. The distance among measured points was 10 μm.

From the measured concentrations data of elements the basic statistical parameters (c_{st} - arithmetic mean, s_{n-1} - standard deviation and others) have been estimated and using the process described in the works, the values of effective distribution coefficients k_x have been calculated. Furthermore the indexes of heterogeneity $I_H=s_{n-1}/c_{st}$ for each element and each sample have been estimated. This results are completely described in the work.

It was estimated, that the main values of chemical heterogeneity indexes I_H of elements in slab are decreasing in the range: Al (0,858), P (0,492), S (0,421), Ti (0,329), Cr (0,269), Si (0,251), Mn (0,167) and Fe (0,00139). The maximal microheterogeneity index has aluminium, and the minimal microheterogeneity indexes have manganium and iron. The differences of the microheterogeneity indexes of individual elements among samples in slab (see fig.3) are statistically insignificant.

The main values of the effective distribution coefficients k_x of elements in slab are increasing in the range: Al (0,470), P (0,651), S (0,709), Ti (0,750), Cr (0,791), Si (0,806), Mn (0,866) and Fe (1,00125). We can see, the minimal values of k_x has aluminium and the maximal one has iron. The differences of the effective distribution coefficients of individual elements among samples in slab are also statistically insignificant. The dependence between microheterogeneity index and distribution coefficient of individual elements can be expressed analytically through the equation

$$I_H = 0{,}005534 - 1{,}134.\ln(k_x) \qquad (2)$$

in which the correlation coefficient r = 1,00, is very statistically significant.

CONCLUSION

The numerical model must also be applicable to solving other individual thermokinetical problems like: oscillations of the crystallizer and their amplitude or frequency, different ways of cooling the crystallizer, non-traditional methods included, choosing and considering the influence of the bevel of crystallizer working surface (a very modern problem nowadays), optimization of the choice of casting powders and their influence on the surface quality of a blank, problems with the contact sow- casting powder-crystallizer including the prediction of the effect of casting powders on the formation of gap at this interface, prediction of the position of the apex of solidification cone in cross and lengthwise sections, the optimization of the feed speed of a blank according to a given intensity of cooling in individual ECC zones or the optimization of both the method and intensity of cooling at a given feed speed, etc. It is assumed, that the model of dendritic segregation will enable to evaluate in advance the critical points of slabs from the viewpoint of their increased predisposition to form cracks.

This publication is based on work sponsored by the GA ČR Project No.106/98/0296, by the EUREKA Project No.1867 CONMOD, by the COST-Action P3 Project No.P3.20 and by the KONTAKT No. ME 380

REFERENCES

1. Chvorinov, N.: Crystallization and inhomogeneity of steel. NČSAV, Praha 1954
2. Dobrovská, V. - Dobrovská, J. - Rek, A. - Stránský, K.: Prediction of distribution curves of dendrite segregation. Kovové Mater., 33, 1995, No 1, pp.8-
3. Dobrovská, J. - Dobrovská, V. - Rek, A. - Stránský, K.: In: Diffusion and thermodynamics of materials. ÚFM AVČR, Tři Studně, 1998, pp.29-32.
4. Rek, A.-Stránský, K.: The heterogeneity of continuously casting slab. Research report. VTÚO Brno, 1998
5. Kavička F.-Hloušek J.-Štětina J.: Analysis of the effect of thermodynamic properties and boundary conditions on the calculation accuracy of solidification thermokinetics, The 62th World Foundry Congres, Philadelphia, 1996.

LIQUID-VAPOUR TRAVELLING WAVES BY A KINETIC MODEL OF VAN DER WAALS FLUIDS

Bogdan Kaźmierczak*, Kazimierz Piechór**

*Polish Academy of Sciences, IPPT PAN, Świętokrzyska 21, PL 00-049 Warszawa, Poland,

**Pedagogical University of Bydgoszcz, Dept. of Environmental Mechanics Chodkiewicza 30, PL 85-064 Bydgoszcz, Poland, also Polish Academy of Sciences, IPPT PAN, Świętokrzyska 21, PL 00-049 Warszawa, Poland.

1 INTRODUCTION

The transition zone separating the liquid and vapour phases is very narrow and the gradients of the flow parameters are very large. Hence, the flow is very non-uniform with a strong heat and mass transfer. Therefore a kinetic theory approach to such types of flows seems to be the most suitable one. As the medium can be very dense, every kinetic equation has to take into account the following fundamental phenomena

1. the finite size of the molecules;
2. the strong correlation between interacting molecules;
3. the attractive forces with which the molecules interact and which "keep the molecules together" when in the liquid state.

These three conditions are satisfied by a model proposed by Grmela[1,2] and called by him the Enskog-Vlasov equation. In his model, the intermolecular potential is split into a hard-core and an attractive tail. The hard-core is treated as in the standard or revised Enskog equation, whereas the tail enters the equation only linearly in a mean-field term.

Unfortunately, the Enskog-Vlasov equation is too complicated for a study of any flow. That is why we constructed such a mathematical model of this equation in which the molecular velocity space is not all R^3, but a set of four, fixed in advance, two-dimensional vectors.

Although, from the physical point of view this model is very simple, mathematically it is quite complicated. We look for travelling wave solutions to these simplified versions. We introduce a simplified model and present some numerical results concerning the hydrodynamic and kinetic shock wave structures paying special attention to the impending shock splitting. We show numerically that kinetic effects alone are unable to kill the artificial phenomenon of impending shock splitting.

2 THE MODEL

We consider the plane 4-velocity model of the Enskog-Vlasov equation as a system of evolution equations for the probability density functions $N_i = N_i(\boldsymbol{r}, t)$, $i = 1,2,3,4$, $t \in [0,\infty)$, $\boldsymbol{r} = (x,y) \in R^2$ of the particles of the „gas" travelling with the velocities $\boldsymbol{c}_i$: $\boldsymbol{c}_1 = (1,0) = -\boldsymbol{c}_3$, $\boldsymbol{c}_2 = (0,1) = -\boldsymbol{c}_4$

$$\left(\frac{\partial}{\partial t} + \boldsymbol{c}_i \cdot \frac{\partial}{\partial \boldsymbol{r}}\right) N_i = \frac{1}{\varepsilon} E_i(N,\varepsilon) + F_i, \tag{2.1}$$

where $E_i(N,\varepsilon)$, $i = 1,2,3,4$, model the Enskog collision operator, and ε is the Knudsen number. We omit the rather complicated expressions for E_i since they can be found in the paper by Piechór[3] F_i's represent terms containing the attractive tail.

The problem we want to consider consists in a study of propagation of plane non-linear waves, what admits the introduction of a few simplifying assumptions. They are:

- the flow is in the direction of the molecular velocity $c_1 = (1,0)$;
- all densities N_i depend on time t and one position variable x measured in the direction of c_1, and do not depend on the other position variable y measured in the direction perpendicular to this vector
- the flow is symmetric with respect to the x-axis, what results in $N_4(t, x) = N_2(t, x)$.

Under these simplifying assumptions, the equations of our model cease to be so complicated and take the following form[3]. To simplify further the equations we expand the integrals in power series in ε. In this way we obtain a system of three purely differential equations which, when written in the Lagrangian co-ordinates, read

$$\frac{\partial}{\partial t} w - \frac{\partial}{\partial X} u = 0, \tag{2.2}$$

$$\frac{\partial}{\partial t} u + \frac{\partial}{\partial X}\left[p(w,u) + \frac{1}{2}q\right] = \varepsilon \frac{\partial}{\partial X}\left(\frac{b^2\rho(w)}{4w^3}\frac{\partial}{\partial X}u\right) + A\varepsilon^2 \frac{\partial}{\partial X}\left[\frac{5}{w^6}\left(\frac{\partial}{\partial X}w\right)^2 - \frac{2}{w^5}\frac{\partial^2}{\partial X^2}w\right], \tag{2.3}$$

and

$$w\frac{\partial}{\partial t}q - 2u\frac{\partial}{\partial X}q + \frac{1-u^2}{w}\frac{\partial}{\partial X}u = -\frac{4\rho(w)}{\varepsilon}q, \tag{2.4}$$

where X is the Lagrange mass co-ordinate, and $n = N_1 + 2N_2 + N_3$ is the number density, $nu = N_1 - N_3$ defines the mean velocity, and $nq = N_1N_3 - N_2^2$. In the above equations: $p(w,u)$ is the pressure, $b>0$ is a constant characterizing the close packing density, $A>0$ is a constant characterizing the capillarity-to-viscosity effects, $w = 1/n$ is the specific volume, finally $\rho = \rho(w)$ represents the pair correlation function.

The pressure in our model is given by the following formula

$$p = p(w,u) = \frac{1-u^2}{2w}\left(1 + \frac{b}{w}\rho(w)\right) - \frac{a}{w^2}. \tag{2.5}$$

If we take $\rho = \frac{w}{w-b}$ and denote $T = \frac{1-u^2}{2}$ then (2.5) takes the form of the van der Waals equation of state, if T is interpreted as the temperature. From now on we assume that $\rho(w)$ is given by this formula.

Hydrodynamic approximation

From Eq.(2.4) we obtain easily the following approximate formula

$$q = -\varepsilon \frac{1-u^2}{4w\rho(w)}\frac{\partial u}{\partial X}.$$

Using it in Eq.(2.3) we obtain a system of two equations for two physical quantities the specific volume w and the flow velocity u. These equations read

$$\frac{\partial}{\partial t} w - \frac{\partial}{\partial X} u = 0, \tag{2.6}$$

$$\frac{\partial}{\partial t} u + \frac{\partial}{\partial X}\left[\frac{1-u^2}{2w}\left(1+\frac{b}{w}\rho\right) - \frac{a}{w^2}\right] = \varepsilon \frac{\partial}{\partial X}\left(\mu \frac{\partial}{\partial X} u\right) + A\varepsilon^2 \frac{\partial}{\partial X}\left[\frac{5}{w^6}\left(\frac{\partial}{\partial X} w\right)^2 - \frac{2}{w^5}\frac{\partial^2}{\partial X^2} w\right], \tag{2.7}$$

where

$$\mu = \mu(w,u) = \frac{w^2\left(1-u^2\right) + 2b^2\rho^2}{8w^3\rho} \tag{2.8}$$

is the coefficient of viscosity.

3 THE TRAVELLING WAVE PROBLEM

Travelling waves in the kinetic model

A travelling wave solution to the kinetic equations (2.2)-(2.4) is a solution of the form

$$(w,u,q)(t,X) = (w,u,q)(\xi), \quad \xi = \frac{X - st}{\varepsilon} \in R^1, \tag{3.1}$$

where s = const is the wave-speed, such that

$$\lim_{\xi\to-\infty}(w,u,q) = (w_l,u_l,0), \qquad \lim_{\xi\to+\infty}(w,u,q) = (w_r,u_r,0), \tag{3.2}$$

$$\lim_{\xi\to\pm\infty}(\dot{w},\dot{u},q) = (0,0,0), \qquad \lim_{\xi\to\pm\infty}(\ddot{w},\ddot{u}) = (0,0), \tag{3.3}$$

where the dot above a character means differentiation with respect to ξ.
Now, we act in a very standard way. Namely, we substitute (3.1) into Eqs.(2.2)-(2.4), perform one integration with respect to ξ, and use the limit conditions (3.2)-(3.3). As the result we find the velocity u is given by

$$u = u_l - s(w - w_l), \tag{3.4}$$

whereas w is coupled to q through the following system of ordinary differential equations

$$\alpha\left[\frac{2\ddot{w}}{w^5} - \frac{5\dot{w}^2}{w^6}\right] + \frac{sb^2\rho(w)}{4w^3}\dot{w} + f(w;w_l,u_l,s) + \frac{1}{2}q = 0, \tag{3.5}$$

$$\left[2(u_l + sw_l) - sw\right]\dot{q} + s\frac{1-(u_l - s(w-w_l))^2}{w}\dot{w} - 4\rho(w)q = 0, \tag{3.6}$$

where

$$f(w; w_l, u_l, s) = s^2(w - w_l) + p(w, u_l - s(w - w_l)) - p(w_l, u_l) \tag{3.7}$$

The limit conditions for the solutions of this system are

Travelling waves in the hydrodynamic approximation

The travelling wave solutions to the capillarity equations (2.6), (2.7) are defined similarly to the travelling wave solution of the kinetic equations, only the third component in (3.1)-(3.3) referring to q is missing. Also, a procedure like that described in the first part of the present section yields equation (3.4) and the equation for $w(\xi)$:

$$\alpha\left[\frac{2\ddot{w}}{w^5} - \frac{5\dot{w}^2}{w^6}\right] + s\mu(w; w_l, u_l, s)\dot{w} + f(w; w_l, u_l, s) = 0, \tag{3.8}$$

where $f(w;w_l,u_l,s)$ is the same as previously, and $\mu(w;w_l,u_l,s) = \mu(w,u_l-s(w-w_l))$, with $\mu(w,u)$ given by (2.8). The limit conditions for Eq.(3.8) are

$$\lim_{\xi\to-\infty} w = w_l, \quad \lim_{\xi\to+\infty} w = w_r, \quad \lim_{\xi\to\pm\infty}(\dot{w}, \ddot{w}) = (0,0) \tag{3.9}$$

States of rest

The state (w_0, q_0) is called state of rest if it nullifies the right hand side of Eqs.(3.5), (3.6). We check easily that $q_0 = 0$, and w_0 is a solution of

$$f(w_0; w_l, u_l, s) = 0, \tag{3.10}$$

The fundamental question which now arises concerns the number of solutions of Eq.(3.10). In general it can have either two or four different solutions. In the first case they are $w_0 = w_l$, and $w_0 = w_r$, in the second case of four solutions we have two other states of rest in addition to the asymptotic ones w_l and w_r. In this paper we consider the case when Eq.(3.10) has two solutions only.

4 A SIMPLIFIED MODEL[4]

The model kinetic equations (2.2)-(2.4) as well as their hydrodynamic limit equations (2.6),(2.7) contain dissipation and dispersion terms which can be viewed as unnecessarily complicated for qualitative considerations. That is why we present a simplified version of the model, and believe that it correctly reflects the qualitative features of the original one.

We leave the mass conservation equation (2.2) unchanged

$$\frac{\partial}{\partial t}w-\frac{\partial}{\partial X}u=0. \tag{4.1}$$

Also we do not change the left-hand side of Eq. (2.3), but we simplify the right hand side of it and, instead of (2.3), we take

$$\frac{\partial}{\partial t}u+\frac{\partial}{\partial X}\left[\frac{1-u^2}{2w}\left(1+\frac{b}{w}\rho\right)-\frac{a}{w^2}+\frac{1}{2}q\right]=\varepsilon\beta b^2\frac{\partial^2}{\partial X^2}u-\alpha\varepsilon^2\frac{\partial^3}{\partial X^3}w, \tag{4.2}$$

where α, ε and ρ are the same as previously, and $\beta>0$ is a constant. Finally we replace Eq.(2.4) by the following one

$$w\frac{\partial}{\partial t}q-u\frac{\partial}{\partial X}q+\gamma\frac{\partial}{\partial X}u=-\frac{\chi}{\varepsilon}q, \tag{4.3}$$

where γ, χ are constants of the same sign. Assuming $\gamma = O(1)$, $\chi = O(1)$ as $\varepsilon \to 0$ we obtain from the last equation

$$q=-\varepsilon\frac{\gamma}{\chi}\frac{\partial u}{\partial X}u+O\left(\varepsilon^2\right)$$

Using this in (4.2) we obtain an approximate system of two equations called the simplified capillarity equations. They read

$$\frac{\partial}{\partial t}w-\frac{\partial}{\partial X}u=0. \tag{4.4}$$

and

$$\frac{\partial}{\partial t}u+\frac{\partial}{\partial X}\left[\frac{1-u^2}{2w}\left(1+\frac{b}{w}\rho\right)-\frac{a}{w^2}\right]=\varepsilon\mu\frac{\partial^2}{\partial X^2}u-\alpha\varepsilon^2\frac{\partial^3}{\partial X^3}w, \tag{4.5}$$

where μ is the coefficient of viscosity now given by

$$\mu=\frac{\gamma}{2\chi}+\beta\ b^2=const.>0. \tag{4.6}$$

The travelling wave solutions to (4.1)-(4.3) are defined by (3.1)-(3.5). Consequently, Eq.(3.6) is also satisfied in the present case, and w is coupled to q through the following system of ordinary differential equation

$$\begin{aligned}&\alpha\ \dddot{w}+\beta\ sb^2\dot{w}+f\left(w;w_l,u_l,s\right)+\frac{1}{2}q=0,\\ &q+\frac{s\gamma}{u_l+sw_l}\dot{w}-\frac{\chi}{u_l+sw_l}q=0,\end{aligned} \tag{4.6}$$

where $f\left(w;w_l,u_l,s\right)$ is given by (3.7). Of course, we are interested in those solutions to Eqs.(4.6) which satisfy the limit conditions (3.2), (3.3).
We define

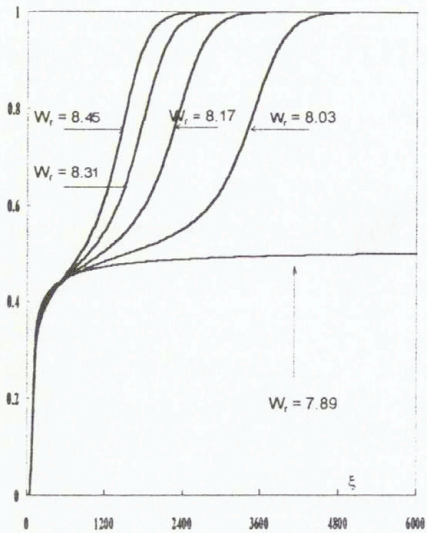

Fig. 1 Capillarity shock waves for α =1.

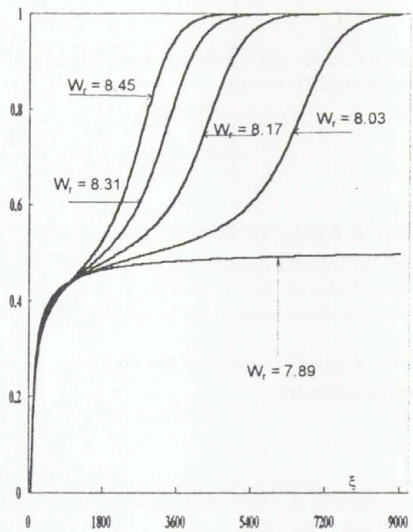

Fig. 2 Kinetic shock waves for α = 1

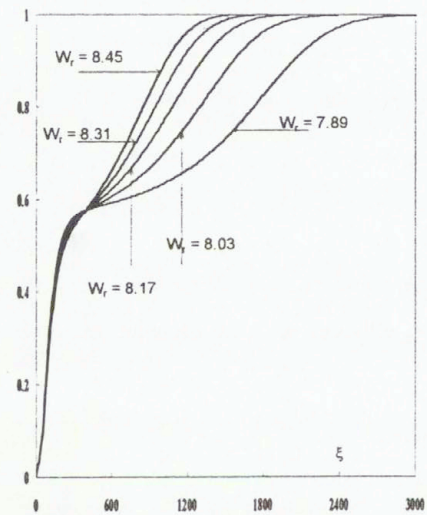

Fig. 3 Capillarity shock waves for α = 5.

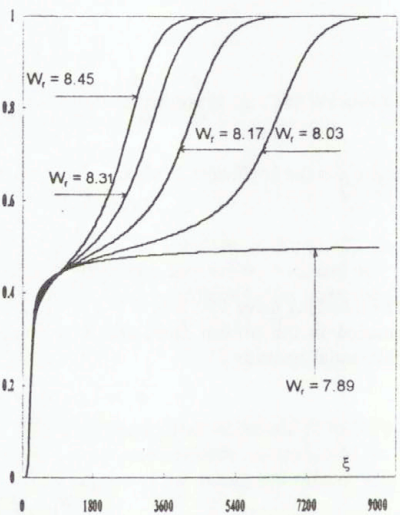

Fig. 4 Kinetic shock wave for α =5.

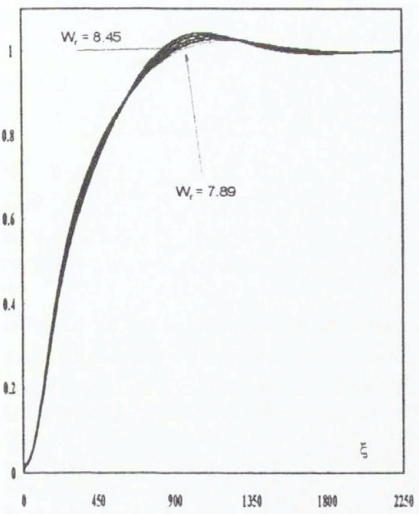

Fig.5 Capillarity shock waves for α =15.

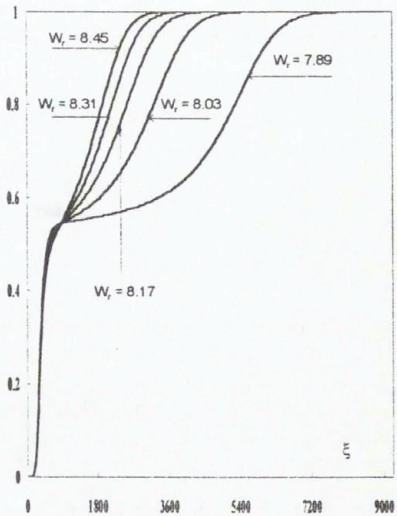

Fig.6 Kinetic shock waves for α =15.

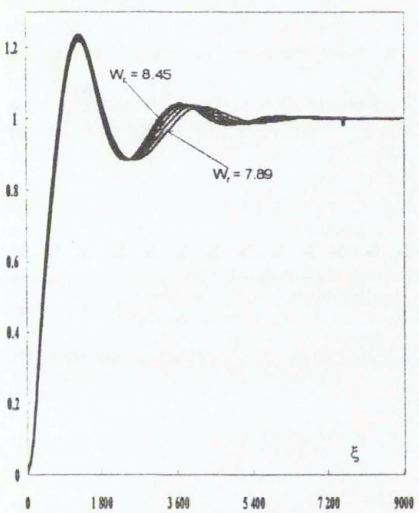

Fig.7 Capillarity shock waves for α =50.

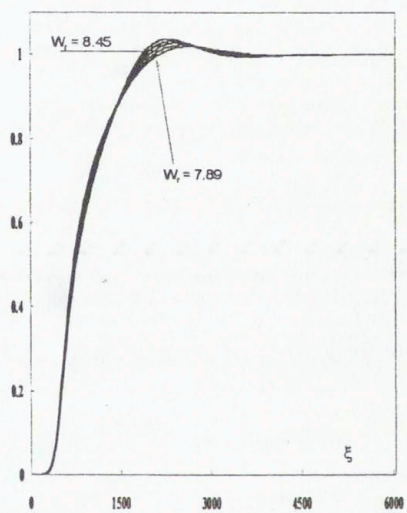

Fig.8 Kinetic shock waves for α =50.

$$\tilde{u}_l = u_l + s(w_l - b) = const. \qquad \text{and} \qquad \tilde{T}_l = \frac{1-\tilde{u}_l^2}{2} = const.$$

In Figs. 1-8 the normalised specific volume v defined by

$$v = \frac{w - w_l}{w_r - w_l}$$

is shown for α = 1, 5, 15, and 50.The other parameters are $\tilde{T}_l = 0.295$, a = 1.004, b = 1, $w_l = 2.1$, and w_r = 7.89, 8.03, 8.17, 8.31, and 8.45. We took also $\beta = 0.0625$, $\gamma = -2$, $\chi = -1$. When preparing these graphs we kept w_l and $\tilde{T}_l$ fixed and changed s. Consequently we changed u_l, i. e. we took $u_l = u_l(s)$.

The states of equilibrium are so chosen that the function $f(w; w_l, u_l, s)$ takes for a certain $w_{crit}, w_l < w_{crit} < w_r$ a positive value, but very close to zero. This results in the fact that the shock profiles for small values of the capillarity parameter α consist as if of two shocks. This phenomenon was discovered by Cramer and Crickenberger[5], who called it „impending shock splitting". The following features of this phenomenon are noticeable

- the shock wave thickness is very sensitive to the choice, for fixed value of the capillarity parameter α, of the values of the states of equilibrium; quite small differences between them can result in very great differences of the thickness. We see from Figures 1, 2, 4 that the thickness of the wave corresponding to $w_r = 7.89$ is much greater than that for $w_r = 8.03$;
- the increase of the capillarity parameter α kills the effect of the impending shock splitting, the shock thickness ceases to be so sensitive to the values of the states of equilibrium. For sufficiently large values of the capillarity parameter α the shocks become oscillatory, both in the hydrodynamic and kinetic descriptions;
- the kinetic approach to the shock wave structure is not able to kill the effect of the shock splitting. Our results seem to suggest that the leading mechanism of the damping of this effect is sufficiently intensive capillarity.

REFERENCES

1. M. Grmela, M. Kinetic approach to phase transitions. J. Statistical Physics 3: 347-364, 1971
2. M. Grmela M. On the approach to equilibrium in kinetic theory. J. Math. Physics 1: 35-40, 1974
3. K. Piechór K. A four-velocity model for van der Waals fluids. Arch. Mech. 6: 1089-1111, 1995
4. B. Kaźmierczak, K. Piechór, Shock waves by a kinetic model of van der Waals flows, ARI –Springer-Verlag, **51**, 1998.
5. M. S. Cramer, A. B. Crickenberger The dissipative structure of shock waves in dense gases. J. Fluid Mech. 223: 325-355, 1991

GENERALIZED INTEGRAL FORMS OF WALL FRICTION, HEAT AND MASS TRANSFER FACTORS FOR DRIFT FLUX MODEL OF TWO-PHASE FLOW IN AXISYMMETRICAL CHANNELS

Yuri N. Kornienko & Elena V. Kornienko
Institute of Physics and Power Engineering, Bondarenko Sq.1, Obninsk, Kaluga Region, Russia, 249020
Fax: 7-095-230-2326, E-mail: kornienk@ippe.rssi.ru

Summary. This paper describes the problem of the generalized representations of constitutive equations required in the lumped parameter code. The paper has the following objectives: 1) to draw attention to an improved approach of constructing analytical local and integral relationships for wall friction, heat and mass transfer factors based on boundary layer model, drift flux model of two-phase flow, Reynolds flux concept and generalized substance transfer coefficient; 2) to show the way in which the suggested integral equation is used to derive relations for wall friction, heat and mass transfer coefficients.

Thermo-hydraulic analysis of nuclear reactor cores depends on an availability of realistic and accurate descriptions of both field and constitutive equations. Therewith such analyses are usually carried out using Lumped Parameter Analysis (LPA) codes. One of the difficulties is associated with the establishment of the constitutive relationships between flows in one-dimensional annular channels and those in subchannels in rod bundles. In the use of the one-dimensional model in such an LPA code as the subchannel analysis code, a number of serious shortcomings of the conventional modeling are pointed out and new formulations to eliminate them are presented in this paper.

SUBSTANCE FLUX DISTRIBUTION

This initial mathematical formulation is relying on three-dimension (r-θ-z) description in the frame of the boundary layer conception. To have a possibility to extend the method being developed to two-phase flows, it is convenient to use the conservation laws in a form equally acceptable both for single-phase and two-phase flows. For this purpose it appears expedient to describe the two-phase flow on the basis of the drift flux model of Ishii[1]. Table 1*) shows appropriate designations, definitions and the drift flux model modified in accordance with the purposes of the present paper. The law of the light phase propagation is described by the convective diffusion equation. The terms with the subscript d taking into account the light phase drift are added to the corresponding turbulent substance fluxes with the subscript t.

For fully stabilized longitudinal flows through concentric annulus and unbaffled assemblies of fuel rods with constant cross-sections, a variation of local value changes of the S-variable (by which we mean axial velocity, enthalpy or concentration) proves to be identical at every position normal to the wall. The main assumption is the validity of gradient formulation of substance transfer along the normal direction to the wetted perimeter. Shown in Table 1, the conservation equations can write in a generalized and unified form by means of the single equation:

$$\frac{1}{r}\frac{\partial}{\partial r}(rJ_{r\theta}) = \rho w\frac{\partial S}{\partial z} + \rho v\frac{\partial S}{\partial r} + \rho v_\theta \frac{1}{r}\frac{\partial w}{\partial \theta} - \frac{1}{r}\frac{\partial J_\theta}{\partial \theta} - I_{v\theta}\,, \qquad (1)$$

where $r=r_1+y$ (r_1- rod radius), w, v and v_θ are axial radial and azimuthal velocities, θ-azimuthal angle; and J_θ is the azimuthal substance flux. In this paper the source term $I_{v\theta}$ unites the pressure gradient and hydrostatic component in the motion equation, whereas in the energy and mass transfer equation it is the heat and mass source (sink).

*) This and others Tables also explain of the notations and symbols used.

Table 1 Non-conservative (transportable) forms of conservation law equations, two-phase flow description is based on drift flux model by Ishii (1975).

Field equations of:	Definitions of parameters
Mixture continuity: $\frac{\partial \rho}{\partial t}+\nabla\cdot(\rho\vec{u})=0,$	$\rho=(\alpha\rho)_g+(\alpha\rho)_f$; $\rho\vec{u}=(\alpha\rho\vec{u})_g+(\alpha\rho\vec{u})_f$; where $\alpha_g=1-\alpha_f$; f-fluid, g- gas, vapor.
Convective diffusion: $\rho\frac{\partial c}{\partial t}+\rho\vec{u}\cdot\nabla c=-\nabla\cdot(\vec{N}_T)+\bar{I}^c,$	$c=(\alpha\rho)_g/\rho,$ $\vec{N}_T=\vec{N}_t+\vec{N}_d$; $\vec{N}_d=c(\alpha\rho)_g\vec{u}_{gf}$; $\vec{u}_{gf}=\vec{u}_g-\vec{u}_f$.
Mixture energy: $\rho\frac{\partial h}{\partial t}+\rho\vec{u}\cdot\nabla h=-\nabla\cdot(\vec{q}_T)+q_v,$	$h=[(\alpha\rho h)_g+(\alpha\rho h)_f]/\rho$; $\vec{q}_T=\vec{q}_t+\vec{q}_d$; $\vec{q}_d=c\rho_f\vec{u}_{gf}(h_g-h_f)$.
Mixture momentum: $\rho\frac{\partial \vec{u}}{\partial t}+\rho\vec{u}\cdot\nabla\vec{u}=\nabla\cdot(\bar{\bar{\tau}}_T)-\nabla P+\rho\vec{g}_T$.	$\vec{u}=[(\alpha\rho\vec{u})_g+(\alpha\rho\vec{u})_f]/\rho$; $\bar{\bar{\tau}}_T=\bar{\bar{\tau}}_t+\bar{\bar{\tau}}_d$; $\bar{\bar{\tau}}_d=\frac{c}{1-\alpha}\rho_f\vec{u}_{gf}\vec{u}_{gf}$; $\rho\vec{g}_T=\rho(\vec{g}+\frac{\bar{I}^c}{\rho}\vec{u}_{gf})$.
General form: $\rho\frac{\partial S}{\partial t}+\rho\vec{u}\cdot\nabla S=-\nabla\cdot(\bar{\bar{J}})+I_v,$	Variable $S\rightarrow(c,\ h(T),\ w)$; Substance flux $\bar{\bar{J}}\rightarrow(\vec{N},\vec{q},\bar{\bar{\tau}})$; Source (sink) $I_v\rightarrow(\Gamma,q_v,\rho\vec{g}_T)$

After scaling the variables in Eq. 1 and having integrated it first with the variable upper limit $Y=y/\delta_s$ and then up to the boundary layer ($Y=1$) and having combined the integrals obtained we can derive the equation for the local substance flux (see also Table 2, with designation $Y_s=1+2\tilde{\delta}_s Y$):

$$\tilde{\bar{J}}_{Y\theta}=\left\{1-G^{\curvearrowright}\left[1+\tilde{\bar{I}}_v f_v-S_z f_z-S_n f_n-2\tilde{\delta}_s\left(S_\theta f_\theta+\tilde{\bar{J}}_\Delta f_\Delta\right)\right]\right\}\Big/\ Y_s \quad . \tag{2}$$

Table 2 Definitions of *local substance profile* (LSP) components and coefficients f and weighted functions G.

$\tilde{\bar{I}}_v=\int_\theta^{\theta+\Delta 1}\int_0^1\tilde{\bar{I}}_v Y_s dY d\theta$ (3)	$f_v=1-\int_\theta^{\theta+\Delta Y}\int_0^1\tilde{\bar{I}}_v Y_s dY d\theta\Big/\int_\theta^{\theta+\Delta 1}\int_0^1\tilde{\bar{I}}_v Y_s dY d\theta\Big/G^{\curvearrowright}$ (4)
$S_z=\int_\theta^{\theta+\Delta 1}\int_0^1\tilde{\rho}w^+\frac{\partial S^+}{\partial z}Y_s dY d\theta$ (5)	$f_z=1-\int_\theta^{\theta+\Delta Y}\int_0^1\tilde{\rho}w^+\frac{\partial S^+}{\partial z}Y_s dY d\theta\Big/\int_\theta^{\theta+\Delta 1}\int_0^1\tilde{\rho}w^+\frac{\partial S^+}{\partial z}Y_s dY d\theta\Big/G^{\curvearrowright}$ (6)
$S_n=\int_\theta^{\theta+\Delta 1}\int_0^1\tilde{\rho}v^+\frac{\partial S^+}{\partial Y}Y_s dY d\theta$ (7)	$f_n=1-\int_\theta^{\theta+\Delta Y}\int_0^1\tilde{\rho}v^+\frac{\partial S^+}{\partial Y}Y_s dY d\theta\Big/\int_\theta^{\theta+\Delta 1}\int_0^1\tilde{\rho}v^+\frac{\partial S^+}{\partial Y}Y_s dY d\theta\Big/G^{\curvearrowright}$ (8)
$S_\theta=\int_\theta^{\theta+\Delta 1}\int_0^1\tilde{\rho}v_\theta^+\frac{\partial S^+}{\partial\theta}dY d\theta$ (9)	$f_\theta=1-\int_\theta^{\theta+\Delta Y}\int_0^1\tilde{\rho}v_\theta^+\frac{\partial S^+}{\partial\theta}dY d\theta\Big/\int_\theta^{\theta+\Delta 1}\int_0^1\tilde{\rho}v_\theta^+\frac{\partial S^+}{\partial\theta}dY d\theta\Big/G^{\curvearrowright}$ (10)
$\tilde{\bar{J}}_\Delta=\int_\theta^{\theta+\Delta 1}\int_0^1\frac{\partial\tilde{\bar{J}}_\theta}{\partial\theta}dY d\theta$ (11)	$f_\Delta=1-\int_\theta^{\theta+\Delta Y}\int_0^1\frac{\partial\tilde{\bar{J}}_\theta}{\partial\theta}dY d\theta\Big/\int_\theta^{\theta+\Delta 1}\int_0^1\frac{\partial\tilde{\bar{J}}_\theta}{\partial\theta}dY d\theta\Big/G^{\curvearrowright}$ (12)
$G_a^{\curvearrowright}=Y(1+\tilde{\delta}_s Y)/(1+\tilde{\delta}_s)$, for $\rho w\neq f(Y)$ (13)	$G^{\curvearrowright}=\int_\theta^{\theta+\Delta Y}\int_0^1\tilde{\rho}w^+Y_s dY d\theta\Big/\int_\theta^{\theta+\Delta 1}\int_0^1\tilde{\rho}w^+Y_s dY d\theta$ (14)

As seen from Eq. (2), the contribution of each LSP components under consideration (convective

axial, radial and azimuthal direction transfer, sources (sinks), etc.) to the substance flux can be considered as a correction to the linear distribution. It is obvious that, when the boundary layer is very thin, $\widetilde{\delta}_s << 1$. Then, we see just a small correction to the linear flux distribution $\widetilde{J}_{Y\theta}$ accounting for the influence of above-mentioned transversal profile terms. It is worthwhile here to note that the local substance flux profile in the pin wall region is a function of the weighted functions and of LSP components and coefficients, boundary conditions and geometry.

To unify the designations used and to reduce transpositions in deriving relationships for parameter profiles as well as friction, heat and mass transfer coefficients, it is helpful to use the concepts of generalized substance transfer coefficients (see Reynolds[2]) and the gradient transfer model. A detailed description of the substance fluxes is presented in the next paragraph and the key to decode the designations are quite obvious from the first six lines of Table 3.

WALL FRICTION FACTOR, HEAT AND MASS TRANSFER COEFFICIENTS

Assuming that the axial pressure gradient does not change in the annular, we obtain the following relationship for the wall friction factor from Eq. (2) and ζ_θ from Table 3:

$$\frac{8}{\zeta_\theta}=\mathrm{Re}_\theta \int_{\theta}^{\theta+\Delta 1}\int_{0}^{1}\frac{\widetilde{\rho}}{\prec\widetilde{\rho}\succ}\left(\int_0^Y\left\{1-G_a^{\frown}\left[1+\frac{\widetilde{\rho}\,f_v}{Fr_\theta}+W_z f_z+V_n f_n+2\widetilde{\delta}_\tau\left(\Psi_\theta f_\theta-T_\Delta f_\Delta\right)\right]\right\}\frac{dY}{\widetilde{\rho\nu}_T Y_\tau}\right) Y_t\,dY d\theta\,, \qquad (15)$$

where $Fr_{w\theta}=\tau_{w\theta}/(\rho_{v\theta} g r_w)$, $Y_\tau=1+2\widetilde{\delta}_\tau Y$ and integrals of LSP components (i.e., W_z, V_n, V_θ, T_Δ) and coefficients are given by Eqs. (5)-(12) with the velocity w for the variable S. The local void profile[3] component and coefficient for annular sector are:

$$\rho_v=\int_{\theta}^{\theta+\Delta 1}\int_{0}^{1}\rho_v Y_\tau\,dY d\theta \qquad (16)$$

$$f_v=1-\int_{\theta}^{\theta+\Delta Y}\int_{0}^{1}\rho_v Y_\tau\,dY d\theta\Big/\int_{\theta}^{\theta+\Delta 1}\int_{0}^{1}\rho_v Y_\tau\,dY d\theta\Big/G_a^{\frown} \qquad (17)$$

Assuming as above that the axial enthalpy (and concentration) gradients are not a function of radial position, we obtain the following relationship for the Stanton number:

$$\frac{1}{St_\theta}=Pe_\theta\widetilde{\eta}\int_{\theta}^{\theta+\Delta 1}\int_{0}^{1}\frac{\rho_M}{\prec\rho_M\succ}\int_0^Y\left\{\left[1-G^{\frown}\left(1+H_n f_n-\widetilde{\bar{q}}_v f_{qv}+2\widetilde{\delta}_q\left(H_\theta f_\theta-Q_\Delta f_\Delta\right)\right)\right]\frac{dY}{\widetilde{\rho}\,\widetilde{k}_T Y_q}\right\} Y_q\,dY d\theta\,, \qquad (18)$$

where $Y_q=1+2\widetilde{\delta}_q Y$ and the integrals of LSP components H_n, H_θ, Q_Δ and coefficients are identical to Eqs. (7)- (12) when $S=h$. The internal heat sources (sinks) profile component and coefficient are:

$$q_v=\int_{\theta}^{\theta+\Delta 1}\int_{0}^{1}q_v Y_q\,dY d\theta \qquad (19)$$

$$f_{qv}=1-\int_{\theta}^{\theta+\Delta Y}\int_{0}^{1}q_v Y_q\,dY d\theta\Big/\int_{\theta}^{\theta+\Delta 1}\int_{0}^{1}q_v Y_q\,dY d\theta\Big/G^{\frown} \qquad (20)$$

Equations 15 and 18 generalize the known integral obtained by Petukhov[4] for the friction factor and Lyon[5] for heat transfer and also Kornienko[6] (for circular tube) with respect to the functional way of taking into account the LSP components and coefficients. With this approach, one can formulate the integral analytical expressions for the wall friction, heat and mass transfer factors accounting for the contribution of various above mentioned complementary effects.

REFERENCES

1. Ishii, M.: «Thermo-Fluid Dynamic Theory of Two-Phase Flow», Eyrolles, Paris, 1975.
2. Reynolds, A.J.: «Turbulent Flows in Engineering», J. Wiley & Sons, 1974.
3. Kornienko, Yu.N. Proc. 5-th Int. Conf. On Nuclear Engineering, Paper ICONE-5-2433, (1997).
4. Petukhov, B.S.: «Heat Transfer Problems» Nauka, Moscow, 1987, in Russian.
5. Lyon, R.N.: Chem. Eng. Progr., Vol.47, N 2, pp.75-79, 1951.
6. Kornienko, Yu.N. Int. J. Heat Mass Transfer, Vol. 38, No. 16 pp. 3103-3108, 1995.

Table 3 Formulations of local substance transfer fluxes, numbers and coefficients for annular and subchannel boundary layer model

	Substance flux $J=\rho\gamma_T\frac{\partial S}{\partial y}$	Momentum flux $\tau=\rho\nu_T\frac{\partial w}{\partial y}$	Heat flux $q=-\rho k_T\frac{\partial h}{\partial y}$	Mass flux $N=-\rho D_T\frac{\partial c}{\partial y}$
1	Transfer coefficient $\gamma_T=\gamma+\varepsilon_t$; $(\tilde{\gamma}_T=\gamma_T/\gamma_w)$	$\tilde{\nu}_T=\tilde{\nu}+\tilde{\nu}_t$	$\tilde{k}_T=k+\tilde{\nu}_t\ Pr/Pr_t$	$\tilde{D}_T=\tilde{D}+\tilde{\nu}_t\ Sc/Sc_t$
2 Variable S → (w, h, (T), c)	$S_w^+-S^+=\frac{S}{S_*}=Pe_{S_*}\int_0^Y\frac{\tilde{J}}{\tilde{\rho}\tilde{\gamma}_T}dY'$	$w^+=\mathrm{Re}_*\int_0^Y\frac{\tilde{\tau}}{\tilde{\rho}\tilde{\nu}_T}dY'$, for $w_w=0$	$h_w^+-h^+=Pe_*\int_0^Y\frac{\tilde{q}}{\tilde{\rho}\tilde{k}_T}dY'$	$c_w^+-c^+=Pe_{D_*}\int_0^Y\frac{\tilde{N}}{\tilde{\rho}\tilde{D}_T}dY'$
3	Substance of friction $S_{*\theta}=J_{w\theta}/(\rho_{w\theta}w_{*\theta})$	$w_{*\theta}^2=\tau_{w\theta}/\rho_{w\theta}$	$h_{*\theta}=q_{w\theta}/(\rho_{w\theta}w_{*\theta})$	$c_{*\theta}=N_{w\theta}/(\rho_{w\theta}w_{*\theta})$
4	$\bar{S}_\theta=\frac{\int_\theta^{\theta+\Delta\theta}\int_0^{A_\delta}\rho w^\sigma S dA_\delta d\theta}{\int_\theta^{\theta+\Delta\theta}\int_0^{A_\delta}\rho w^\sigma dA_\delta d\theta}$	$\bar{w}_\theta=\frac{\int_\theta^{\theta+\Delta\theta}\int_0^{A_\delta}\rho w dA_\delta d\theta}{\int_\theta^{\theta+\Delta\theta}\int_0^{\delta_\tau}\rho 2\pi(\eta+y)dyd\theta}$	$\bar{T}_{f\theta}=\frac{\int_\theta^{\theta+\Delta1}\int_0^1\rho wT(1+2\tilde{\delta}_qY)dYd\theta}{\int_\theta^{\theta+\Delta1}\int_0^1\rho w(1+2\tilde{\delta}_qY)dYd\theta}$	$\bar{c}_\theta=\frac{\int_\theta^{\theta+\Delta1}\int_0^1 c(1+2\tilde{\delta}_NY)dYd\theta}{\Delta\cdot(1+\tilde{\delta}_N)}$ if (ρw) is not function of Y.
5	Transfer number $Pe_{s\theta}=\prec\rho w\succ\delta_s/(\rho_{w\theta}\gamma_{w\theta})$ $Pe_{s*\theta}=w_{*\theta}\delta_s/\gamma_{w\theta}$	$\mathrm{Re}_\theta=\prec\rho w\succ\delta_\tau/(\rho_{w\theta}\nu_{w\theta})$ $\mathrm{Re}_{*\theta}=w_{*\theta}\delta_\tau/\nu_{w\theta}$	$Pe_\theta=\prec\rho w\succ\delta_q/(\rho_{w\theta}k_{w\theta})$ $Pe_{*\theta}=w_{*\theta}\delta_q/k_{w\theta}$	$Pe_{D\theta}=\prec\rho w\succ\delta_N/(\rho_{w\theta}D_{w\theta})$ $Pe_{D*\theta}=w_{*\theta}\delta_N/D_{w\theta}$
6	Friction, heat or mass-transfer coefficient	$\zeta_\theta=\frac{8\tau_{w\theta}}{\prec\rho\succ(\bar{w}_\theta)^2}=\frac{8\tau_{w\theta}}{\prec\rho w\succ\bar{w}_\theta}$	$\alpha_{q\theta}=q_{w\theta}/(\bar{T}_{w\theta}-\bar{T}_{f\theta})$; $St_\theta=\alpha_\theta/\prec\rho w\succ C_p$	$\alpha_{N\theta}=\frac{N_{w\theta}}{c_w-\bar{c}_\theta}$; $St_{D\theta}=\frac{\alpha_{N\theta}}{\prec\rho w\succ}$
7	Reynolds flux $Rm_{s\theta}=J_{w\theta}/\eta(S_{w\theta}-\bar{S}_\theta)$	for $w_w=0$, $Rm_{\tau\theta}=\tau_{w\theta}/\bar{w}_\theta$	$Rm_{q\theta}=q_{w\theta}/(\bar{h}_{w\theta}-\bar{h}_{f\theta})$	$Rm_{N\theta}=N_{w\theta}/(c_{w\theta}-\bar{c}_\theta)$
8	Substance Stanton number $\frac{1}{St_{s\theta}}=\tilde{\eta}Pe_{s\theta}\int_\theta^{\theta+\Delta1}\int_0^1\frac{\rho w^\sigma}{\prec\rho w^\sigma\succ}\cdot\left[\int_0^Y\frac{\tilde{J}}{\tilde{\rho}\tilde{\gamma}_T}dY'\right](1+2\tilde{\delta}_sY)dYd\theta$	for $w_w=0$, $\tilde{\eta}=1$, $\sigma=0$ $\frac{1}{\zeta_\theta}=\frac{Re_\theta}{8}\int_\theta^{\theta+\Delta1}\int_0^1\frac{\rho}{\prec\rho\succ}\cdot\left[\int_0^Y\frac{\tilde{\tau}}{\tilde{\rho}\tilde{\nu}_T}dY'\right](1+2\tilde{\delta}_\tau Y)dYd\theta$	for $\sigma=1$, $\tilde{\eta}=C_{pw\theta}/\tilde{C}_{p\theta}$ $\frac{1}{St_{q\theta}}=\tilde{\eta}Pe_\theta\int_\theta^{\theta+\Delta1}\int_0^1\frac{\rho w}{\prec\rho w\succ}\cdot\left[\int_0^Y\frac{\tilde{q}}{\tilde{\rho}\tilde{k}_T}dY'\right](1+2\tilde{\delta}_qY)dYd\theta$	for $\sigma=1$, $\tilde{\eta}=1$ $\frac{1}{St_{D\theta}}=Pe_{D\theta}\int_\theta^{\theta+\Delta1}\int_0^1\frac{\rho w}{\prec\rho w\succ}\cdot\left[\int_0^Y\frac{\tilde{N}}{\tilde{\rho}\tilde{D}_T}dY'\right](1+2\tilde{\delta}_NY)dYd\theta$

EXPERIMENTAL VALIDATION OF TEMPERATURE AND VELOCITY FIELDS FOR THE FREEZING WATER

T.A. Kowalewski*[1], A. Cybulski[1] & M. Rebow[2]
[1]Polish Academy of Sciences, IPPT PAN, PL 00-049 Warszawa
[2]Warsaw University of Technology, ITC PW, PL 00-665 Warszawa

Summary A new experimental technique based on a computational analysis of the colour and displacement of thermochromic liquid crystal tracers (TLCs) was applied to determine both the temperature and velocity fields of freezing water. The method was used to verify and validate numerical solutions for water freezing in the cube shaped cavity.

INTRODUCTION

Application of numerical methods for freezing problem necessitate to solve non-linear partial differential equations of variable properties fluid coupled with moving solid/liquid interface. Due to the problem complexity, it is not a trivial task to determine precisely an error of the numerical results impeded by inevitable model simplifications. Errors appearing due to limited accuracy of different numerical methodologies, and due to inevitable simplifications introduced in the models, are usually difficult to predict a priori [1]. Hence, full field measurements of velocity and temperature gained great importance for the flow problems accompanied by the phase change. With this objective in view new experimental technique based on a computational analysis of the colour and displacement of Thermochromic Liquid Crystal tracers (TLCs) was applied to determine both the temperature and velocity fields of the flow. It combines Digital Particle Image Thermometry (DPIT) and Digital Particle Image Velocimetry (DPIV). Full 2-D temperature and velocity fields are determined from a pair or a longer sequence of colour images taken for the selected cross-sections of the flow. We consider convective flow of freezing water in a simple geometry, a cube shaped cavity of 38mm internal size. Two configurations are investigated. In the first one flow develops in the cavity with a horizontal temperature gradient set between two opposite isothermal walls. The other four walls, made of 6mm thick Plexiglas, are nominally insulators of finite thermal diffusivity. In the second configuration, the top wall of the cavity is isothermal and kept at low temperature T_c. The other five walls are non-adiabatic, allowing a heat flux from an external water bath kept at the temperature T_h. Due to forced convection in the bath it can be assumed that the temperature at the external surfaces of the box is close to the bath temperature. The temperature field at the inner surfaces of the walls adjusts itself depending on both the flow inside the box and the heat flux through and along the walls.

*E-mail: tkowale@ippt.gov.pl

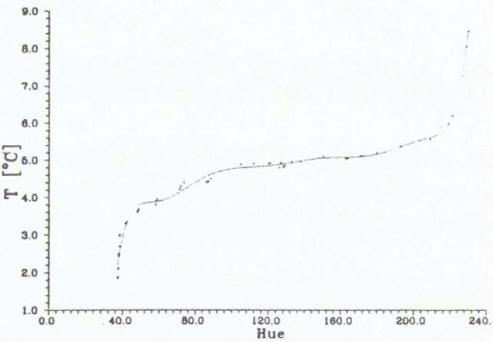

Figure 1: Temperature vs. Hue for TLCs used. Calibration curve is obtained by 8th order polynomial fitted to the experimental points

EXPERIMENTAL METHOD

Thermochromic liquid crystals are used as temperature indicators. They modify incident white light and display colour whose wavelength is proportional to temperature. The displayed colour is red at the low temperature margin of the colour-play interval and blue at the high end. Application of TLCs as tracers opens new possibility of instantaneous full field measurements of temperature and velocity in thermally driven flow. Dispersed liquid crystals into the liquid become small thermometers monitoring local fluid temperature [3, 2]. For flow visualization classical *light sheet* technique is used. The collimated source of white light illuminates selected cross-section of the flow and colour images are acquired at the perpendicular direction. Illuminated TLCs tracers appear on images as cloud of colour spots conveyed by the fluid. Digital acquisition of the images allows quantitative measurement of both temperature as well as displacement of the tracers. The temperature measurements are based on a digital colour analysis of *RGB* images. For evaluating the temperature the *HSI*[1] representation of the *RGB* colour space is used. The incoming *RGB* signals are transformed pixel by pixel into Hue Saturation, and Intensity. Temperature is determined by relating the hue to a temperature calibration function. Our 8-bit representation of the hue value ensures resolution better than 1%. However, the colour-temperature relationship is strongly non-linear (Fig. 1). Hence, the accuracy of the measured temperature depends on the colour (hue) value. The relative error, based on the temperature range defined by the TLCs colour-play limits, varies from 3% to 10%. For the TLCs used (TM from Merck) there results an absolute accuracy of 0.15°C for lower temperatures (red-green colour range) and 0.5°C for higher temperatures (blue colour range).

The 2-D velocity vector field has been measured by digital particle image velocimetry (DPIV). By this method, the motion of the TLC tracers observed in the plane of the illuminating light sheet, is analysed. In the classical DPIV FFT-based cross-correlation analysis the spatial resolution of the method is limited by the interogation window size. Further improvement of the evaluation accuracy allows the recently developed ODP-PIV method

[1]Hue, Saturation, Intensity

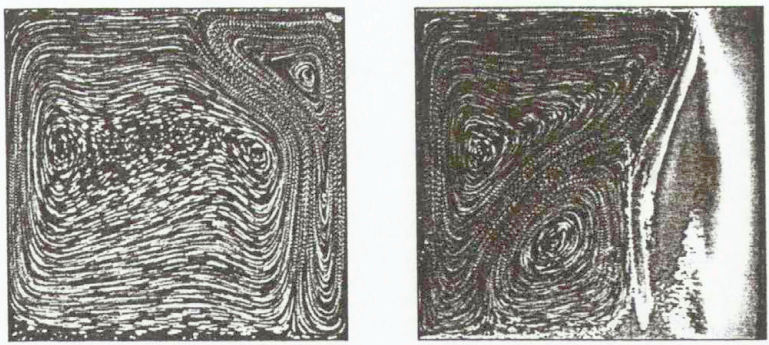

Figure 2: Flow structure observed for the centre plane (z=0.5) in the differentially heated cavity at 60s *(left)* and 2600s *(right)* after cooling started

of image analysis [4]. Due to an iterative search algorithm used, a dense velocity field is obtained, with displacement value calculated at each image pixel. The accuracy of the FFT-based DPIV and that of the ODP-PIV method is 0.6 pixels and 0.15 pixels, respectively. This means that for a typical displacement vector of 10 pixels the relative accuracy of the velocity measurement (for a single point) is better than 6%.

SELECTED RESULTS

Differentially heated cavity

The two opposite metal walls of the cube are assumed to be isothermal. Due to temperature gradients existing between the walls the recirculating flow is generated in the cavity. This flow configuration resembles a popular "bench mark" case, natural convection in a cubical cavity with differentially heated end walls. However, the behaviour of natural convection of water in the vicinity of the freezing point creates interesting and also difficult features for numerical modelling of flow structures. It is mainly due to the strongly non-linear temperature dependence of the density function with the extremum at 4°C. The competing effects of positive and negative buoyancy force result in a flow with two distinct circulations (Figs. 2,3). There is "normal" clockwise circulation, where the water density decreases with temperature (upper-left cavity region) and "abnormal" convection with the opposite density variation and counter-clockwise rotation (lower-right region). At the upper part of the cold wall the two circulations collide with each other, intensifying the heat transfer and effectively decreasing the interface growth. Below, the convective heat transfer from the hot wall is limited by the abnormal circulation, separating it from the freezing front. Hence, the phase front is only initially flat. As time passes it deforms strongly, getting a characteristic "belly" at its lower part.

This type of flow structure appeared to be very sensitive to thermal boundary conditions at the side walls. Despite improvements in the numerical model we used, the computational results differ in detail from their experimental counterparts [5]. An eventual source of observed discrepancies could be the supercooling of water, which delays creation of the first

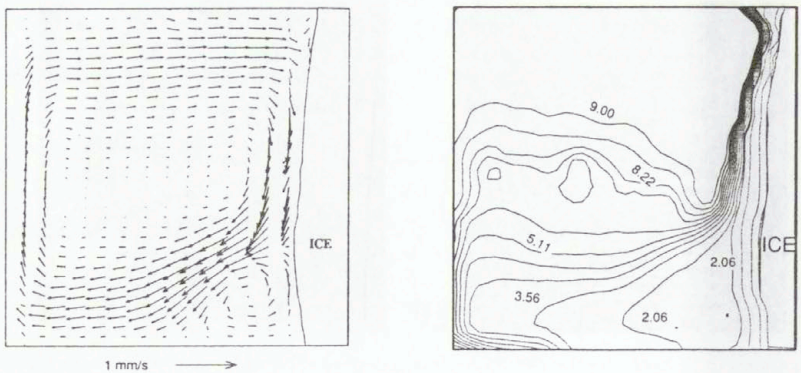

Figure 3: Velocity *(left)* and temperature isotherms *(right)* field evaluated for water freezing in the differentially heated cube at 500s, T_h=10°C, T_c=-10°C

ice layer and deforms the flow pattern at the top of the cavity (comp. Fig. 2a). It is well known that pure water may supercool as far as -40°C, before freezing occurs. Seeding of the flow with thermochromic liquid crystals allowed us to visualize that in fact initial water temperature reaches about -7°C before freezing starts.

Lid cooled cavity

The problem of melt-flow in a lid-cooled cavity has a practical application in a number of manufacturing processes and physical situations. A large scale example is the freezing of water reservoirs, where at night, cooling from above initiates freezing and generates convective flow beneath the ice. On a smaller scale, it has been recognized in crystal growth problems that the flow pattern beneath the solidifying surface is of critical importance to crystal quality. The occurrence of convective flow in the presence of vertical temperature gradients is known to be stable only within a relatively narrow range of Rayleigh number. In our experiments on a lid-cooled cavity there was heat flux into the liquid through the sides and bottom walls. It has been found that these boundary conditions have a stabilising effect on the overall flow, and stable flow structures are possible at $Ra > 10^6$, well above the second critical number for the Rayleigh-Bénard instability. However, various modes of instabilities are observed during the onset of convection. Before a stable final flow structure is achieved, several oscillatory changes in its pattern are observed [6]. The initial flow instabilities, clearly visible in the TLCs visualized temperature field, are also reproduced in the numerical simulations [7]. When a phase change takes place, in our case freezing on a lid surface, strongly non-linear coupling of the flow and interface is responsible for the interface geometry. Despite the fact that freezing starts at a planar surface, the ice surface does not remain planar. Its distortion in turn affects the convection in the whole cavity. A complex interaction between the flow, the moving boundary and the latent heat removed at the solid/liquid interface determines the flow pattern which is established. Fig. 4 shows the

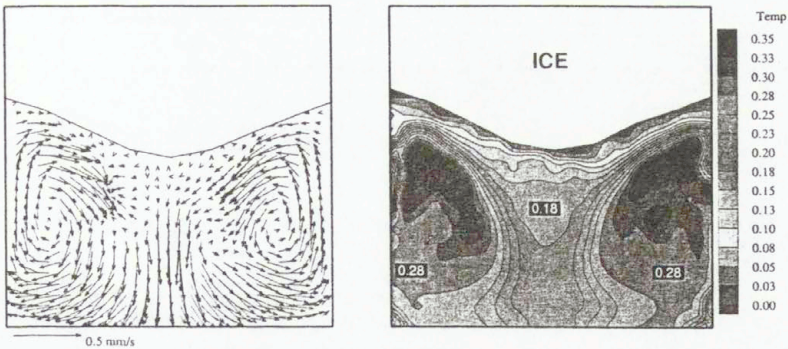

Figure 4: Velocity *(left)* and non-dimensional temperature *(right)* field evaluated for water freezing in the lid cooled cavity after 5 hours, T_h=20°C, Tc=-10°C

temperature and velocity field evaluated for the quasi-steady state, i.e. 5 hours after the experiment was started.

The flow visualisation performed in the lid cooled cavity shows the existence of a complex spiralling structure transporting fluid up along the side walls and down in a central cold jet along the cavity axis. A colour play of TLCs seeded flow images taken directly under the lid shows this flow structure in the temperature pattern. Both the particle tracks and temperature distribution measured underneath the lid indicate the existence of eight symmetric cells created by the flow (comp. Fig. 5). This is also manifested in the complex structure of the ice surface. In both the computed and observed ice surface, a star-like grooving reflects eight-fold symmetry of the flow [7]. It was found that heat flux through, as well as along the walls has to be incorporated in the numerical model to obtain observed flow pattern. It was only as a result of the use of both the experimental and numerical methods that the fine structures of the thermal flow were fully understood.

CONCLUSIONS

The present study has demonstrated the applicability of cholesteric liquid crystals to the quantitative measurements of full field instantaneous temperature distribution in freezing water. The simultaneous measurement of the velocity and temperature fields using TLC tracers, allows a detailed experimental description of the complex flow structures appearing in the convective flow associated with phase change, and their direct comparison with the numerical counterparts. Several discrepancies found between predicted and observed flow indicates the necessity of careful experimental verification of the numerical codes used for simulating phase change problems. It seems that the presented experimental technique offers a valuable tool for the code validation procedure.

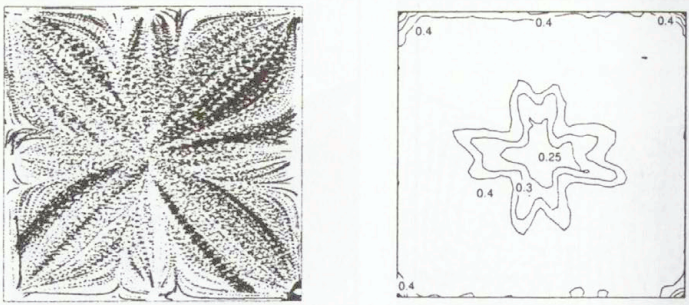

Figure 5: Flow structure observed for the horizontal plane (y=0.9) underneath the cooled lid; particle tracks *(left)* and non-dimensional temperature isotherms evaluated from the colour of TLC tracers *(right)*

References

[1] Kowalewski T. A.: Experimental validation of numerical codes in thermally driven flows. Adv. in Comput. Heat Transfer CHT-97, 1–15, Begel House Inc., New York, 1998.

[2] Hiller W., Kowalewski T. A.: Simultaneous measurement of the temperature and velocity fields in thermal convective flows. Flow Visualization IV, 617–622, Hemisphere, 1987.

[3] Hiller W., Koch St., Kowalewski T. A., Stella, F.: Onset of natural convection in a cube. Int. J. Heat Mass Transfer **36**, pp. 3251–3263, 1993.

[4] Quénot G., Pakleza J., Kowalewski T. A.: Particle Image Velocimetry with Optical Flow. Exp. in Fluids **25**, pp. 177–189, 1998.

[5] Kowalewski T. A., Rebow M.: Freezing of water in the differentially heated cubic cavity. Int. J. of Comp. Fluid Dyn. **11**, no. 3-4, pp. 193–210, 1999.

[6] Kowalewski T. A., Cybulski A.: Experimental and numerical investigations of natural convection in freezing water. Int. Conf. on Heat Transfer with Change of Phase, Kielce, Mechanics **61**/2, 7–16, 1996.

[7] Kowalewski T. A., Cybulski A.: Natural convection with phase change (in polish). IPPT Reports **8**/97, IPPT PAN, Warszawa, 1997.

ANALYSIS OF FREE SURFACE FLOWS WITH SOLIDIFICATION

A.V. Kuznetsov
North Carolina State University, Dept. of Mechanical and Aerospace Engineering,
Raleigh, NC 27695-7910, USA; E-mail: avkuznet@eos.ncsu.edu

Summary. The objective of this paper is to present a theory of free surface flows with continuous solidification. This type of open-channel flows is relevant to a number of important technological processes, such as the horizontal continuous casting of carbon steel. Since carbon steel is a binary alloy, in formulating a mathematical model in addition to accounting for fluid flow and heat transfer it is also necessary to account for the solute transport and for the two-phase region (the mushy zone) effects. Extensive numerical simulations provide valuable insight into this process.

Classical free surface flows received considerable attention in the literature. A good overview on open-channel flows is given in Chow[1]. Both analytical and numerical investigations of open-channel flows is presented in Garcia-Navarro et al.[2], Thomas et al.[3], Rahman et al.[4]. However, open channel flows with solidification have not received so far sufficient attention. This gap needs to be filled, because these flows are relevant to a number of important industrial applications, such as the strip casting of carbon steel.

In recent years, there has been a number of papers devoted to modeling of the heat transfer and fluid flow for different schemes of both vertical[5-9] and horizontal[10-14] strip casting processes. These papers present extensive investigations of both fluid flow and heat transfer in the solidifying strip. However, further insight into this process is needed, such as investigation of coupling flow and heat transfer with solute transport and accounting for the free surface behavior.

In recent publications a number of models for describing fluid flow of binary alloys during solidification have been proposed, mainly for the case when the flow is caused by natural convection. Unlike pure substances, binary alloys solidify over extended temperature ranges and solid formation usually occurs within a two-phase region (the mushy zone), where solid and liquid phases coexist. Sound theories for transport processes in the mushy zone have been developed only recently.

Derivation of the set of governing equations for the mushy zone based on the mixture theory approach was originally reported in refs.[15-16] and recently extended to account for microscopic phenomena in refs.[17-18]. The derivation of the set of governing equations based on a volume-averaging procedure is presented in refs.[19-21]. An excellent review of different models with basic features of each model summarized is given in ref.[22]. Very recently, a three-phase model (solid, liquid and gas phases) of the mushy zone has been proposed[23, 24] and comparisons against the two-phase model have been carried out. Since the appearance of these models, the solidification of alloys has been extensively investigated. Numerical results of these studies along with the main features of the numerical procedures are reported in[25-39]. Reference[40] is one of the first research

works on modeling flow, heat and solute transport in a *multicomponent* steel. Different from the investigations reported in refs.[25-40], where fluid flow is mainly caused by a relatively weak natural convection, in this research we consider the case of a strong forced convection, caused by the change of the height of the free surface.

STATEMENT OF THE PROBLEM

The schematic of the problem is displayed in Figure 1. We consider free surface flow of a binary alloy, for example, carbon steel, on a horizontal surface (casting table) which moves with a constant velocity, U. We assume that the binary alloy enters the moving surface with the fully developed relative velocity profile, where relative means relative to the surface. In the beginning of the computational domain the binary alloy is completely in the liquid state, that is its temperature is above the liquidus temperature. A constant heat flux is withdrawn from the surface, and this causes solidification of the alloy as it flows downstream. At the end of the computational domain the alloy is completely solidified, and the solid strip leaves the moving surface with the same constant velocity, U. This process is an example of a free surface flow with solidification. It also should be noted that in the beginning of the casting table, when $0 \le x \le X^*$, alloy at the free surface is in the liquid state while farther downstream, when $x > X^*$, alloy at the free surface is in the mushy state.

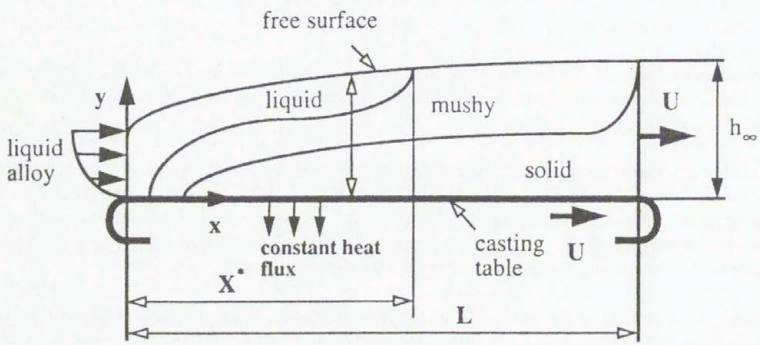

Figure 1. Definition sketch

In establishing the mathematical model for this process, the following assumptions and simplifications are utilized:

- The transport process is steady, two-dimensional and laminar;
- The properties of the solid and liquid phases are homogeneous and isotropic, the solid phase is stationary and rigid, no microporosity forms in the strip;
- The solid and liquid in the mushy zone are in local thermal and phase equilibrium, the thermophysical properties are constant, but may be different for liquid and solid phases;
- No species diffusion in the solid phase between the averaging volumes and complete diffusion in the solid phase within the averaging volume (lever rule) is assumed;
- Heat transfer by radiation and convection from the free surface is negligible;

- The thin layer approximation can be invoked;
- The surface tension effects are negligible;
- The flow resistance due to the growing dendrites is accounted for only in the direction perpendicular to the primary dendrite arms (in the x-direction), resistance in the y-direction is neglected because of the small thickness of the strip;
- The density difference between the fluid and solid phases is accounted for only in the continuity and the species transport equations, but it is neglected in the energy equation. It other words, the term accounting for the density change is incorporated into the latent heat term and the temperature dependence of the "effective latent heat" is then neglected. Thus the energy equation then takes the form suggested in Beckermann and Viskanta[27].

MAJOR RESULSTS AND CONCLUSIONS

This paper suggests a model of free surface flow with solidification. This model is applied to numerically investigate coupled fluid flow, heat transfer and solute transport in horizontal continuous casting process. It is shown that the solute diffusion in the liquid phase causes a formation near the casting table a thin diffusion boundary layer. This boundary layer is essentially depleted of the solute. The formation of this boundary layer can be explained by considering the effect of diffusion near an intensively cooled impermeable wall. It is established that increasing of heat transfer rate from the casting table results in considerable decrease of macrosegregation level in the strip. This is because larger heat transfer rate results in smaller width of the mushy zone, which in turn results in smaller macrosegregation. It is also established that increasing of casting velocity results in slight increase of macrosegregation level in the strip. This is because larger casting velocity results in larger width of the mushy zone, which in turn results in larger macrosegregation.

ACKNOWLEDGMENT

The support provided by the Alexander von Humboldt Foundation and the assistance of the North Carolina Supercomputing Center (NCSC) under an Advanced Computing Resources Grant are greatly appreciated.

REFERENCES

1. Chow, V.T. 1959. Open-channel hydraulics. McGraw-Hill, NY.

2. Garcia-Navarro, P., Alcrudo, F. & Savirón, J.M. 1992. J. Hydraulic Eng. 118, 1359-1371.

3. Thomas, S., Hankey, W.L., Faghri, A. & Swanson, T. 1990. J. Heat Transfer 112, 728-735.

4. Rahman, M.M., Hankey, W.L. & Faghri, A. 1991. Int. J. Heat Mass transfer 34, 103-114.

5. Shiomi, M., Mori, K. & Osakada, K. 1995. In: Proceedings of the Seventh International Conference on Modeling of Casting, Welding, and Advanced Solidification Processes VII, 793-800.

6. Raihle, C.-M., Fredriksson, H. & Östlund, S.: 1995. In: Proceedings of the Seventh International Conference on Modeling of Casting, Welding, and Advanced Solidification Processes VII, 817-824.

7. Hwang, S.M. & Kang, Y.H. 1995. ASME Journal of Heat Transfer 117, 304-315.

8. Saitoh, T., Hojo, H., Yaguchi, H. & Kang, C.G. 1989. Metallurgical Transactions 20B, 381-390.

9. Hwang, J.D., Lin, H.J., Hwang, W.S. & Hu, C.T. 1995. ISIJ International 35, 170-177.

10. Bradbury, P.J. & Hunt, J.D. 1995. In: Proceedings of the Seventh International Conference on Modeling of Casting, Welding, and Advanced Solidification Processes VII, 739-746.

11. Caron, S., Essadiqi, E., Hamel, F.G. & Masounave, J. 1990. Light Metals, 967-973.

12. Mallik, R.K. & Mehrotra, S.P. 1993. ISIJ International 33, 595-604.

13. Jimbo, I. & Cramb, A.W. 1994. ISS Transactions 15, 145-150.

14. Digruber, M., Haas, S. & Schneider W. 1998. In: Proceedings of the Eighth International Conference on Modeling of Casting, Welding, and Advanced Solidification Processes VIII, 663-670.

15. Bennon, W.D. & Incropera, F.P. 1987. Int. J. Heat Mass Transfer 30, 2161-2170.

16. Prescott, P.J., Incropera, F.P. & Bennon, W.D. 1990. Int. J. Heat Mass Transfer 34, 2351-2359.

17. Ni, J. & Incropera, F.P. 1995. Int. J. Heat Mass Transfer 38, 1271-1284.

18. Ni, J. & Incropera, F.P. 1995. Int. J. Heat Mass Transfer 38, 1285-1296.

19. Ganesan, S. & Poirier, D.R. 1990. Metallurgical Transactions 21B, 173-181.

20. Poirier, D.R., Nandapurkar, P.J. & Ganesan, S. 1991. Metallurgical Transactions 22B, 889-990.

21. Ni, J. & Beckermann, C. 1991. Metallurgical Transactions 22B, 349-361.

22. Viskanta, R. 1990. JSME Int. J., Series II 33, 409-423.

23. Kuznetsov, A.V. & Vafai, K. 1995. Int. J. Heat Mass Transfer 38, 2557-2567.

24. Kuznetsov, A.V. & Vafai, K. 1996. Numerical Heat Transfer Part A 29, 859-867.

25. Bennon, W.D. & Incropera, F.P. 1987. Int. J. Heat Mass Transfer 30, 2171-2187.

26. Voller, V.R. & Prakash, C. 1987. Int. J. Heat Mass Transfer 30, 1709-1719.

27. Beckermann, C. & Viskanta, R. 1988. PhysicoChemical Hydrodynamics 10, 195-213.

28. Bennon, W.D. & Incropera, F.P. 1988. Numerical Heat Transfer 13, 277-296.

29. Engel, A.H.H. & Incropera, F.P. 1989. Wärme- und Stoffübertragung 24, 279-288.

30. Voller, V.R., Brent, A.D. & Prakash, C. 1989. Int. J. Heat Mass Transfer 32, 1719-1731.

31. Prakash, C. & Voller, V. 1989. Numerical Heat Transfer B 15, 171-189.

32. Neilson, D.G., Incropera, F.P. & Bennon, W.D. 1990. Int. J. Heat Mass Transfer 33, 367-380.

33. Felicelli, S.D., Heinrich, J.C. & Poirier, D.R. 1991. Metallurgical Transactions 22B, 847-859.

34. Yoo, H. & Viskanta, R. 1992. Int. J. Heat Mass Transfer 35, 2335-2346.

35. Felicelli, S.D., Heinrich, J.C. & Poirier, D.R. 1993. Numerical Heat Transfer B 23, 461-481.

36. Lee, S.L. & Tzong, R.Y. 1995. Int. J. Heat Mass Transfer 38, 1237-1247.

37. Schneider, M.C. & Beckermann, C. 1995. Int. J. Heat Mass Transfer 38, 3455-3473.

38. Kuznetsov, A.V. 1997. Int. J. Heat Mass Transfer 40, 2949-2961.

39. Kuznetsov, A.V. 1998. Numerical Heat Transfer, Part A: Applications 33, 515-532.

40. Böhmer, W.F.A., Schneider, M.C., Beckermann, C. & Sahm, P.R. 1995. In: Proceedings of the Seventh International Conference on Modeling of Casting, Welding, and Advanced Solidification Processes VII, 617-624.

FINITE ELEMENT ANALYSIS OF MELTING DRIVEN BY BUOYANCY AND SURFACE TENSION FORCES

Marc MEDALE, Marc JAEGER & Ahmed KAISS

Institut Universitaire des Systèmes Thermiques Industriels, CNRS U.M.R. 6595
Technopôle de Château-Gombert, 5 rue Enrico Fermi, 13454 Marseille Cedex 13, France.

Summary A finite element model has been developed for the computation of melting/solidifying process under the action of both buoyancy and surface tension forces. Validated on the square cavity benchmark of Gobin & Le Quéré [3], it is further extended to the free surface case where surface tension can drive the flow (capillary flow). A comparison of the results obtained for three boundary conditions applied at the top of the melting pool is performed. It shows that the flow is dominated by buoyancy effect when the pool is deep enough as in the square cavity case of the benchmark.

MODEL DESCRIPTION

The aim of our presentation concerns the numerical model we have developed for the computation of industrial solid-liquid phase change problems. It is based on the macroscopic Voller and Prakash physical description of the phenomenon [1], recast in the finite element framework. It solves on a fixed mesh the coupled incompressible Navier-Stokes and energy equations the later being solved also in the solid phase. According to the original model, the energy equation is written in an enthalpy formulation in order to take into account the latent heat release during phase change. This model is especially well suited to handle the phase change of mixture like metallurgical alloys. In that case the phase change which occurs over a temperature range, leads to a stretched solidifying/melting front (mushy region) instead of a steeple one (pure materials). Thus the momentum equations have been slightly modified by a Darcy like modeling to simulate the fluid flow in this region. The natural convection flow in the liquid phase can originate from two types of forces depending whether there is a free surface or not. In the first case buoyancy alone induces the flow whereas in the second case surface tension forces act too. It is noteworthy that both can depend on temperature and/or species concentration gradients, whenever in the present study only the thermal effect is considered. In our model, buoyancy is taken into account through the Boussinesq's approximation and the surface tension depends linearly on temperature.

The numerical model is formulated in primary variables ($\vec{V}$, p, T). The fluid flow and heat transfer problems are solved using a non-stationary uncoupled approach. It consists in sequentially solving at each time step the energy equation with the latest available velocities and then the fluid flow problem with the updated temperature field. The time discretization is performed with the first order backward finite difference scheme (implicit Euler) for both problems. The space discretization is achieved with standard Q2/P1 quadrilateral elements for the fluid flow problem together with linear C^0 elements for the temperature.

The finite element model has been programmed with the PETSc toolkit [2] in order to achieve parallel computations and it has been implemented on a CRAY T3E computer (IDRIS, France). The fluid flow and heat transfer algebraic systems are solved in a segregated manner, using the faster iterative solver available in PETSc for each of them.

APPLICATIONS

Validation on the melting driven by natural convection benchmark

As validation, we have contributed to the comparison exercise proposed by Gobin and Le Quéré [3] (synthesis given at PCC99). Whenever our model is especially devoted to non-isothermal phase change problems, this benchmark focuses on the melting of two pure materials (Tin and Octadecane) in a square cavity (heated on the left vertical wall and maintained at the melting temperature on the opposite one). Thus this benchmark represents a challenging validation for our model, since one has to simulate this isothermal phase change as a non-isothermal one with a mushy region width tending to zero. However the results of our computations for the four test cases proposed in the benchmark are in good agreement with others contributor's ones.

Combined action of buoyancy and thermocapillary forces

In many actual situations, the upper boundary of the melting pool is a free surface. Therefore it becomes relevant to analyze the influence of the free surface modeling on the melting problem. For this aim we have reconsidered the test case number two (Pr=0.02, Ste=0.01, $Ra=2.5x10^5$) of the above benchmark problem with two other boundary conditions at the upper liquid boundary (assumed to remain flat): perfect slipping or surface tension gradient (Ma=1250). The Nusselt number along the heated wall and the liquid fraction (melt volume / total volume) are plotted respectively on Figures 1 and 2 versus non-dimensional time (Stefan number times Fourier number). On both figures we have plotted the results for the three kinds of boundary condition on the upper liquid boundary: 1) no slipping; 2) perfect slipping; 3) surface tension gradient. The solid line curves correspond to the Jany & Bejan's correlation (used in the aforementioned benchmark) on Figure 1 and to the pure conductive case on Figure 2, respectively. For the considered case the free surface modeling influences very slightly these results. Actually the value of the ratio Ra/Ma=200 (ratio of the magnitude of the two driving forces) demonstrates that buoyancy is by far dominant. As a result, the free surface modeling only influences a thin layer in the upper part of the cavity. This can be observed on Figure 3, which presents isotherms and streamlines at four instants for the three models.

CONCLUSION

Our study demonstrates that the results obtained in the benchmark framework (closed cavity) can be reasonably extended to melting squared open in the limit of high Ra/Ma ratios. However, since this ratio varies as the square of the melting pool depth, it's obvious that capillary effect will become dominant for thin fluid layers as can be found for example in welding processes or surface processing. Thus it's useful to develop and validate models able to deal with such situations.

REFERENCES

1. V. R. Voller and C. Prakash: A fixed grid numerical modeling methodology for convection-diffusion mushy region phase-change problems, *Int. J. Heat Mass Transfer*, **30**, N°8, pp 1709-1719, 1987.

2. S. Balay, W. Gropp, L. C. McInnes and B. Smith: *PETSc 2.0.21 Users Manual*, Mathematics and Computer Science Division, Argone National Laboratory, 1998.

3. D. Gobin and P. Le Quéré: Melting Driven by Natural Convection. A Comparison Exercise: First results, *Int. J. Thermal Sciences*, **38**, pp 5-26, 1999.

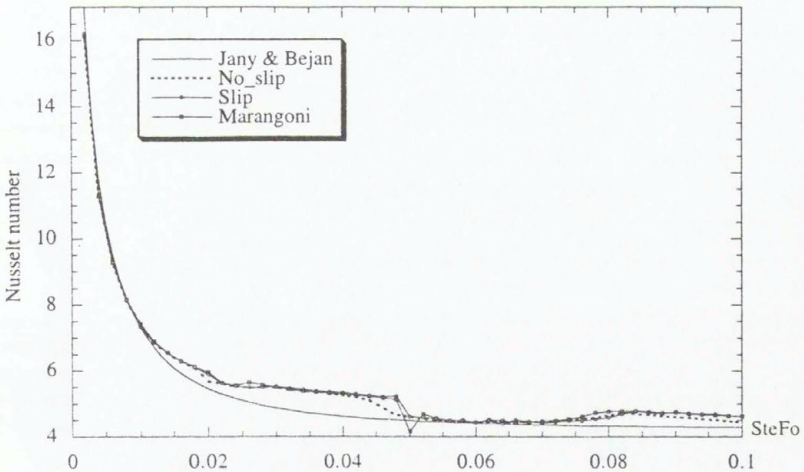

Figure 1. Time evolution of the average Nusselt number along the heated wall for the three kinds of boundary conditions together with Jany and Bejan's correlation

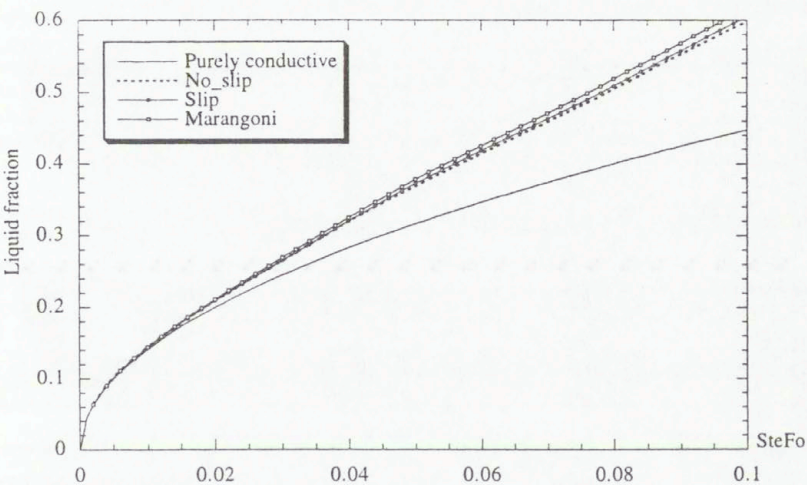

Figure 2. Time evolution of the liquid fraction for the three kinds of boundary conditions together with pure conductive case

Figure 3. Next page: Isotherms (three upper rows) and streamlines (three lower rows) at four instants for the three kinds of boundary conditions

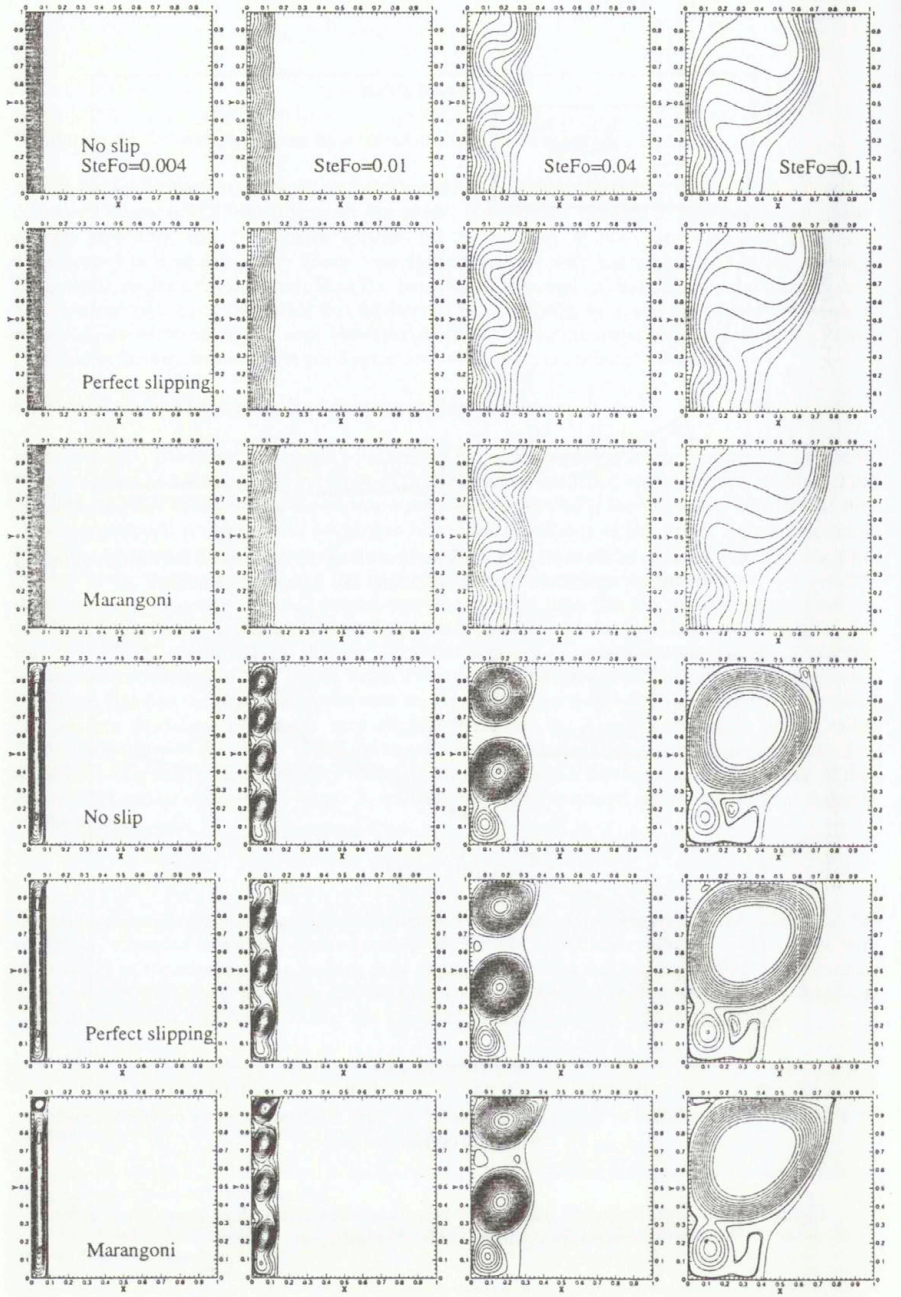

COMPARISON OF UPWIND AND CHARACTERISTIC SCHEMES FOR SOLVING MULTIPHASE DIFFUSION-CONVECTION EQUATION

Jali Pieskä, Erkki Laitinen

Department of Mathematical Science, University of Oulu, Infotech
PL 3000, 90401 Oulu, FINLAND

Summary In this paper the multiphase diffusion-convection problem is solved numerically by using upwind and characteristic schemes. Discretization for the schemes is performed by finite difference method. For solving the algebraic equations at every time level the modified S.O.R. method is used. In the numerical results computing time, number of iterations and accuracy of the schemes are analysed.

INTRODUCTION

In this paper two different numerical schemes for solving multiphase diffusion-convection equation are presented. The equation considered is involved in many physical problems of practical interest for example in melting, solidification[1], multi-component fluid flows, flows through porous media, meteorology, pollution problems etc. Usually these problems are discretized by using finite difference, finite element or boundary element method on a fixed or on a moving grid[2,3,4].

The physical situation considered here is involved in steel continuous casting problem[5,6]. In this problem a one-directional time dependent flow of liquid steel is cooled down in a rectangular geometry.

Let Ω be a regtangular domain in $\mathbb{R}^2$ with the boundary $\Gamma = \Gamma_N \cup \Gamma_D$. Let $T > 0$, and $\Omega_T = \Omega \times]0, T[$. We denote by $H(u(x;t);t)$ the enthalpy and by $u(x;t)$ the temperature of steel at the point $(x;t) \in \Omega_T$.

Using enthalpy method we can formulate the continuous casting problem as a following multiphase diffusion-convection equation which we solve numerically on a fixed grid.

$$(P) \qquad \begin{cases} \frac{\partial H}{\partial t} - \Delta u + v(t)\frac{\partial H}{\partial x_2} = f(x;t) & \text{on } \Omega \\ u(x;t) = g_D(x;t) & \text{on } \Gamma_D \\ \frac{\partial u}{\partial n} = g_N(x;t) & \text{on } \Gamma_N \\ H(x;0) = H_0(x) & \text{on } \Omega. \end{cases}$$

The graph of $H(u)$ is a non-decreasing function $\mathbb{R} \to \mathbb{R}$ involving near vertical segments corresponding to the phase transition state. The speed of the fluid flow to direction x_2 is $v(t)$.

DISCRETIZATION OF PROBLEM (P)

Let us consider the case where the problem (P) is solved in rectangle domain $\Omega =]0, l_1[\times]0, l_2[$, with the boundary Γ divided into two parts: $\Gamma_D = \{ (x_1, x_2) \mid x_2 = l_2 , x_1 \in [0, l_1] \}$ and $\Gamma_N = \Gamma \setminus \Gamma_D$.

Let the number of the grid points in both x_1- and x_2-directions be N. Hence the grid parameters are respectively h_1 and h_2. The grid parameter in time is denoted by τ.

Denote

$$\bar{\partial}_1 u(x) = h_1^{-1}(u(x_1, x_2) - u(x_1 - h_1, x_2))$$
$$\partial_1 u(x) = h_1^{-1}(u(x_1 + h, x_2) - u(x_1, x_2))$$

and similary for $\bar{\partial}_2$ and ∂_2. By using normal 5-point difference formula the Laplacian Δ can be discretized

$$\Delta_h = \partial_1 \bar{\partial}_1 + \partial_2 \bar{\partial}_2$$

Upwind scheme

The semi-discrete upwind scheme approximation for the problem (P) is

$$\begin{cases} \frac{\partial H}{\partial t} - \Delta_h u + v\partial_2 H = f & \text{on } \Omega \\ u = g_D & \text{on } \Gamma_D \\ \frac{\partial u}{\partial n} = g_N & \text{on } \Gamma_N \\ H(x;0) = H_0(x) & \text{on } \Omega, \end{cases}$$

where

$$\frac{\partial u}{\partial n} = \begin{cases} \partial_1 u & \text{if } x_1 = 0, \quad x \in \Gamma \\ \bar{\partial}_1 u & \text{if } x_1 = l_1, \quad x \in \Gamma \\ \bar{\partial}_2 u & \text{if } x_2 = 0, \quad x \in \Gamma. \end{cases}$$

For time discretization we denote

$$\partial_\tau H = \frac{H^{k+1} - H^k}{\tau}.$$

Using the implicit Euler method in time and normal difference quotients in space we can write the fully discrete form of equation (P) as follows. For all $k = 0, 1...nt - 1$ find the pair u^{k+1}, H^{k+1}

$$(P_h) \qquad \begin{cases} \partial_\tau H - \Delta_h u^{k+1} + v\partial_2 H^{k+1} = f^{k+1} & \text{on } \Omega \\ u^{k+1} = g_D & \text{on } \Gamma_D \\ \frac{\partial u^{k+1}}{\partial n} = g_N & \text{on } \Gamma_N \\ H_0 = H(x;0) & \text{on } \Omega, \end{cases}$$

Taking into account boundary conditions and discretizing them by using normal difference quotients we can write the problem (P_h) in the matrix form

$$MH^{k+1} + AU^{k+1} = F^{k+1}. \tag{1}$$

In the equation (1) the vector H^{k+1} contains the nodal values of the enthalpy and the vector U^{k+1} nodal values of the temperature at the time level $k+1$. The matrix A is the usual 5-point difference approximation for the Laplacian operator, and M is the matrix form for the operator $\partial_t + v\partial_2$. The right-hand side vector $F^{k+1} = \tilde{F}^{k+1} + \tau^{-1}H^k$ contains all known nodal values of the problem (P_h).

Characteristic scheme

For the characteristic scheme the discretization of the convection term differs from the upwind scheme. To approximate the term $\left(\frac{\partial}{\partial t} + v(t)\frac{\partial}{\partial y}\right)H$ we use the characteristics of this first order differential operator. Namely if (x_1, x_2, t) is the grid point on the time level t we choose the point $(x_1, \tilde{x}_2, t-\tau) = (x_1, x_2 - \int_{t-\tau}^{t} v(\xi)d\xi, t-\tau)$ on time level $t-\tau$ and approximate the term

$$\left(\frac{\partial}{\partial t} + v(t)\frac{\partial}{\partial x_2}\right)H \approx \frac{H(x_1, x_2, t) - H(x_1, \tilde{x}_2, t-\tau)}{\tau}.$$

Generally the point $(x_1, \tilde{x}_2)$ is not the grid point so we use linear interpolation for the function H. If

$$(x_1, \tilde{x}_2) = \alpha(x_i, x_{j-1}) + (1-\alpha)(x_i, x_j), \qquad \alpha \in (0,1),$$

where (x_i, x_{j-1}) and (x_i, x_j) are grid points, then we put

$$H(x_1, \tilde{x}_2, t-\tau) \equiv \tilde{H}(x_1, x_2, t-\tau) = \alpha H(x_i, x_{j-1}, t-\tau) + (1-\alpha)H(x_i, x_j, t-\tau).$$

Near the boundary $\{x_1 \in [0, l_1],\ x_2 = 0\}$ it can happen that $(x_1, x_2) \notin \Omega$. In that case we write

$$\tilde{H}(x_1, x_2, t-\tau) = \alpha(2h_2 H(g_i) + H(x_i, x_{j+1}, t-\tau)) + (1-\alpha)H(x_i, x_j, t-\tau).$$

Thus we can write the approximation as

$$\partial_\tau \tilde{H} = \left(\frac{\partial}{\partial t} + v(t)\frac{\partial}{\partial x_2}\right)H \approx \frac{H(x_1, x_2, t) - \tilde{H}(x_1, x_2, t-\tau)}{\tau}.$$

The problem (P) for the characteristic scheme can be written

$$(\tilde{P}_h) \qquad \begin{cases} \partial_\tau \tilde{H} - \Delta_h u^{k+1} = f^{k+1} & \text{on } \Omega \\ u^{k+1} = g_D & \text{on } \Gamma_D \\ \frac{\partial u^{k+1}}{\partial n} = g_N & \text{on } \Gamma_N \\ H_0 = H(x;0) & \text{on } \Omega, \end{cases}$$

Taking account boundary conditions and discretizing them by using normal difference quotients we can write the above equation also in the matrix form

$$\tilde{M}H^{k+1} + AU^{k+1} = F^{k+1}. \tag{2}$$

In the equation (2) the vectors H^{k+1}, U^{k+1} and the matrix A are the same as in the equation (1). In this case $\tilde{M}$ is a diagonal matrix of the form $\tilde{M} = \tau^{-1}I$, where the I is the identity matrix.

SOLVING ALGORITHM

For solving the problem (P_h) respectively $(\tilde{P}_h)$ at time level $k+1$ by using upwind or characteristic scheme we must solve the corresponding algebraic equation (1) or (2). The following calculation algorithm is used at every time step t^{k+1}, $k = 0, ..., nt-1$. For each time level t^{k+1}, set the initial guess $u^0 = u(x; t^{k+1} - \tau)$ moreover we assume that

$$H(u) = \begin{cases} \alpha_1 u + \gamma_1, & u < u_M - \varepsilon \\ \alpha_2 u + \gamma_2, & u \in [u_M - \varepsilon, u_M + \varepsilon] \\ \alpha_3 u + \gamma_3, & u > u_M + \varepsilon \end{cases}$$

where u_M is the phase change temperature. For theoretical backround of the algorithm see Elliot et Ockendon[7].

1 $j := 0$ (number of iterations)

2 $j := j + 1$; $i := 0$ (number of node)

3 $i := i + 1$

4 $z_i^j = f_i^{j-1} - \left(\sum_{l<i} A_{il} u_l^j + m_{il} H_l^j \right) - \left(\sum_{l>i} A_{il} u_l^{j-1} + m_{il} H_l^{j-1} \right)$

5

$$v_i^j = \begin{cases} \frac{z_i^j - m_{ii}\gamma_1}{m_{ii}\alpha_1 + a_{ii}}, & \text{if } z_i^j < (u_M - \varepsilon)(m_{ii}\alpha_1 + a_{ii}) + m_{ii}\gamma_1 \\ \frac{z_i^j - m_{ii}\gamma_3}{m_{ii}\alpha_3 + a_{ii}}, & \text{if } z_i^j > (u_M + \varepsilon)(m_{ii}\alpha_3 + a_{ii}) + m_{ii}\gamma_3 \\ \frac{z_i^j - m_{ii}\gamma_2}{m_{ii}\alpha_2 + a_{ii}}, & \text{else} \end{cases}$$

6 $u_i^j = u_i^{j-1} + \omega(v_i^j - u_i^{j-1})$

7 if $i < N$ (N=total number of nodes) goto 3

8 if $\|u^j - u^{j-1}\| > \epsilon$ goto 2, else STOP

NUMERICAL EXAMPLE

To illustrate the calculation speed and accuracy of the described above numerical schemes the following numerical example is considered.

Let $\Omega =]0,1[\times]0,1[$, with the boundary Γ divided in two parts $\Gamma_D = \{x_1 \in [0,1], x_2 = 1\}$ and $\Gamma_N = \Gamma \setminus \Gamma_D$, moreover let $T = 1$. Let us consider the case where the phase change temperature $u_M = 1$ and the latent heat $L = 1$. Let the phase change interval be $[u_M - \varepsilon, u_M + \varepsilon]$, $\varepsilon = 0.01$, and the velocity is $v(t) = \frac{1}{5}$.

Our numerical example is

$$\begin{cases} \frac{\partial H}{\partial t} - \Delta K + v(t)\frac{\partial H}{\partial x_2} = f(x;t) & \text{on } \Omega \\ u(x_1, 1; t) = (x_1 - \frac{1}{2})^2 + \frac{5}{4} - \frac{1}{2}e^{-4t} & \text{on } \Gamma_D \\ \frac{\partial u}{\partial n} = 1 & \text{on } \Gamma_N \\ u(x_1, x_2; 0) = (x_1 - \frac{1}{2})^2 + (x_2 - \frac{1}{2})^2 + \frac{1}{2} & \text{on } \Omega, \end{cases}$$

where

$$H(u) = \begin{cases} 2u & u < u_M - \varepsilon \\ \left(\frac{1+8\varepsilon}{2\varepsilon}\right)(u-1) + \frac{5+4\varepsilon}{2} & u \in [u_M - \varepsilon, u_M + \varepsilon] \\ 6u - 3 & u > u_M + \varepsilon \end{cases}$$

and

$$K(u) = \begin{cases} u & u < u_M - \varepsilon \\ \frac{3}{2}u - \frac{1-\varepsilon}{2} & u \in [u_M - \varepsilon, u_M + \varepsilon] \\ 2u - 1 & u > u_M + \varepsilon. \end{cases}$$

Furthermore

$$f(x;t) = \begin{cases} 4e^{-4t} + \frac{1}{5}(4x_2 - 2) - 4 & u < u_M \\ 12e^{-4t} + \frac{1}{5}(12x_2 - 6) - 8 & u > u_M. \end{cases}$$

The exact solution of our problem is

$$u(x_1, x_2, t) = (x_1 - \frac{1}{2})^2 + (x_2 - \frac{1}{2})^2 - \frac{1}{2}e^{-4t} + 1$$

The numerical test was run in the Sun Ultra Enterprise 4000 for different grid parameters h and τ. In table 1 the maximum iteration number, maximum cpu-time and maximum L_2-error of time levels $k = 1, ..., nt$ is presented as a function of parameter values.

		Upwind scheme			Characteristic scheme		
h	τ	ite	cpu [s]	L_2-error	ite	cpu [s]	L_2-error
$\frac{1}{4}$	$\frac{1}{8}$	23	$2.61 \cdot 10^{-2}$	$4.285 \cdot 10^{-2}$	21	$1.156 \cdot 10^{-2}$	$9.077 \cdot 10^{-2}$
$\frac{1}{8}$	$\frac{1}{16}$	43	0.115	$2.178 \cdot 10^{-2}$	40	$6.919 \cdot 10^{-2}$	$3.34 \cdot 10^{-2}$
$\frac{1}{16}$	$\frac{1}{32}$	76	0.346	$1.122 \cdot 10^{-2}$	74	0.246	$1.498 \cdot 10^{-2}$
$\frac{1}{32}$	$\frac{1}{64}$	127	0.647	$9.199 \cdot 10^{-3}$	127	0.427	$7.053 \cdot 10^{-3}$
$\frac{1}{64}$	$\frac{1}{128}$	205	0.794	$9.056 \cdot 10^{-3}$	205	0.623	$4.915 \cdot 10^{-3}$

Table 1. The comparison of upwind and characteristic methods. The parameters ite, cpu and L_2-error are the maximum number of iterations, calculation time and L_2-error of the time levels, respectively.

In this case it turned out that the both schemes need approximately the same amount of iterations to achieve the required accuracy of stopping criterion in the calculation algorithm.

However, the characteristic scheme was at least 30% faster than the upwind scheme. The main reason for that is the difference of the numerical approximation of the convection term. In the

characteristic method the convection term is included in time derivative and, hence, updated only once at every time level. In the upwind scheme the convection term is updated at every iteration step.

The both schemes seems to converge properly with respect to the change of grid parameters. The slower convergence of the upwind method, when the grid parameters are small, is probably due to the round off errors in the computer program.

CONCLUSIONS

The problem considered here is closely involved in continuous casting of metal alloys (steel, copper, aluminium). The study of fast calculation methods has practical interest because of the development of large and realistic simulation models which can be used in process simulation, control and optimization. Our future work is related to the study of the domain decomposition method (DDM) for solving the continuous casting problem[8]. The DDM is suitable for calculating the solution in multiprocessor computer.

References

1. Flemings, M.C.: Solidification Processing, McGraw-Hill, New York 1974.

2. Samarkii, A.A., Vabischchevich, P.N., Iliev, O.P., Churbanov, A.G.: Numerical Simulation of convection/diffusion problems. *Int. J. Heat Mass Transfer* **36**, pp 4095-4106, 1993

3. Swaminathan, C.R., Voller, V.R.: A general enthalpy method for modeling solidification processes. *Metall. Trans. B* **23**, pp 651-664, 1992

4. Swaminathan, C.R., Voller, V.R.: On the enthalpy method. *Int. J. Num. Meth. Heat Fluid Flow* **3**, pp 233-244, 1993

5. Laitinen, E., Rekkilä, M., Tolvanen, M.: Control of steel solidification in continuous casting process. *9th CIMTEC-World Forum on New Materials Symposium I-Computational Modelling and Simulation of Materials*, Techna Srl. 1999, pp. 487-494

6. Louhenkilpi, S., Laitinen, E., Nieminen, R.: Real-time simulation of heat transfer in continuous casting. *Metall. Trans. B* **24**, pp 685-693, 1993

7. Elliot, C.M., Ockendon, J.R.: Weak and variational methods for moving boundary problems, Pitman, Boston, 1982.

8. Laitinen, E., Lapin, A.: Semi-implicit mesh scheme and splitting iterative methods for the solution of continuous casting problem. *Preprint, March 1999, Dep. of Math. Sci., University of Oulu, Finland*, pp. 19

A NOTE ON POSSIBLE FLOW INSTABILITIES IN MELTING FROM THE SIDE

Patrick Le Quéré[1] & Dominique Gobin[2]

[1]*LIMSI-CNRS, BP 133, F-91403 Orsay Cedex France*
[2]*Laboratoire FAST Bât. 502, Campus Universitaire F-91405 Orsay Cedex France*

We present a scale analysis of the parameters for which flow instabilities can be expected in coupled phase change-natural convection in cavities heated from the side. The results are in agreement with what was observed numerically for very low Prandtl number fluids, where multiple cells were found to appear at early time as a result of the instability of the conduction regime. For very large Prandtl number flow instabilities, if any, would only occur at very large nominal Rayleigh number.

CONVERGENCE OF PHASE–FIELD EQUATIONS TO THE STEFAN MODEL

Giulio Schimperna*

*Dipartimento di Matematica, Università di Pavia, via Ferrata 1, 27100 Pavia, Italy

Summary We discuss the convergence of the Caginalp–Fix phase–field model to the weak formulation of the Stefan problem. In particular, we address two related situations: first, we study the case of a single substance subject to this change of the solidification model; then, we try and repeat the convergence analysis to the case of two different adjoining fluids obeying to transmission conditions at the common boundary both for the temperature and for the phase field. In particular, we assume that the solidification law undergoes a variation only on one side: in this case, the convergence problem is solvable only under additional compatibility conditions, which we try and justify from both the mathematical and the thermodynamical viewpoints.

The phase–field problem

We consider a bounded smooth domain $\Omega \subset \mathbb{R}^n$ and fix $T > 0$; we also set $Q := \Omega \times]0, T[$. We begin by presenting the initial–boundary value problem for the standard (parabolic) phase–field model[1]: suppose that Ω is filled with an homogeneous and incompressible fluid and denote its temperature by θ and its *phase–field* by χ; then, the heat and phase diffusion inside Ω can be described by means of the system

$$\partial_t(\theta + \lambda\chi) - \operatorname{div}(k\nabla\theta) = f \quad \text{in } Q, \tag{1}$$

$$\mu_\varepsilon \partial_t \chi - \operatorname{div}(\nu_\varepsilon \nabla\chi) + \beta_\varepsilon(\chi) - c_\varepsilon \chi = \lambda\theta \quad \text{in } Q, \tag{2}$$

where the subscript ε is related to the subsequent limit procedure (for the present, do not consider it). Here, we have indicated by λ the latent heat, by k the thermal conductivity, by f a heat source term, by μ_ε the phase–relaxation parameter, by ν_ε the interfacial energy coefficient, and by $\beta_\varepsilon - c_\varepsilon$ the derivative of a Ginzburg–Landau double–well free energy potential. In particular, $\beta_\varepsilon(\chi)$ stays for its monotone part and $-c_\varepsilon\chi$ for the rest; in most physical cases, we have that $\beta_\varepsilon(r) = \kappa r^3$; anyway, also $\beta_\varepsilon(r) = \kappa|r|^p r$, for any $p \geq 0$, is a thermodynamically consistent choice, and other possibilities have also been considered in literature. For this reason, under a mathematical point of view, we assume β_ε to be a general *maximal monotone graph* in $\mathbb{R} \times \mathbb{R}$, while, at present, on account of the homogeneity of the fluid, $\lambda, k, \mu_\varepsilon, \nu_\varepsilon, c_\varepsilon$ are supposed to be strictly positive constant values.

If the above system is complemented through the initial and homogeneous Neumann conditions, it is not difficult to prove, by means of standard variational techniques, a related existence and uniqueness result[5] (which we do not report for brevity).

Convergence to the Stefan model

We now present, in the simple framework introduced above, the question of the convergence of the system (1–2) to a Stefan–like problem (in the weak formulation[2]) as the coefficients $\mu_\varepsilon, \nu_\varepsilon, c_\varepsilon$ tend simultaneously to 0 and the monotone graphs β_ε converge in a suitable sense to the inverse H of the Heaviside graph, which is given by $H(r) =]-\infty, 0]$ for $r = 0$, $H(r) = 0$ for $0 < r < 1$ and $H(r) = [0, +\infty[$ for $r = 1$. In particular, we have the following result

Theorem 1. *Suppose that, as $\varepsilon \to 0$, $\mu_\varepsilon, \nu_\varepsilon, c_\varepsilon$ and the ratio $c_\varepsilon/\mu_\varepsilon$ tend to 0; assume also that the operators β_ε G–converge to H in $\mathbb{R}$. Then, we have that the solutions (θ, χ) of the system (1–2) (which naturally depend on ε) tend in the suitable spaces to the solution $(\overline{\theta}, \overline{\chi})$ of the Stefan–like problem given by the equations*

$$\partial_t(\overline{\theta} + \lambda\overline{\chi}) - \operatorname{div}(k\nabla\overline{\theta}) = f \quad \text{in } Q, \tag{3}$$

$$H(\overline{\chi}) \ni \lambda\overline{\theta} \quad \text{in } Q, \tag{4}$$

together with homogeneous Neumann conditions (only for $\overline{\theta}$) at the boundary and with the initial condition for the variable $(\overline{\theta} + \lambda\overline{\chi})$, which has the physical meaning of enthalpy. ∎

The proof[6] of the above result relies on the derivation of some a priori estimates, independent of ε, for the solution of the system (1–2), together with a classical variational argument for general monotone operators, which is used to pass to the limit in the term $\beta_\varepsilon(\chi)$; note the inclusion symbol in (4), whose presence is due to H being a multivalued operator.

A transmission problem for the phase–field system

We now try and extend the preceding analysis to the more complicated case of a transmission problem; we begin by giving a related reinterpretation of the system (1–2) in this new situation. So, suppose that the set Ω is now split by a fixed smooth interface Γ into two subdomains Ω_1, Ω_2 of Lipschitz regularity; assume that Ω_1, Ω_2 are filled with two fluids, still homogeneous and incompressible, but of possibly different thermodynamical characteristics; set also $\Sigma := \Gamma\times]0,T[$, $Q_1 := \Omega_1\times]0,T[$, $Q_2 := \Omega_2\times]0,T[$.

As a first step, we suppose that both the substances in Ω_1, Ω_2 obey to diffusion equations similar to (1–2) and we make the constitutive assumption that transmission conditions hold at the interface Γ not only for the temperature, but also for the phase–field (later we shall discuss this point in some detail). To write the corresponding mathematical system in its precise form, anyway, it is not necessary to distinguish between the contributions of Ω_1 and of Ω_2; the expression (1–2) is still correct, provided that we interpret it as a differential system with discontinuous coefficients; so, we now suppose the $\lambda, k, \mu_\varepsilon, \nu_\varepsilon, c_\varepsilon$ be piecewise constant strictly positive functions assuming the constant values $\lambda_1, k_1, \mu_1, \nu_1, c_1$ on Ω_1 and $\lambda_2, k_2, \mu_{\varepsilon,2}, \nu_{\varepsilon,2}, c_{\varepsilon,2}$ on Ω_2 (again, for the present, do not consider the dependence on ε). More generally, in the following, for any function g defined on Ω, we shall write g_i to denote its restriction to Ω_i, the index i taking the values 1, 2. Furthermore, we also provide a reinterpretation of the graph β_ε, which is now supposed to be a nonlocal operator depending also on space, in the form

$$\beta_\varepsilon(x, v(x)) := \begin{cases} \beta_{\varepsilon,1}(v_1(x)) & \text{if } x \in \Omega_1, \\ \beta_{\varepsilon,2}(v_2(x)) & \text{if } x \in \Omega_2, \end{cases} \tag{5}$$

where $\beta_{\varepsilon,1}$ and $\beta_{\varepsilon,2}$ are still general maximal monotone graphs in $\mathbb{R}\times\mathbb{R}$.

In this setting, system (1–2) contains also (in an implicit form) the required compatibility and transmission conditions at the interface Γ; anyway, for clarity, we prefer to report them in detail:

$$\theta_1 = \theta_2 \quad \text{and} \quad \chi_1 = \chi_2 \quad \text{on } \Sigma, \tag{6}$$

$$\partial_{\mathbf{n}}\theta_1 = \partial_{\mathbf{n}}\theta_2 \quad \text{and} \quad \nu_1\partial_{\mathbf{n}}\chi_1 = \nu_2\partial_{\mathbf{n}}\chi_2 \quad \text{on } \Sigma. \tag{7}$$

Again, initial and Neumann boundary conditions on θ and χ have to be assumed in order that the above system (1–2)–(6–7) be solvable. In this case, it is worthwhile to state the related existence and uniqueness theorem in its precise formulation.

Theorem 2. *Suppose that $f \in L^2(Q)$, that homogeneous Neumann conditions are assumed on the unknowns θ and χ (more general choices are allowed) and that the initial conditions are required, in the form*

$$\theta(\cdot,0) = \theta_0, \qquad \chi(\cdot,0) = \chi_0 \quad \text{in } \Omega, \tag{8}$$

for some $\theta_0 \in L^2(\Omega)$ and $\chi_0 \in H^1(\Omega)$, also verifying $\beta_\varepsilon(\chi_0) \in L^2(\Omega)$. Then, the system (1–2) admits a unique solution of suitable regularity properties, provided that the graphs $\beta_{\varepsilon,1}$, $\beta_{\varepsilon,2}$ verify either of the following:

(CC)[4] *$\beta_{\varepsilon,2}(r) = \beta_{\varepsilon,1}(r) + \phi_\varepsilon(r)$ for any $r \in \mathbb{R}$ and for some Lipschitz-continuous function ϕ_ε (compatibility condition);*

(GC)[5] *$\beta_{\varepsilon,1}$ and $\beta_{\varepsilon,2}$ have at most a linear growth at infinity (growth condition; we point out that it could be slightly relaxed, particularly in a lower space dimension).* ∎

Why does the phase–field system seem not to be solvable in the general case? We can identify both a mathematical reason and a physical one and we start discussing the first: suppose to multiply equation (2) by the test function $\beta_\varepsilon(\chi)$ and to integrate over Q. In the case of a single substance, we can use the Gauss–Green formula to derive

$$-\int_0^T \int_\Omega \operatorname{div}(\nu_\varepsilon \nabla\chi)\, \beta_\varepsilon(\chi)\, dx\, ds = \int_0^T \int_\Omega \nu_\varepsilon\, \beta_\varepsilon'(\chi) |\nabla\chi|^2\, dx\, ds \geq 0 \tag{9}$$

(also on account of the monotonicity of β_ε); this allows to construct an L^2–a priori bound for $\beta_\varepsilon(\chi)$. However, this procedure is not always applicable in the transmission case, since the discontinuity of β_ε gives rise to nontrivial boundary terms on Γ, which can be controlled only under hypothesis (CC), i.e., when $\beta_{\varepsilon,1}$ and $\beta_{\varepsilon,2}$ "are not too different" (in the case of (GC) this problem does not appear, since the above estimate is no longer needed[5]). Indeed, this suggests also the physical reason: we believe that, for very different fluids, it is not thermodynamically plausible that transmission conditions for the phase–field are verified at the common boundary; maybe, it would be more suitable to consider a model with no diffusion across Γ for the unknown χ.

Convergence to the Stefan model: transmission case

We finally want to discuss in some detail the convergence of the above model to a mixed heat transmission problem between two fluids, one of which (Ω_1) obeys to the phase–field system, and the other (Ω_2) to the Stefan model; this corresponds to keeping fixed the contribution of Ω_1 to the system (1–2) and to perform the limit similarly as before, but now *only in the domain* Ω_2. We first state the convergence theorem and then give a number of related remarks.

Theorem 3. *Suppose that, for any $\varepsilon > 0$, (θ, χ) are solutions to system (1–2) in the transmission case and that $\beta_{\varepsilon,1}$, $\beta_{\varepsilon,2}$ are Lipschitz-continuous approximations (for instance Yosida-approximations) of the graphs $\beta_1(r) = \kappa r^3$ and $\beta_2 = H$, converging to them in the sense of G-convergence in $\mathbb{R}$. Indicate by L_ε the Lipschitz norm of $\beta_{\varepsilon,2}$. Assume also that $\mu_{\varepsilon,2}, \nu_{\varepsilon,2}, c_{\varepsilon,2}$, the ratio $c_{\varepsilon,2}/\mu_{\varepsilon,2}$ and the product $L_\varepsilon \nu_{\varepsilon,2}^p$ tend to 0 as $\varepsilon \to 0$, for some exponent $p \in]0, 1/4[$. Then, we have that, as $\varepsilon \to 0$, the solutions to the systems (1–2) converge in the appropriate spaces to a couple of functions $(\overline{\theta}, \overline{\chi})$, verifying*

$$\partial_t(\overline{\theta} + \lambda\overline{\chi}) - \operatorname{div}(k\nabla\overline{\theta}) = f \quad \text{in } Q, \tag{10}$$

$$\mu_1 \partial_t \overline{\chi}_1 - \operatorname{div}(\nu_1 \nabla \overline{\chi}_1) + \beta_1(\overline{\chi}_1) - c_1 \overline{\chi}_1 = \lambda_1 \overline{\theta}_1 \quad \text{in } Q_1, \tag{11}$$

$$\beta_2(\overline{\chi}_2) \ni \lambda_2 \overline{\theta}_2 \quad \text{in } Q_2. \tag{12}$$

Moreover, initial value conditions hold now for $(\overline{\theta} + \lambda\overline{\chi})$ *and for* $\overline{\chi}_1$, *the Neumann boundary conditions are verified for* $\overline{\theta}$ *on* $\partial\Omega\times]0,T[$ *and for* $\overline{\chi}_1$ *on* $\partial\Omega_1\times]0,T[$, *while the transmission conditions (6–7) hold now only for the unknown* $\overline{\theta}$. ∎

Concerning the above statement, we first remark that the limit operators β_1 and β_2 do not satisfy any of assumption (CC), (GC) (at the ε-step, instead, the Lipschitz continuity of $\beta_{\varepsilon,1}$, $\beta_{\varepsilon,2}$ guarantees both (CC) and (GC)). Anyway, the boundary conditions on Γ are now different: the fluid in Ω_1 is insulated as far as the phase transmission is concerned and the only diffusion which occurs across Γ is that of heat, as one would expect on behalf of physical considerations. Correspondently, the resolution of the limit system does not present the troubles described in (9).

Finally, we want to give an idea of the nontrivial mathematical procedure which we used to perform the passage to the limit; indeed, we notice that, as ε tends to 0, the Lipschitz norm of the ϕ_ε in (CC) blows up to infinity. Also, there is no hope of uniformity with respect to ε in condition (GC), since it is evident that L_ε tends to infinity too. We bypassed this difficulty by means of a different interpretation of system (1-2), essentially due to Damlamian, Kenmochi and Sato[3], in terms of the following monotone operators in the space $L^2(Q)$

$$\mathcal{A}_\varepsilon(v) = -\operatorname{div}(\nu_\varepsilon \nabla v) + \beta_\varepsilon(v), \qquad \mathcal{A}(v) = -\operatorname{div}(\nu_1 \nabla v_1) + \beta(v), \tag{13}$$

which also account for the space diffusion of phase and include, in their effective domains, the correct boundary conditions. In this way, the terms $-\operatorname{div}(\nu_\varepsilon \nabla \chi)$ and $\beta_\varepsilon(\chi)$ are estimated together and the integration by parts of (9) is no more required; however, we are now forced to prove a G-convergence for $\mathcal{A}_\varepsilon$ to $\mathcal{A}$ in the space $L^2(Q)$. This requires a careful use of singular perturbation techniques together with a fine interpolation inequality[6]; furthermore, the hypothesis $L_\varepsilon \nu_{\varepsilon,2}^p \to 0$ $(p < 1/4)$ seems essential in order to control some boundary terms still appearing on Γ.

The problem of the numerical study of the phase-field transmission problem and of its convergence to the above mixed statement is still open: in particular, it could be interesting to verify if the assumptions (CC) or (GC), required for the theoretical resolution of (1–2), result necessary also at the numerical exam; another problem could be that of investigating the optimality of the critical exponent 1/4 in the hypothesis $L_\varepsilon \nu_{\varepsilon,2}^p \to 0$, which we have assumed in the last limit procedure.

REFERENCES

1. Caginalp G.: An analysis of a phase field model of a free boundary, *Arch. Rational Mech. Anal.* **92**, pp. 205–245, 1986.

2. Damlamian A.: Some results on the multi-phase Stefan problem, *Comm. Partial Differential Equations* **10**, pp. 1017–1044, 1977.

3. Damlamian A., Kenmochi N., Sato N.: Subdifferential operator approach to a class of nonlinear systems for Stefan problems with phase relaxation, *Nonlinear Anal.* **23**, pp. 115–142, 1994.

4. Schimperna G.: Singular limit of a transmission problem for the parabolic phase–field model, *Appl. Math.*, to appear.

5. Schimperna G.: Abstract approach to evolution equations of phase–field type and applications, *J. Differential Equations*, submitted.

6. Schimperna G.: Some convergence results for a class of nonlinear phase–field evolution equations, *J. Math. Anal. Appl.*, submitted.

ERROR CONTROL OF FRÉMOND MODELS OF SHAPE MEMORY ALLOYS

Ulisse Stefanelli

Dipartimento di Matematica, Università di Pavia,
via Ferrata 1, 27100 Pavia, Italy

Summary. Existence results for the Frémond model of shape memory alloys have been often investigated by using a *time discretization* approach. Here, we present some error estimates for such approximations with respect to the full one-dimensional model and some three-dimensional models. These estimates show optimal rates of convergence, depend solely on data, and impose no costraints between consecutive time steps.

This communication is concerned with the following system of partial differential equations in terms of the unknown functions ϑ, $\boldsymbol{u}$, χ_1, and χ_2

$$\partial_t\big(c_0\vartheta - L\chi_1\big) + \partial_t\big((\alpha(\vartheta) - \vartheta\alpha'(\vartheta))\chi_2 \operatorname{div}\boldsymbol{u}\big) - h\Delta\vartheta \;=\; F + \alpha(\vartheta)\chi_2\partial_t \operatorname{div}\boldsymbol{u} \tag{1}$$

$$\operatorname{div}\big(-\nu\Delta(\operatorname{div}\boldsymbol{u})J + \lambda \operatorname{div}\boldsymbol{u}\, J + 2\mu\varepsilon(\boldsymbol{u}) + \alpha(\vartheta)\chi_2 J\big) + \boldsymbol{G} = \boldsymbol{0}, \tag{2}$$

$$k\partial_t\begin{pmatrix}\chi_1\\ \chi_2\end{pmatrix} \;+\; \begin{pmatrix}\ell(\vartheta - \vartheta^\star)\\ \alpha(\vartheta)\operatorname{div}\boldsymbol{u}\end{pmatrix} \;+\; \partial I_{\mathcal{K}}(\chi_1, \chi_2) \;\ni\; \begin{pmatrix}0\\ 0\end{pmatrix}, \tag{3}$$

fulfilled a.e. in $Q := \Omega \times (0, T)$, where Ω is a bounded open subset of $\mathbb{R}^d$, $1 \le d \le 3$, with smooth boundary $\partial\Omega$ and $T > 0$ stands for some final time. In addition, c_0, L, h, λ, μ, k, ℓ, and $\vartheta^\star$ are positive parameters, J is the identity matrix in $\mathbb{R}^d$, and ν is a nonnegative constant. Here, ε denotes the tensor

$$\varepsilon_{ij}(\boldsymbol{u}) = \frac{1}{2}\left(\frac{\partial u_i}{\partial x_j} + \frac{\partial u_j}{\partial x_i}\right) \quad \text{for } i, j = 1, \dots, d, \tag{4}$$

while $\partial I_{\mathcal{K}}$ stands for the subdifferential of the indicator function of $\mathcal{K}$, which is a nonempty, bounded, convex, and closed subset of $\mathbb{R}^2$, $F : Q \to \mathbb{R}$, and $\boldsymbol{G} : Q \to \mathbb{R}^d$ are source terms, and $\alpha : \mathbb{R} \to \mathbb{R}$ is a smooth function.

The nonlinear system (1)-(3) is concerned with the behaviour of *shape memory alloys* subject to thermo-mechanical treatments. These materials are metallic alloys which could be permanently deformed (avoiding fractures) and consequently be forced to recover the original shape just by thermal means.

At the microscopic scale, this phenomenon is interpreted as the effect of a structural phase transition between different configurations of the metallic lattices, namely the *austenite* and

its shared counterparts termed *martensites*[1]. Various models have been proposed to describe this behaviour from the macroscopic point of view. If we assume the different phases to coexist at each point of the shape memory sample and suppose that just two martensitic variants are present besides one austenite (in the three-dimensional space, 24 martensitic variants are actually present), indeed we deal with the approach proposed by Frémond[2]. In this context, ϑ has to be regarded as the absolute temperature of the shape memory body, while $\boldsymbol{u}$ accounts for its actual displacement and ε stands for the (linearized) strain tensor. Besides, $\alpha(\vartheta)$ represents the thermal expansion of the system, and thus it vanishes at high temperatures[1]. In our analysis α is also required to fulfil some compatibility conditions and properties complying with its actual physical behaviour[2]. Moreover, χ_1 and χ_2 are related to the volumetric proportions of the phases.

Existence of solutions to various problems concerning the system (1)-(3), supplied with suitable initial and boundary conditions, are well known[3]. These results often rely on a *time-discretization, a priori estimates, passage to the limit* procedure. Moreover, the uniqueness of the solution to these problems has also been proved either in one[4] or in three[5] space dimension.

On the basis of above cited results, this work[6,7] is addressed to the analysis of some estimates of the discretization error of (a variable step version of) such an approximation. For instance, letting $\mathcal{P}$ be a partition of the time interval $[0,T]$, namely

$$\mathcal{P} := \left\{0 = t^0 < t^1 < \cdots < t^{N-1} < t^N = T\right\}, \tag{5}$$

with variable step $\tau^i := t^i - t^{i-1}$ and diameter $\tau := \max_{1\le i\le N}\tau^i$, and denoting by F^i and $\boldsymbol{G}^i$ suitable appoximations of the functions F and $\boldsymbol{G}$, respectively, we deal with (a variational version of) the following scheme[3],

$$\begin{aligned}\left(c_0 - \Theta^{i-1}\alpha''(\Theta^{i-1})\mathcal{X}_2^{i-1}\operatorname{div}\boldsymbol{U}^{i-1}\right)\frac{\Theta^i-\Theta^{i-1}}{\tau^i} - h\Delta\Theta^i &= F^i + L\frac{\mathcal{X}_1^i-\mathcal{X}_1^{i-1}}{\tau^i}\\ &+ \left(\Theta^{i-1}\alpha'(\Theta^{i-1}) - \alpha(\Theta^{i-1})\right)\operatorname{div}\boldsymbol{U}^{i-1}\frac{\mathcal{X}_2^i-\mathcal{X}_2^{i-1}}{\tau^i}\\ &+ \Theta^{i-1}\alpha'(\Theta^{i-1})\mathcal{X}_2^{i-1}\frac{\operatorname{div}\boldsymbol{U}^i - \operatorname{div}\boldsymbol{U}^{i-1}}{\tau^i},\end{aligned} \tag{6}$$

$$\operatorname{div}\left(-\nu\Delta(\operatorname{div}\boldsymbol{U}^i)J + \lambda\operatorname{div}\boldsymbol{U}^iJ + 2\mu\varepsilon(\boldsymbol{U}^i) + \alpha(\Theta^i)\mathcal{X}_2^iJ\right) + \boldsymbol{G}^i = \boldsymbol{0}, \tag{7}$$

$$\frac{k}{\tau^i}\begin{pmatrix}\mathcal{X}_1^i-\mathcal{X}_1^{i-1}\\ \mathcal{X}_2^i-\mathcal{X}_2^{i-1}\end{pmatrix} + \begin{pmatrix}\ell(\Theta^i-\vartheta^*)\\ \alpha(\Theta^i)\operatorname{div}\boldsymbol{U}^{i-1}\end{pmatrix} + \partial I_{\mathcal{K}}(\mathcal{X}_1^i,\mathcal{X}_2^i) \ni \begin{pmatrix}0\\0\end{pmatrix}, \tag{8}$$

for $i = 1,\ldots,N$, along with proper initial and boundary conditions.

The main novelty of this work consists in dealing with three models derived from (1)-(3) and the corresponding discrete schemes obtained from (6)-(8), and deducing error estimates for such discretizations. Namely, we investigate the following models:

- 3-D MODEL. Consider (2)-(3) and replace (1) with

$$\partial_t\big(c_0\vartheta - L\chi_1\big) + \partial_t\big((\alpha(\vartheta) - \vartheta\alpha'(\vartheta))\chi_2 \operatorname{div} \boldsymbol{u}\big) - h\Delta\vartheta \;=\; F$$

- 3-D LINEARIZED MODEL[1]. Consider (2)-(3) and replace (1) with

$$\partial_t\big(c_0\vartheta - L\chi_1\big) - h\Delta\vartheta \;=\; F$$

- 1-D FULL MODEL[4]. Consider (1)-(3) in one dimension of space.
  Moreover, let $\nu = 0$, thus avoiding the regularizing fourth-order term in (2).

Concerning the 3-D model, we prove existence and uniqueness of the solution to an initial-boundary value problem. Consider that existence and uniqueness of solutions to both the 3-D linearized model and the 1-D full model have already been proved[1,4].

Next, we state the main results of this work by using a convenient notation. Given $\{W^i\}_{i=0}^N$ in the linear space $\mathcal{W}$, set

$$\overline{W}_{\mathcal{P}}(t) := W^i, \quad W_{\mathcal{P}}(t) := W^i + \frac{W^i - W^{i-1}}{\tau^i}(t - t^i) \tag{9}$$

for $t \in (t^{i-1}, t^i]$, $i = 1, \ldots, N$. Moreover, let $*$ denote the standard convolution product on $(0, t)$, namely $(a*b)(t) := \int_0^t a(t-s)b(s)ds$. Letting $(\vartheta, \boldsymbol{u}, \chi_1, \chi_2)$ and $\{\Theta^i, \boldsymbol{U}^i, \mathcal{X}_1^i, \mathcal{X}_2^i\}_{i=0}^N$ be solutions to the continuous 3-D model stated above and the related discrete scheme, respectively, and $\Theta_{\mathcal{P}}$, $\overline{\Theta}_{\mathcal{P}}$, $\mathcal{X}_{1,\mathcal{P}}$, $\mathcal{X}_{2,\mathcal{P}}$, $\boldsymbol{U}_{\mathcal{P}}$, $\overline{\boldsymbol{U}}_{\mathcal{P}}$, be defined as in (9), we have the existence of a positive constant C_1 such that

$$\text{3-D MODEL} \quad \begin{cases} \|\vartheta - \Theta_{\mathcal{P}}\|_{L^2(0,T;L^2(\Omega))} + \|1 * (\vartheta - \overline{\Theta}_{\mathcal{P}})\|_{C^0([0,T];H^1(\Omega))} \\ + \|\boldsymbol{u} - \boldsymbol{U}_{\mathcal{P}}\|_{L^2(0,T;(H^1(\Omega))^3)} + \|\operatorname{div} \boldsymbol{u} - \operatorname{div} \boldsymbol{U}_{\mathcal{P}}\|_{L^2(0,T;H^1(\Omega))} \\ + \displaystyle\sum_{j=1}^{2} \|\chi_j - \mathcal{X}_{j,\mathcal{P}}\|_{C^0([0,T];L^2(\Omega))} \le C_1\sqrt{\tau}. \end{cases} \tag{10}$$

Indeed, the same analysis applied to the 3-D linearized model allows the choice of a positive constant C_2 such that the order of convergence $o(\tau)$ is achieved. Namely, we establish the estimates

$$\text{3-D LINEARIZED MODEL} \quad \begin{cases} \|\vartheta - \Theta_{\mathcal{P}}\|_{L^2(0,T;L^2(\Omega))} + \|1 * (\vartheta - \overline{\Theta}_{\mathcal{P}})\|_{C^0([0,T];H^1(\Omega))} \\ + \|\boldsymbol{u} - \boldsymbol{U}_{\mathcal{P}}\|_{L^2(0,T;(H^1(\Omega))^3)} + \|\operatorname{div} \boldsymbol{u} - \operatorname{div} \boldsymbol{U}_{\mathcal{P}}\|_{L^2(0,T;H^1(\Omega))} \\ + \displaystyle\sum_{j=1}^{2} \|\chi_j - \mathcal{X}_{j,\mathcal{P}}\|_{C^0([0,T];L^2(\Omega))} \le C_2\,\tau, \\ \qquad\qquad \text{and} \\ \|\vartheta - \Theta_{\mathcal{P}}\|_{C^0([0,T];L^2(\Omega))\cap L^2(0,T;H^1(\Omega))} \le C_2\sqrt{\tau}. \end{cases} \tag{11}$$

Finally, with regard to the 1-D full model, hence retaining all the nonlinearities of equation (1), we achieve that the following estimate

$$\text{1-D FULL MODEL} \quad \begin{cases} \|\vartheta - \Theta_\mathcal{P}\|_{L^2(0,T;L^2(\Omega))} + \|1 * (\vartheta - \overline{\Theta}_\mathcal{P})\|_{C^0([0,T];H^1(\Omega))} \\ + \|u - \overline{U}_\mathcal{P}\|_{L^2(0,T;H^1(\Omega))} + \displaystyle\sum_{j=1}^{2} \|\chi_j - \mathcal{X}_{j,\mathcal{P}}\|_{C^0([0,T];L^2(\Omega))} \leq C_3\,\tau \end{cases} \tag{12}$$

holds for some positive constant C_3.

We point out that the constants C_1, C_2, and C_3 depend solely on data and, in particular, exponentially on T, since (10)-(12) are proved by using Gronwall's lemma. Moreover, let us stress that the first estimate in (11) and (12) are *optimal* with respect to the order of convergence, as we used the backward Euler's method to approximate time derivatives in (6) and (8). Since no *a priori* constraints between consecutive time steps are imposed in the present analysis, (10)-(12) ensure the possibility of implementing a step-by-step choice of time step sizes[8].

REFERENCES

[1] P. Colli, M. Frémond, and A. Visintin, *Thermo-mechanical evolution of shape memory alloys*, Quart. Appl. Math, 48:31–47, 1995.

[2] M. Frémond, *Matériaux à mémoire de forme*. C. R. Sci. Paris Sér. II Méc. Phys. Chim. Sci. Univers Sci. Terre, 304:239–244, 1987.

[3] P. Colli, *Global existence for the three-dimensional Frémond model of shape memory alloys*, Nonlinear Anal., 24(11):1565–1579, 1995.

[4] P. Colli and J. Sprekels, *Global existence for a three-dimensional for the thermodinamical evolution of shape memory alloys*, Nonlinear Anal., 18:873–888, 1992.

[5] N. Chemetov, *Uniqueness results for the full Frémond model of shape memory alloys*, Z. Anal. Anwendungen, 17(4):877–892, 1998.

[6] U. Stefanelli, *Error control of a three-dimensional Frémond model of shape memory alloys*, IAN-CNR, Pavia, Italy, preprint, 1999

[7] U. Stefanelli, *Error control of the full one-dimensional Frémond model of shape memory alloys*, IAN-CNR, Pavia, Italy, preprint, 1999

[8] R. Nochetto, G. Savaré, and C. Verdi, *Error control of nonlinear evolution equations*, C. R. Acad. Sci. Paris Sér. I Math., 326:1437-1442, 1998.

THE ENTRAINMENT OF FLUX INTO THE LUBRICATION GAP IN CONTINUOUS CASTING OF STEEL

Herbert Steinrück
Christian Doppler Laboratory for Continuous Solidification Processes
University of Technology Vienna, Wiedner Hauptstr. 7, 1040 Vienna, Austria

Summary In continuous casting flux powder is added on top of the melt. Due to the large temperatures the flux melts and flows into a small gap between the soldified strand shell and the mould. Due to the vertical oscillation of the mould depressions on the strand surface, so called oscillation marks, are formed. In this paper a model describing the interaction of the liquid flux with the solidifying strand shell is presented.

In continuous casting liquid metal is fed into a mould through a submerged nozzle. Intense coolig causes the metal to solidify. The solid shell is withdrawn downwards with casting speed u_c. Casting powder ('flux') is added on top of the mould. The flux melts and flows into a narrow gap between the mould and the solid strand. The mould oscillates vertically, causing depressions, so-called oscillation marks, on the strand surface. The forming of the oscillation marks and the early stages of solidification cannot be observed directly due to the large temperatures. Only indirect information is available. The depth of the oscillation marks and the net consumption of flux can be easily measured. More detailed information can be gained from break out shells. Metallurgists can deduce from the dendritic structure the cooling conditions. Thus two mechanisms of the formation of oscillation marks are proposed: *overflow* and *meniscus bending*. In the first case the steel shell solidifies at the meniscus and is overflown by liquid steel. In the second case due to the periodic motion of the mould the pressure in the flux varies periodically deforming the weak steel shell. Due to the withdrawl of the shell these deformations are frozen in as oscillation marks. Since these marks are the location of possible shell ruptures or breakouts an understanding of the early stages of solidification is needed.

In this investigation an attempt is made to model the interaction between the flow of flux, the molten steel and the solidified steel shell. The scope of the model is limited to the case of meniscus bending. Estimating the size of the meniscus region, where the oscillation marks are formed, gives a meniscus radius of about 5 mm. A typical gap width is below 1 mm. Compared with the dimensions of the mould, which has a cross section of about 0.2m×1.5m this is very small. Therefore a coupling of a computation of the strand shell dynamics and the global flow field in the melt does not seem appropriate. Hence a local model describing the interaction of the steel shell and the fluid flow of flux is developed.

The basic idea of the model is to use a thin layer approximation for the fluid flow of flux in the gap and the deformation of the steel shell. According to the three different states of steel (liquid, mushy, solid), the interface flux/steel can be devided into three different regions. At the top of the meniscus region the flux is in contact with the liquid steel. There the form of the interface is primarily determined by the pressure difference in both liquids and the interfacial tension. Near the meniscus the Reynolds lubrication approximation used for the flow of flux in the gap is not valid. There the velocity profiles differ significantly from parabolic profiles. However an asymptotic analysis with respect to a small Capillary number shows that the form of the interface obtained by the lubrication theory is in first order correct. As long as the apex of the steel shell is in the range where the lubrication theory holds we can expect reasonable results.

The mushy zone is modelled as a thin layer of a Newtonian fluid with a large effective viscosity depending on the fraction of solid. Using an asymptotic analysis with respect to a large aspect ratio of the mushy zone the flow field turns out to be extensional. However the pressure is transmitted perpendicular through the mushy zone. Thus the form of the interface is again determined primarily by the interfacial tension.

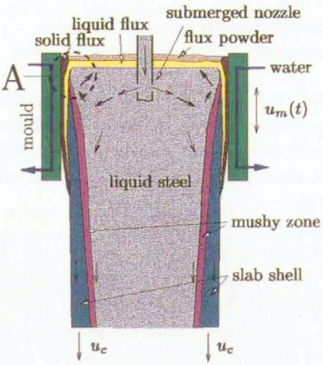

Fig. 1a: Continuous casting process

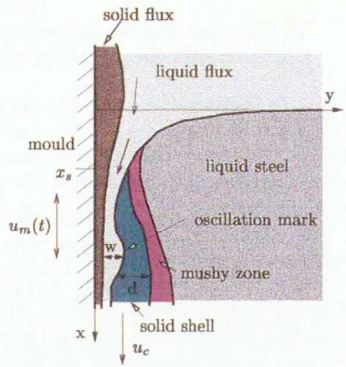

Fig. 1b: Detail A: Meniscus region

If the fraction of solid is above a certain value the steel shell is considered as solid. It is modelled as an elastic beam. However, it turns out, that even in the high temperature range the Young's modulus is so large, that the shell is almost rigid. Thus the deformations created at the meniscus remain almost unchanged.

The thichkness of the solid steel shell and the mushy zone are determined by the solution of the energy equation. The most primitve version of the model assumes a constant heat flux density across the mould and the flux gap. For the steel shell an integral method is employed using a parabolic temperature profile. Then the energy balance for a cross section of the steel shell is solved. Finally the thickness of the steel shell is determined, so that the boundary conditions at the interfaces to melt and the flux are satisfied.

At the interface to the melt the heat flux density has to be prescribed. It can be obtained from a flow and heat transfer simulation of the melt. Here we persue a different approach. The heat transfer coefficient between the shell and the melt is estimated on the basis of a turbulent flow in a channel.

The resulting equations are solved numerically. Starting from an arbitrary initial condition for the shape of the steel shell and the temperature distribution the equation are integrated. The numerical solution shows the expected behaviour: During the downstroke of the mould the gap opens at the meniscus and flux is sucked into the lubrication gap. During the upstroke the gap closes again and the deformation of the shell is frozen in as an oszillation mark.

As reference quantities the average flux consumption and the depth of the oscillation marks are computed and compared with plant observations.

It has been expected that after some initial transient behaviour a peridioc solution will develop. However, the numerical results show, that in genereral this is not the case. Moreover the solution, in particular the average gap width, seem to depend on the gap width of the prescribed initial condition. In conclusion although the local model of the meniscus behaviour gives some insight into the interaction od the strand shell with the flux further research is necessary.

NATURAL CONVECTION DURING ICE FORMATION: NUMERICAL SIMULATION VS. EXPERIMENTAL RESULTS

F. Stella[1], M. Giangi[1] & T.A. Kowalewski[2]
[1]Univ. Di Roma "*La Sapienza*", Via Eudossiana 18, I - 00184 Rome
[2]IPPT PAN, Polish Academy of Science, PL - 00049 Warsaw

Summary A numerical and experimental study of unsteady natural convection during freezing of water is presented. Mathematical model for the numerical simulation is based on the enthalpy-porosity method in vorticity-velocity formulation, equations are discretised on a fixed grid by means of a finite volume technique. Experiments are performed for water in a small differentially heated cube surrounded by air. In order to improve the capability of the numerical method to predict experimental results, a conjugate heat transfer problem was solved, with finite thickness and internal heat conductivity of the non-isothermal walls. These results have been compared with the simulations obtained for the idealised case of perfectly adiabatic side walls, and with our experimental findings. Results obtained for the improved numerical model show a very good agreement with the experimental data only for pure convection and initial time of freezing process. As time passes the discrepancies between numerical predictions and the experiment become evident, suggesting necessity for further improvements of the physical model used for freezing water.

MATHEMATICAL MODEL AND NUMERICAL TECHNIQUE

We consider convective flow in a cubic box filled with a viscous heat conducting liquid, which in this case is distilled water. Two opposite vertical walls of the box are assumed isothermal. One of them is held at temperature T_c= -10°C. It is below the freezing temperature of the liquid T_f= 0°C, hence the solid forms there. The opposite vertical wall is held at temperature T_h = 10°C. The other four walls of low thermal conductivity allow the entry of heat from the environment (air at temperature T_{ext}=25°C).

To improve our definition of the initial condition, so called „warm start" is performed. The freezing starts after the steady convection pattern is established in the cavity. This initial flow state corresponds to natural convection without phase change in the differentially heated cavity, with the temperature of the cold wall set to T_c=0°C. The freezing experiment starts, when at time t=0, the cold wall temperature suddenly drops to T_c= -10°C. In the numerical runs, the solution obtained for steady state natural convection was used as the initial flow and temperature fields to start the freezing calculations.

The numerical study of freezing water has been conducted on a fixed-grid by using a mathematical formulation based on the enthalpy porosity method [1]. One of the advantages of the fixed grid method is that an unique set of equations and boundary conditions is used for the whole domain, including both solid and liquid phase. It allows to avoid the problem of tracking the solid/liquid interface. The governing equations are obtained using averaged quantities [2] so the continuum velocity, density, and thermal conductivity are defined respectively as:

$$\mathbf{v}_m = f_s\mathbf{v}_s + f_l\mathbf{v}_l \tag{1a}$$

$$\rho_m = g_s\rho_s + g_l\rho_l \tag{1b}$$

$$k_m = g_s k_s + g_l k_l \tag{1c}$$

where $\mathbf{v}_l$, $\mathbf{v}_s$ are the velocity of the liquid and solid phase, f_l, f_s are the liquid and solid mass fraction, g_l, g_s are the liquid and solid volume fraction, ρ_l, ρ_s are the density of the liquid and solid phase. The volume fraction g is related to the mass fraction f_l and f_s via:

$$\rho f_s = \rho_s g_s$$
$$\rho f_l = \rho_l g_l$$

According to the saturated mixture conditions the mass and volume fractions must add to unity:

$$f_s + f_l = 1$$
$$g_s + g_l = 1$$

Under the assumptions that the liquid is Newtonian and incompressible, that the densities (ρ) and the specific heat (c) in the liquid $(\cdot)_l$ and solid $(\cdot)_s$ phases are equal and constant, the dimensionless governing equations in vorticity-velocity formulation result:

$$\frac{\partial \omega_m}{\partial t} + \nabla\times(\omega_m \times \mathrm{v}_m) = \mathrm{Pr}\,\nabla^2\omega_m + Ra\,\mathrm{Pr}\left\{-\theta - \sum_{i=2}^{N}\frac{a_i}{a_1}\Delta T^{(i-1)}\theta^i\right\}\left(\frac{g}{|g|}\right) + \nabla\times S \tag{2}$$

$$\frac{D\theta}{Dt} = \nabla\cdot\left(\bar{k}\nabla\theta\right) + B \tag{3}$$

$$\nabla^2\cdot\mathbf{v} = -\nabla\times\omega_m \tag{4}$$

Where a_i $(i = 1, N)$ are the coefficients in the polynomial density expression and $\Delta T = T_h - T_r$ is the temperature difference of the hot wall T_h and the phase interface T_r.
The dimensionless conductivity is defined as

$$\bar{k} = (1 - f_l)\frac{k_s}{k_l} + f_l,$$

in such a way in the liquid zone ($f_l = 1$) $\bar{k} = 1$ and in the solid zone ($f_l = 0$) $\bar{k} = k_s / k_l$.
In the momentum equation the Boussinesq approximation has been assumed, so the non linear density variation has been considered only into the buoyancy term.
The source term of Darcy type [2] has been adopted in the momentum equation to gradually reduces velocity in the solidifying zone:

$$S = \frac{-C(1 - f_l)^2}{(f_l^3 + q)}\mathrm{v}_m$$

Where C is a large constant value and q is a computational small quantity used to avoid singularity in solid zone ($\cong 10^{-3}$).

In the energy equation (3) the last term at the right-side:

$$B = -\frac{1}{\mathrm{Ste}}\frac{\partial f_l}{\partial t}$$

takes into account the latent heat due to the phase change.
The governing equation eq. (2-4) are discretized using a finite volume method technique on a staggered grid. A fully implicit method has been adopted for the mass and momentum equations, while the temperature field is solved separately in order to evaluate the variation in the local liquid phase. The two linearised algebraic systems are solved using a preconditioner BI-CGStab method [3].
At each time step the liquid fraction f_l and the temperature field θ in eq. (3) are solved by using an iterative procedure. At the time step $n+1$ the initial iterative fields are initialized to previous time step n then the following iterative system (5)-(7) is solved:

$$Ste\left(\frac{\theta^{i}-\theta^{n}}{\Delta t}\right)+Ste\nabla\cdot\left(\mathrm{v}^{n}\cdot\theta^{i}\right)=Ste\nabla\cdot\left(\bar{\mathrm{k}}\nabla\theta^{i}\right)+\frac{f_l^{i}-f_l^{i-1}}{\Delta t} \tag{5}$$

$$f_l^{i}=f_l^{i-1}+Ste\left(\theta^{i}-\theta_s\right) \tag{6}$$

Subject to the following constraint:

$$f_l^{i}=\max\left[0,\min\left(f_l^{i},1\right)\right] \tag{7}$$

where i is the index of iteration level, Δt the time step discretization and θ_s the phase change temperature.
The steps (5)-(7) are repeated until $\left\|f_l^{i}-f_l^{i-1}\right\|<\varepsilon$ and $\left\|\theta^{i}-\theta^{i-1}\right\|<\varepsilon$ with $\varepsilon\cong 10^{-8}$.

SELECTED RESULTS

Experimental validation of the numerical model is the main aim of our project. For this purpose quantitative information about the phase front position as well as about velocity and temperature fields within a domain of a mid-height vertical plane of the cavity are collected in the experiments. For this purpose the flow images of liquid crystal tracer have been collected periodically using 3CCD colour camera and frame grabber. Digital evaluation of images allows us to evaluate both velocity (PIV) and temperature fields (PIT) for the selected 2-D flow cross-section [4,5].

Natural Convection

At the beginning, our interest was directed to verify numerical solutions obtained for natural convection of water in the vicinity of the freezing point. In the experiments the cold wall temperature was set to 0°C, and the hot wall to +10°C. The effects of density inversion and of the thermal boundary conditions at non-isothermal walls on the flow structures are studied to compare and eventually improve the numerical code.

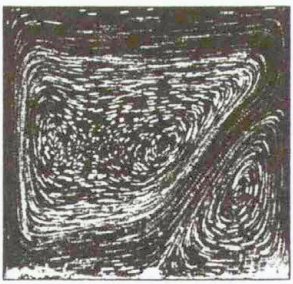

Natural convection flow pattern (traces)

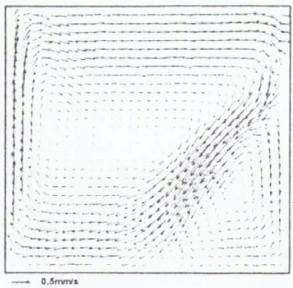

Natural convection velocity field (PIV)

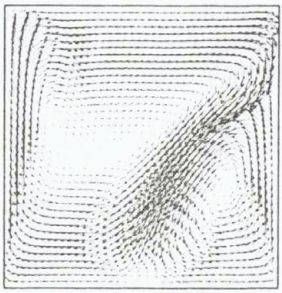

Numerical simulation adiabatic walls. Stream function (left), velocity field (right)

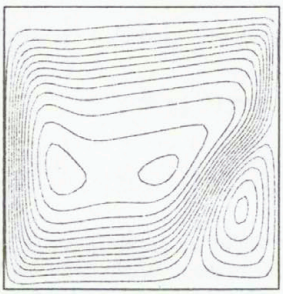

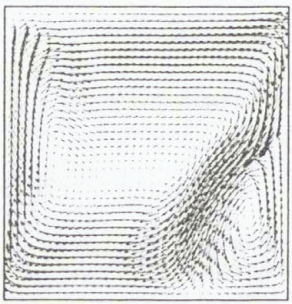

Numerical simulation conducting walls. Stream function (left), velocity field (right)

Figure 1. Velocity field in the centre vertical plane, comparison of the experimental and numerical results for natural convection of water; Th=10°C, Tc=0°C.

A typical flow structure (comp. Figure 1) exhibits two recirculation regions, upper one, where the water density decreases with temperature, and the lower region with an abnormal density variation. Similar flow pattern exhibits numerical solution, however several discrepancies are present. Numerical experimentation with the thermal boundary conditions posed at non-isothermal walls has shown that the calculated flow pattern strongly depends on the modelling used. Small changes of the heat flux through these "passive" walls evidently shifts the saddle point present at the cold wall, modifying dimension of both counter-rotating flow structures.

It was concluded, that neither isothermal or constant heat flux models are sufficiently accurate to obtain observed flow structures. Observed flow configuration, with two interacting cold and warm counter-rotating circulation, appears to be very sensitive to changes of the heat flux through side walls. Hence, direct comparison of the numerical and experimental results is necessary to verify assumptions made for heat transfer coefficients at the external surfaces. Solving the coupled solid-fluid heat conduction problem together with the Navier-Stokes equations evidently improved modelling of the flow pattern, but still empirical values for the air-wall heat flux coefficients have to be used.

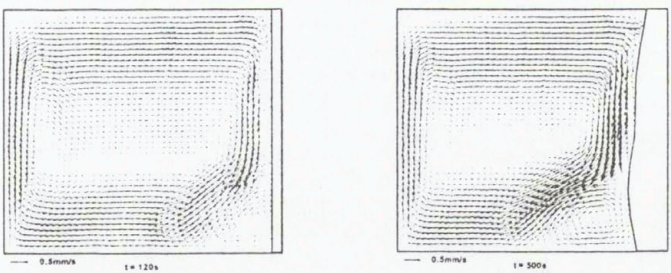

Measured (PIV) velocity field at t=120s t=500s

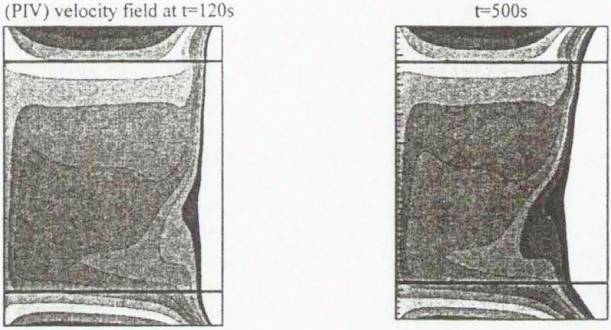

Calculated temperature field at t=120s t=500s

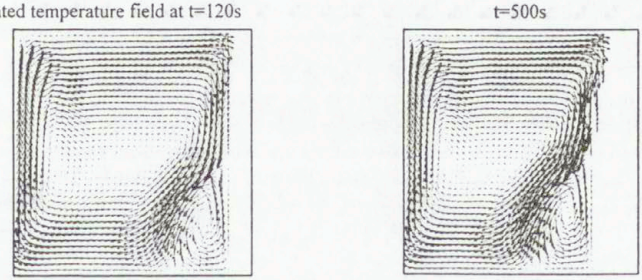

Calculated velocity field at t=120s t=500s

Figure 2. Freezing of water: measured and calculated flow field at 120s and 500s after freezing starts from the steady convective flow; Th= 10°C, Tc= -10°C.

Freezing of water

When freezing starts from developed flow, the thermal boundary conditions at the cold side remain the same, i.e. 0°C isothermal surface. However, interaction of the convective flow with the freezing front causes deformation of initially flat freezing plane. The „hot" circulation melts upper parts of the ice front, diminishing ice growth rate in this region. The „abnormal" flow circulation, located in the lower part of the cavity, transports the cold liquid up along the adjacent ice surface and back to the bottom along the isotherm of the density extreme. This cold water circulation only moderately modifies the heat balance at the interface. The convective heat transfer between both upper and lower regions seems to be limited mainly to the upper right corner of the cavity. There, along the colliding cold and warm fluid layers, the heat is transferred from the hot wall to the lower parts of the cavity. The shape of the freezing front reproduces this interaction, almost doubling the ice growth rate at the bottom.

Comparison of the measured and calculated (comp. Figure 2) ice fronts indicates qualitative agreement. For short time (first 500s), there is also quite good quantitative agreement between simulated and experimental results. However, with progressing development of the solidus differences of the front shape appear to grow. Especially lower parts of the ice front suffer evident errors in modelling. Numerical counter-clockwise circulation at the lower parts seems to be more effective in decreasing ice growth. In the experiments the ice surface remains almost perpendicular to the bottom wall, whereas in the numerical results for large time its shape declines strongly back into the cold wall.

FINAL REMARKS

The results obtained show a very good agreement between numerical and experimental results for initial time of this transient process. The agreement progressively decreases for longer experimental time. One of our future aims is to improve the capacity of the prediction of the numerical model for long time simulation. Since at longer time the ice layer is quite thick, it seems important to correct our model of thermal conductivity inside solidus. Non-uniformity of the ice structure, dendrites, and impurities due to the solved gases may force us to verify the assumption used about isotropy of the thermal properties of the ice. Another important point is the analysis of the effects of by supercooling. Our experiments with freezing water indicate that in most of the cases distilled water cools to about -7°C before phase change begins. The observed effect of supercooling qualitatively changes the onset of freezing.

REFERENCES

1. Voller V.R., Cross M. and Markatos N.C.: An enthalpy method for convection-diffusion phase change, *Int. J. Num. Meth. Eng.*, **24**, pp. 271-284, 1987.
2. Slattery J.C.: Momentum energy and mass transfer in continua, *Kieger*, New York, 1978.
3. Van De Worst H.: A fast and smoothly converging variant of Bi-Cgstab for the solution of non-symmetric linear systems, SIAM, *J. Sci. Stat. Comput.*, **132**, pp. 631-644, 1992.
4. Kowalewski T.A., Rebow M.: *An experimental benchmark for freezing water in the cubic cavity* in Advances in Computational Heat Transfer CHT-97 , Begel House Inc.; pp.149-156; New York, 1998.
5. T.A. Kowalewski, A. Cybulski, M. Rebow: *Particle Image Velocimetry and Thermometry in Freezing Water* 8th Int. Symposium on Flow Visualization, Sorrento, eds. G.M. Carlomagno and I. Grant, CD ROM Proceedings ISBN 0953399109 , pp. 24.1-24.8, Edinburgh, 1998.

Y DISTRIBUTION IN Ba-Cu-O MELT DURING GROWTH OF SUPERCONDUCTING MATERIAL Y123 BY CZOCHRALSKI METHOD

Janusz S. Szmyd*, Krzysztof Gajek* & Kenjiro Suzuki**
*University of Mining and Metallurgy, Mickiewicza 30, 30-059 Krakow, Poland,
**Kyoto University, Kyoto 606, Japan,

Summary Numerical computations of the yttrium distribution in the BaO-CuO melt were performed for the yttrium barium copper oxide superconductor ($YBa_2Cu_3O_{7-x}$) single crystal growth by the Czochralski method. The finite volume method with staggered numerical grid was used to calculate the fluid flow, heat transfer and yttrium distribution in the melt. The flow in the melt was assumed to be axisymmetric and was modelled as an incompressible Newtonian, Boussinesque fluid. Heat transfer was due to both convection and diffusion. Calculations were presented for a combination of buoyancy - driven flow and crystal - rotation driven flow.

INTRODUCTION

Since discovery in 1987 of superconductivity at ~90 K in a new mixed-phase compound system, an enormous amount of attention has been given to the improvement of its quality. One of the most seriously studied compounds is the yttrium barium copper oxide superconductor $YBa_2Cu_3O_{7-x}$ (Y123). In 1993 continuous growth of $YBa_2Cu_3O_{7-x}$ (Y123) large single crystals was achieved by applying a modified Czochralski method.[1] The quality of the crystal of yttrium barium copper oxide superconductor $YBa_2Cu_3O_{7-x}$ (Y123) grown from a melt by this method is significantly affected by heat and mass transfer in the melt during growth. In an Y123 single crystal growth system the Y123 single crystal grows directly from the liquid phase as a primary phase by the migration of Y atoms from the solute Y_2BaCuO_5 (Y211) on the bottom of the melt to the free surface. The Y123 crystal grows continuously as long as the nutrient Y211 exists. In this method, convection in the melt is an important factor in controlling the distribution of Y atoms in the melt, due to the high Schmidt number of the melt ($Sc \cong 7000$). It is well known that the quality of substrates depends on the conditions for crystal growth such as the crystal pulling rate and temperature distribution on the wall of the crucible. Therefore it is very important to understand melt motion, and fluctuation of temperature in the melt to obtain bigger and higher quality single crystal. Studies on the dynamic patterns of convection in a Czochralski melt are numerous. However, a detailed convective flow pattern in the melt for the Y123 single crystal growth process has not yet been clearly presented. A recent publication of Namikawa *et al.*[2] shows some numerical calculation results for steady state melt convection. However, the numerical results obtained by Szmyd *et al.*[3, 4] for similar boundary conditions show periodically oscillating convection, it was found that thermal boundary condition seriously affect the instability of the melt flow.[5, 6] A recent publication of Yamauchi *et al.*[7] shows necessity of unsteady three-dimensional computation for the melt flow of the Y123 production process by Czochralski method. In this study, numerical computation of the flow, thermal and Y atoms concentration fields in the melt were performed for the yttrium barium copper oxide superconductor ($YBa_2Cu_3O_{7-x}$) single crystal growth by the Czochralski method assuming the steadiness of the melt flow. Calculations are presented for a combination of buoyancy-driven flow and flow driven by crystal rotation.

FORMULATION AND NUMERICAL SCHEME

A crystal with radius R_x grew from the cylindrical melt in a crucible with radius R_c and depth H_l. The melt is bounded at the top center by a coaxially mounted crystal rotating with angular velocity

Ω_x. The melt free surface around the crystal is assumed to be flat and free from surface tension effect. The crystal interface is assumed to be kept at temperature T_x, and Y concentration is assumed to be constant there at $C=C_x(T_x)$[8, 9]. Temperature and Y concentration at the bottom of the melt are assumed respectively to be T_c, and $C=C_c(T_c)$ [8, 9] Melt flow is assumed to be axisymmetric. The fluid is considered to be incompressible, Newtonian, Boussinesque and its properties are taken to be constant. The flow, thermal and yttrium concentration fields in the melt were calculated numerically by the control - volume - based finite difference method[10] (numerically solving the finite-difference equivalents of the momentum, energy and concentration equations). Staggered grids were used for the velocity components. The SIMPLER algorithm[10] was used to solve the pressure. The central finite difference approximation was applied for the diffusion terms while for the convection terms the QUICK scheme[11] was used. The present scheme was based on fully implicit discretization schemes taking into account the unsteady terms of governing equations. The ADI (Alternative - Direction - Implicit Method)[12] was combined in the iterative procedure at each time step to solve the algebraic equations. The grid points were uniformly allocated in r - z plane and total number of grid points was 96 x 104. The time step was $\Delta t^* = 10^{-6}$ (where t^* is non-dimensional time $t^* = t \nu / R_x^2$).

Numerical computation was carried out for H_l / R_c = 1.1, 1.0, 0.95, 0.8 and for Grashof number Gr = 10000, for seven different Reynolds numbers, Re_x = 0, 10, 20, 30, 40, 50, 60 (for $Re_x = 0$ the problem is one of natural convection). The Reynolds and Grashof numbers are defined as $Re_x = (R_x^2 \Omega_x) / \nu$, Gr = $[g\beta(T_c-T_x) R_c^3]/\nu^2$. The temperature of the vertical wall of the crucible varies linearly (from $z=0$ to $z=H_c$) from T_c to $T_c-\Delta T$ (where ΔT is temperature difference between the bottom and the top of the crucible vertical wall) and ΔT = 3 [K]. Radiative heat loss from the melt free surface to the surrounding environment was calculated applying following equation: $-\lambda \partial T/\partial n = \sigma \varepsilon(T^4-T_o^4)$, where n is normal to the interface, σ is Stefan Boltzmann constant ($\sigma = 5.6667 \times 10^{-8}$ [W/(m^{2}K^4)], ε is the emissivity from the surface (ε = 0.7) and temperature T_o =1243 [K]. The concentration buoyancy effect is negligible due to a low yttrium concentration in the BaO-CuO melt. Y concentration in the melt is of the order of 3.65 kg/m^3 at the melt surface and 3.76 kg/m^3 at the melt bottom (density of the melt ρ=5500 kg/m^3). Therefore the term $g\beta_c(C - C_m)$ can be assumed to be negligibly small.

NUMERICAL RESULTS

The calculations were performed for the CPU time 10^5 [s] = 27.77 hours (In practices, it takes about two weeks to obtain a Y123 single crystal by applying Czochralski method if H_l and R_c are assumed to be 25mm and 23mm respectively). First is discussed the case where H_l / R_c = 1.1. Figure 1 illustrates some examples of the numerical results for Gr = 10000 and Re_x = 0, 10, 20, 30, 40, 50, respectively. Each figure shows half of the vertical section of the melt, and the vertical lines at the left-hand side of the figures indicate the centre line of the crucible. These figures consist of the Y concentration field (upper part), isotherms of the melt (central part) and the velocity vectors (lower part). Examples of the calculated Y distribution in BaO-CuO melt at $z^* = z / H_l$ = 0.99 for H_l / R_c = 1.1, 1.0, 0.95, 0.8 are shown in Figure 2. The following conclusion may be drawn from these results. Yttrium concentration field in Ba-Cu-O melt is strongly connected with velocity field, due to a high Schmidt number in the melt, and is strongly connected with temperature field, due to the temperature dependence of Y solubility in the BaO-CuO solution.

A comparison of figures demonstrates that thermally driven convection is dominant as crystal rotation Ω_x is low, there is almost no difference between the case Re_x=0 and the case Re_x=10. When the crystal rotation Ω_x is increased flow near the melt bottom becomes less significant. Near the top free surface outward forced convection exists and below the crystal a reticulating flow is

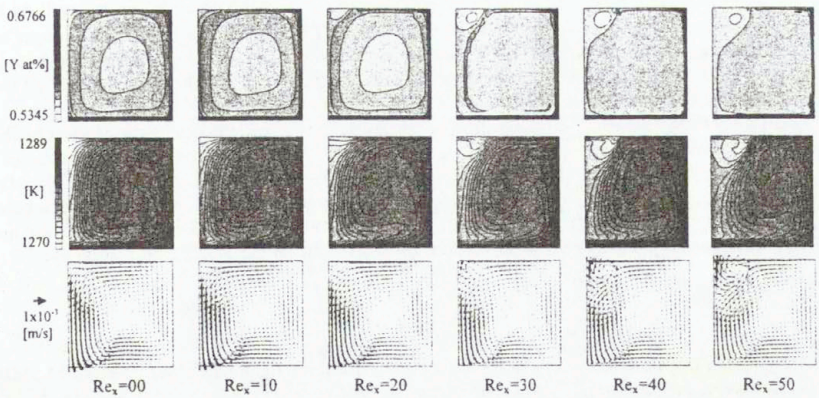

Fig. 1. Y distribution in Ba-Cu-O melt, isotherms and velocity vectors for Gr = 10000

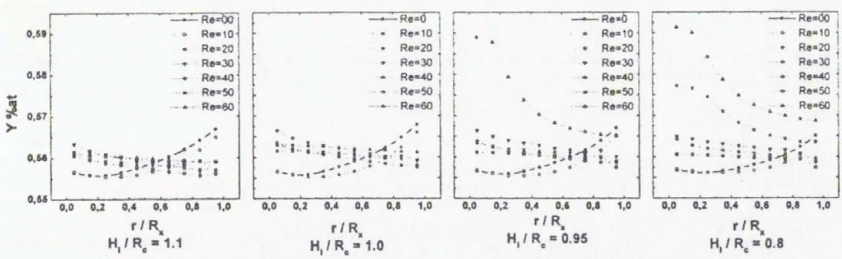

Fig. 2. Y distribution in Ba-Cu-O melt at $z^* = 0.99$ for H_l / R_c = 1.1, 1.0, 0.95, 0,8
(Gr = 10000 and Re_x =0, 10, 20, 30, 40, 50, 60)

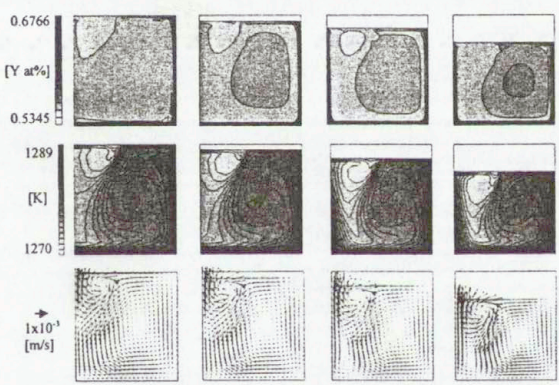

Fig. 3. Y distribution in Ba-Cu-O melt, isotherms and velocity vectors for Gr=10000, Re_x=60
(H_l / R_c=1.1, 1.0, 0.95, 0,8)

incurred. On the other hand, natural convection is generated near the crucible vertical wall by the buoyancy force. As the crystal rotation Ω_x is increased the forced convection becomes stronger and yttrium distribution in the melt BaO-CuO becomes more uniform (see Fig. 1). Figures 2 and 3 present other interesting results. As the melt depth H_l decreases, Y distribution in BaO-CuO melt becomes non-uniform below the crystal ($z^* = z / H_l = 0.99$) for Re_x=60. This is a consequence of the flow structure below the crystal where up – flow appears close to the axis of the crucible. When the melt depth is decreased from $H_l / R_c = 1.1$ to $H_l / R_c = 0.8$, a strong up–flow becomes to prevail below the whole crystal and produces a steep temperature gradient. The interface temperature is increased and yttrium distribution becomes non-uniform in the BaO-CuO melt below the crystal. As evidently seen in Fig.2, the crystal rotation should be reduced with decreasing melt depth in order to keep a nearly uniform yttrium distribution below the crystal.

CONCLUSIONS

Numerical computations of the yttrium distribution in the BaO-CuO melt were performed for the yttrium barium copper oxide superconductor ($YBa_2Cu_3O_{7-x}$) single crystal growth by the Czochralski method. The flow in the melt was assumed to be axisymmetric and was modelled as an incompressible Newtonian Boussinesque fluid. Calculations were presented for different melt depth. for a combination of buoyancy - driven flow and crystal-rotation driven flow. An appropriate crystal rotation rate appears to keep the temperature constant at the crystal – melt interface and the crystal rotation should be reduced with decreasing melt depth in order to keep a nearly uniform yttrium distribution in BaO-CuO solution below the crystal.

Acknowledgements
This research was supported in part by National Committee for Scientific Research, (Grant KBN 7T08B00916).

REFERENCES

1. Yamada Y., Shiohara, Y.: Continuous crystal growth of $YBa_2Cu_3O_{7-x}$ by the modified top - seeded crystal pulling method, *Physica C*, **217**, pp. 182 – 188, 1993.
2. Namikawa Y., Egami M., Shiohara Y.: Numerical calculation of the crystal rotation effect on $YBa_2Cu_3O_{7-x}$ single crystal growth by the puling method, *J. Mater. Res.*, **11**, pp. 288 -295, 1996.
3. Szmyd J.S., Yamamoto T., Bueckle U., Suzuki K.: Flow and thermal field computation of the melt for superconductor $YBa_2Cu_3O_{7-x}$ single crystal growth by the modified Czochralski method, *Proc. 1st JSPS - NUS Seminar on Integrated Engineering; Computer Applications in Engineering*, Kyoto, Vol. 1, pp. 152-163, 1996.
4. Szmyd J.S., Yamamoto T., Suzuki K., Bueckle U.: An analysis of the melt convection for superconductor $YBa_2Cu_3O_{7-x}$ single crystal growth by the modified Czochralski method, *Proc. 10th International Symposium on Transport Phenomena in Thermal Science and Process Engineering;* Kyoto, Vol. 3, pp. 643-648, 1997.
5. Szmyd J.S., Yamamoto T., Suzuki K.: Numerical analysis of oscillatory convection in the melt for superconductor $YBa_2Cu_3O_{7-x}$ single crystal growth by a modified Czochralski method, *Heat Transfer 1998, Proceedings of 11th International Heat Transfer Conference*, ed. J.S. Lee, Taylor & Francis, Levittown, Vol. 4 pp. 289-294, 1998.
6. Szmyd J.S., Mika G., Suzuki K.: Convection in an Y-Ba-Cu-O melt during crystal growth by Czochralski method, Advanced Computational Methods in Heat Transfer, Computational Mechanics Publications, Southampton, pp. 223-232, 1998.
7. Yamauchi T., Mika G., Szmyd J.S., Suzuki K.: Unsteady tree-dimensional melt flow computation of Czochralski single crystal growth of super-conducting material, (to publish elsewhere).
8. Yamada Y., Krauns Ch., Nakamura M., Tagami M., Shiohara Y.: Growth rate estimation of $YBa_2Cu_3O_{7-x}$ single crystal growth by crystal pulling, *J. Mater. Res.*, **10**, No. 7, pp. 1601-1604, 1995.
9. Krauns Ch., Sumida M., Tagami M., Yamada Y., Shiohara Y.: Solubility of RE elements into BA-Cu-O melts and enthalpy of dissolution, *Phys. B*, **96**, pp. 207-212, 1994.
10. Patankar, S.V.: Numerical Heat Transfer and Fluid Flow, Hemisphere, New York, 1980.
11. Leonard, B.P.: A stable and accurate convective modelling procedure based on quadratic upstream interpolation, *Compt. Meths. Appl. Mech. Eng.*, **19**, pp. 59 – 98, 1979.
12. Roache, P.J.: Computational Fluid Dynamics, Hermosa Publishers, Albuquerque, 1976.

EFFECTS OF THERMAL CONDUCTIVITIES ON HEAT AND MASS TRANSFER DURING DIRECTIONAL SOLIDIFICATION

V. Timchenko*, M. El Ganaoui**, E. Leonardi*, P. Bontoux** and G. de Vahl Davis*

*School of Mechanical and Manufacturing Engineering
The University of New South Wales, Sydney, Australia 2052

**Département de Modélisation Numérique
I.R.P.H.E. UMR CNRS 6594
38, rue Frederic Joliot-Curie, 13451 Marseille, France

Summary The effects of unequal thermal conductivities in the liquid and solid phase during directional solidification in Bridgman configurations are investigated. Numerical solutions are obtained based on a fixed grid single domain (enthalpy) method using two different approaches - finite volume with primitive variables and finite difference vorticity-stream function formulation. The cases of transient phase change problems during directional solidification for a pure substance with oscillatory and steady convection in the liquid region in the inverted Bridgman configuration (heated from below) and for a binary alloy in the horizontal Bridgman configuration are presented. The significant effects of the variation of thermal conductivity on the interface shape and flow structures are discussed.

INTRODUCTION

Directional solidification of alloys is used to grow single crystals and to obtain controlled distribution of the composition within the material grown. The most important industrial applications of this type of solidification are for growth of crystals for semiconductors. Bridgman crystal growth is one of the techniques used to produce single crystals from the melt. Bridgman type moving furnaces with an isothermal hot zone, a temperature-gradient zone and an isothermal cold zone are used for directional solidification of the materials and have become popular in ground and space experiments of fundamental studies of crystal growth.

For semiconductors, the resulting crystal structure is strongly affected by heat transfer, diffusion of species and convection occurring in the melt during the directional solidification. To study this problem numerically a fixed grid single domain approach (the enthalpy method) can be used. The main advantage of this method is its ability to solve solidification problems of both pure and alloy materials without the necessity to follow the movements and deformation of the melt-crystal interface. It permits the solution of the conservation equations in the entire domain including the solid, liquid and the mushy zone (it exists for some materials which solidify over a temperature-range). The boundary conditions which applied at the solid-liquid interface in a multi domain method are replaced by source terms in the mass, energy and momentum conservation equations[1].

In this paper we present numerical simulations of directional solidification in both vertical and horizontal Bridgman configurations. The effects of unequal thermal conductivities of material in the solid and liquid phase, on the heat and mass transfer and predicted shape of the solid-liquid interface during solidification are investigated.

MATHEMATICAL FORMULATION

We consider a Bridgman furnace in which a moving temperature profile, consisting of a cold zone (T_c), an adiabatic zone and a hot zone (T_h), is imposed on the boundary of the ampoule. This boundary temperature profile is translated with a constant pulling velocity as a result of the furnace movement, causing the solid/liquid interface to move along the ampoule.

To model the process of directional solidification we have chosen the fixed grid single domain approach, which avoids explicit tracking of the solid/liquid interface. Incorporation of the interface thermal and solutal boundary conditions can be achieved using appropriate source terms in the energy and solute transport equations[1].

Using, L the height of the cavity as the scale factor for length; and L^2/α, α/L and $\rho\alpha^2/L^2$ (where α is the liquid thermal diffusivity) as the scaling factors for time, velocity and pressure; and the non-dimensional temperature defined as $\theta = (T - T_c)/(T_h - T_c)$; the time dependent primitive variable equations can be written in dimensionless form as:

$$\frac{\partial}{\partial x_j}(v_j) = 0 \tag{1}$$

$$\frac{\partial}{\partial t}(v_i) + \frac{\partial}{\partial x_j}(v_j v_i) = -\frac{\partial p}{\partial x_i} + Pr\,\frac{\partial}{\partial x_j}\left(\frac{\partial v_i}{\partial x_j}\right) + Ra\,Pr\,\hat{g}_i(\theta - B_r C_l) - \frac{Pr}{K}v_i \tag{2}$$

$$\frac{\partial \theta}{\partial t} + \frac{\partial}{\partial x_j}(v_j\theta) = \frac{\partial}{\partial x_j}\left(k'\frac{\partial \theta}{\partial x_j}\right) - \frac{1}{Ste}\frac{\partial f_l}{\partial t} \tag{3}$$

$$\frac{\partial C_l}{\partial t} + \frac{\partial}{\partial x_j}(v_j C_l) = \frac{1}{Le}\frac{\partial^2 C_l}{\partial x_j^2} + S_c \tag{4}$$

$$\text{where } S_c = \frac{\partial f_s}{\partial t}(1 - k_p)C_l + f_s\frac{\partial C_l}{\partial t} \tag{5}$$

in which v_j is the velocity vector components, C_l is the solute concentration in the liquid, p is the pressure, and $\hat{g}_i$ is the unit gravitational acceleration vector. The Rayleigh number, $Ra = g\beta(T_h - T_c)L^3/\alpha\nu$, the Prandtl number, $Pr = \nu/\alpha$, the Lewis number, α/D_l, buoyancy ratio, $B_r = (\beta_C \Delta C_r)/(\beta_T \Delta T_r)$, the Stefan number, $Ste = c_p(T_h - T_c)/h_f$ and h_f is the latent heat of fusion. f_l is the local liquid volume fraction, β_C and β_T are the thermal and solutal expansion coefficients, k_p is the partition coefficient and D_l is the diffusivity of the solute. Solute diffusion in the solid phase is negligible. The density, ρ, and specific heat, c_p, are assumed to be equal in the liquid and solid phases. An average conductivity is defined as $k = f_l k_l + (1 - f_l)k_s$ and non-dimensionalized using a reference value at the reference temperature in the liquid, viz., $k' = k/k_l$.

The permeability K which appears in the momentum equation is defined as a function of the local liquid volume fraction (Carman-Kozeny relation),

$$K = K_0\left[\frac{f_l^3}{(1 - f_l)^2}\right] \tag{6}$$

where K_o is a constant which depends on the solidification microstructures[2].

NUMERICAL METHODS

Numerical solutions were obtained using two different approaches – 1) finite volume (FV) with primitive variables and 2) finite differences (FD) with a vorticity - stream function formulation.

In the first approach the set of transport equations (1-3) is discretized using a finite volume method. The approximation of the convective and diffusive flux at the interface between two control volumes is performed using respectively an ULTRA-QUICK and a centred scheme. The pressure-velocity coupling is ensured using a PISO algorithm.

In the second approach the momentum equation (2) was converted into a vorticity-stream function formulation. Latent heat evolution is accounted for by defining an effective heat coefficient (apparent heat capacity method). The release of solute into the liquid during solidification of the binary alloy is incorporated in equations (4) and (5). The governing two dimensional equations are then discretized using finite differences and solved using the Samarskii & Andreyev ADI scheme. Internal iterations on each variable at each time step are performed to ensure satisfaction of boundary conditions and to achieve true simultaneous solution of the non-linear strongly coupled equations.

RESULTS

Two cases are presented. The first one is that of a phase change problem of a pure substance in an inverted Bridgman configuration obtained using the FV approach. The second case is a phase change problem during transient directional solidification of a binary alloy in a horizontal Bridgman configuration solved using the FD method.

Figure 1 shows the interface shape and stream function contours in the case of solidification of gallium in the vertical inverted Bridgman configuration for $k_s / k_l = ½$, 1 and 2 for $Ra=10^3$. The interface is flat in the case of equal solid and liquid conductivities. It becomes concave when thermal conductivity in the melt is greater than the solid thermal conductivity and convex for the reverse case. A flow in the melt for all these cases remains steady and symmetrical.

Figure 2 shows the interface shape and stream function for solidification in the vertical Bridgman configuration for $k_s / k_l = ½$, 1 and 2 for $Ra=10^5$. In this case flow in the melt becomes periodic and asymmetric. The largest effect on the interface from the interaction with the flow is obtained in the case $k_s / k_l = 1$. For $k_s / k_l = ½$ the interface is concave and for $k_s / k_l = 2$ it is mainly convex.

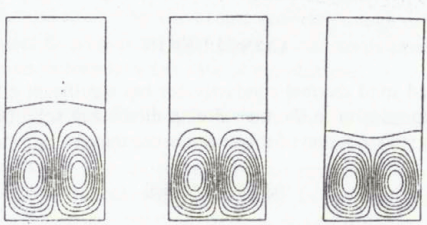

(a) (b) (c)

Figure 1. Interface shape for $Ra = 10^3$;
(a) $k_s / k_l = 1/2$, (b) $k_s / k_l = 1$ and (c) $k_s / k_l = 2$.

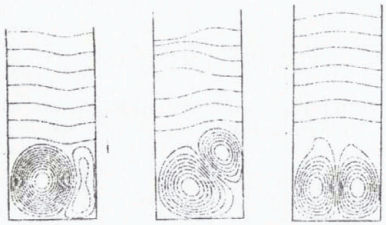

(a) (b) (c)

Figure 2. Interface shape for Ra = 10^5;
(a) $k_s / k_l = 2$, (b) $k_s / k_l = 1$ and (c) $k_s / k_l = 1/2$.

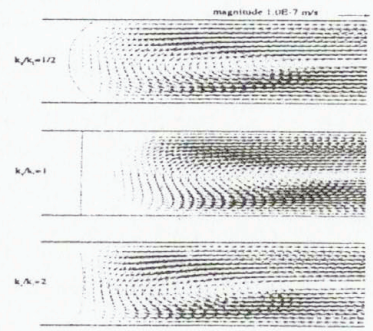

Figure 3. Interface shape and velocity vectors for different conductivity ratio

Figure 3 shows the interface shape and velocity vectors in the case of solidification of Bi-1at%Sn alloy in a horizontal Bridgman ampoule for a gravity level of 9.81×10^{-6} ms^{-2} for $k_s / k_l = ½$, 1 and 2. As in the vertical case, the interface becomes concave when the solid thermal conductivity is less than the liquid conductivity and convex otherwise. The variation in the thermal conductivity strongly affects the temperature gradients in the vicinity of the interface leading to the change of its shape and as a consequence to the redistribution of solute at the interface. Our numerical results showed strong dependence of the radial segregation on the interface curvature. Segregation defined as $(C_{max} - C_{min}) / C_{ave} \times 100\%$ is 1.99% for $k_s / k_l = 1$, 21.3% for $k_s / k_l = 2$ and 36% for $k_s / k_l = ½$.

CONCLUSION

The variation of liquid and solid thermal conductivities has significant effect on the heat transfer, the interface shape and convection in the melt during directional solidification. In the case of a binary alloy it also affects redistribution of solute and hence the resulting structure of the crystal.

REFERENCES

1. Voller, V.R., Brent, A.D. and Prakash, C., The modelling of heat, mass and solute transport in solidification systems, *Int. J. Heat Mass Transfer*, Vol. 32, pp 1719-1731, 1989.
2. Morvan, D., El Ganaoui, M. and Bontoux, P., Application of porous medium approach for the resolution of solidification problems, *Bulletin ERCOFTAC*, Vol. 28, pp. 39-42, 1996.

AN ASYMPTOTIC SOLUTION FOR THE DISSOLUTION OF PARTICLES IN MULTI-COMPONENT ALLOYS

Fred Vermolen[1], Kees Vuik[2] & Sybrand van der Zwaag[3]
[1]Mathematics and Computing Center, Amsterdam, The Netherlands
[2]Faculty of Technical Mathematics and Informatics, & [3]Laboratory for Materials Science
Delft University of Technology, Delft, The Netherlands

Summary Dissolution of stoichiometric multi-component particles is an important process occurring during the heat treatment of as-cast aluminium alloys. A mathematical model is proposed to describe such a process. In this model equations are given to determine the position of the particle-matrix interface in time, using a number of diffusion equations which are coupled by non-linear boundary conditions at the interface. This problem is known as a vector valued Stefan problem. Characteristic for this work is approximation of a vector valued Stefan problem by a scalar Stefan problem, which is solved analytically.

1 Introduction

Heat treatment of metals is often necessary to optimize their mechanical properties. During the heat treatment the metallurgical state of the alloy changes. One of the most important change is the dissolution of second phase (multi-component) particles.

In this paper, we distinguish the alloy into a primary and secondary phase. The primary phase is the metallic phase in which diffusion takes place. The secondary phase (or briefly particle) dissolves in the primary phase. Due to the complex structure and presence of numerous alloying elements in commercial alloys, the secondary phase may consist of several components.

Particle dissolution is assumed to proceed via the following subsequent steps: decomposition of the chemical compound in the particle, crossing the interface between the particle and primary phase (briefly the interface) by the atoms and long-range diffusion in the primary phase. In the present paper it is assumed that the first two steps proceed much faster than the third step, i.e. diffusion determines the rate of dissolution.

Mathematically, we have to solve Fick's second Law in the primary phase around each particle. The total number of atoms stays constant in the alloy, hence the interface moves due to conservation of mass. This is known as a Stefan problem. Some examples of articles and books on this subject are respectively: [1] and [2]. In these studies the technologically important dissolution of multi-component particles is not considered.

Particle dissolution in ternary alloys (alloys with two alloying elements) is treated by Hubert [3] and Vermolen and Vuik [7]. The present work covers an asymptotic solution applicable to multi-component alloys. For more details, we refer to [6].

The mathematical model is given in Section 2. Some remarks about existence are given in Section 3. Section 4 covers an asymptotic solution. Some conclusions are given in Section 5.

2 A MODEL OF DISSOLUTION IN MULTI-COMPONENT ALLOYS

Various particle geometries (planar, cylindrical or spherical) are observed in practice. In this section we consider a one-dimensional problem (in $\mathbb{R}^1$), i.e. the dissolution of a multi-component planar particle in an infinite primary phase. Different geometries are treated in [6]. The initial particle thickness is given by S_0. The particle thickness at time t is given by $S(t)$. The particle consists of n components that diffuse through the primary phase. We assume that the composition of the particle is constant in time.

For dissolution, we assume that there is a $t = T < \infty$ such that $S(T) = 0$. Diffusion is modelled by Fick's second Law:

$$\frac{\partial c_i}{\partial t} = \mathbb{D}_i \frac{\partial^2 c_i}{\partial x^2}, \quad x > S(t) \geq 0, \ 0 < t < T, \ i \in \{1, ..., n\}. \tag{1}$$

Here c_i and $\mathbb{D}_i$ denote the concentration and diffusion coefficient of alloying element i respectively. As initial condition and as 'boundary condition' for $x \to \infty$ we use:

$$(IB): \begin{cases} c_i(x, 0) = c_i^0, & x > S_0, \ i \in \{1, ..., n\}, \\ \\ c_i(x, t) = c_i^0, & as \ x \to \infty, \ 0 < t < T, \ i \in \{1, ..., n\}. \end{cases}$$

For convenience we define at the interface:

$$c_i^{sol}(t) := c_i(S(t), t), \quad 0 < t < T, \ i \in \{0, ..., n\}.$$

From thermodynamics [4] follows:

$$\Pi_{i=1}^{n} (c_i^{sol})^{m_i} = K, \quad 0 < t < T. \tag{2}$$

Here m_i are exponents from the stoichiometry of the particle. We denote the particle concentration of each alloying element by c_i^{part}. The balance of atoms and constant composition of the particle then leads to:

$$\left(c_i^{part} - c_i^{sol}\right) \frac{dS}{dt} = \mathbb{D}_i \frac{\partial c_i(S(t), t)}{\partial x}, \quad 0 < t < T, \ i \in \{1, ..., n\}. \tag{3}$$

Condition 3 implies:

$$\mathbb{D}_i \frac{\partial c_i(S(t), t)}{\partial x} = \mathbb{D}_j \frac{\partial c_j(S(t), t)}{\partial x}, \quad 0 < t < T, \ i, j \in \{1, ..., n\}. \tag{4}$$

The parameters known in the set of equations are the particle concentrations c_i^{part}, diffusion coefficients $\mathbb{D}_i$, initial concentrations c_i^0 and solubility product K. Unknown are here the concentration profiles c_i, the position of the interface S, and the interface concentrations c_i^{sol}.

The moving boundary problem given by equations 1, (IB), 2, 3 and 4 is known as a Stefan-problem. Note that the non-linear conditions in equation 2 are not standard.

3 PROPERTIES OF THE PLANAR STEFAN PROBLEM

In this section we summarize some properties of this Stefan problem. We do not present them in full rigour. For more details we refer to [6]. For convenience we define Q as: $Q := \{(x,t) : x > S(t), 0 < t < T\}$. We are only interested in smooth solutions, i.e. $S \in C^1(0,T]$ and $c_i \in C^{2,1}(Q) \cap C(\overline{Q})$. A solution that satisfies these requirements is unique and satisfies a maximum principle, i.e. (local) extremes can only occur at the boundaries or at $t = 0$. This has been proven for a general parabolic operator by Protter and Weinberger [5] and by Vuik for an unbounded domain [9].

3.1 A necessary condition for existence of a solution

We analyze the existence of a solution for a class of Stefan problems. First we enter the following definition of a conserving solution.

Definition 3.1 A solution to the Stefan problem presented here is called conserving if and only if:

$$\int_{S(t)}^{\infty} (c_i - c_i^0) dx = (c_i^{part} - c_i^0)(S_0 - S(t)). \tag{5}$$

From physical point of view it is required that equations 3 and 5 are equivalent. We reject non-conserving solutions. A sufficient condition for non-existence of a solution of this Stefan is formulated in the following proposition:

Proposition 3.1 The Stefan problem has no conserving solution if for some i

$$\left(c_i^{part} - c_i^0\right)\left(c_i^{part} - c_i^{sol}\right) \leq 0, \text{ and } c_i^{sol} \neq c_i^0 \text{ with } c_i^{part}, c_i^{sol}, c_i^0 \in \mathbb{R}^+ \cup \{0\}.$$

Above proposition is proven in [6] for a bounded domain and in [8] for an unbounded domain. In the next section we approximate the solution of a vector valued Stefan problem. Due to non-linear boundary conditions the approximate solution is not unique. Therefore we use Proposition 3.1 as a means of selecting an acceptable solution.

4 AN ASYMPTOTIC SOLUTION FOR THE VECTOR-VALUED STEFAN PROBLEM

In this section we approximate the solution of the vector valued Stefan problem. Assuming that c_i^{sol} is constant, it can be proven that the solution is:

$$(S1): \begin{cases} c_i(x,t) = \frac{c_i^0 - c_i^{sol}}{\operatorname{erfc}\left(\frac{k}{2\sqrt{D_i}}\right)} \operatorname{erfc}\left(\frac{x - S_0}{2\sqrt{D_i t}}\right) + c_i^0, \\ \\ S(t) = S_0 + k\sqrt{t} \end{cases}$$

Note that the concentration profiles c_i and interface concentrations have to satisfy equations 2 and 4. (S1) and equations 4 and 2 imply:

$$(S2): \begin{cases} \frac{k}{2} = \frac{c_i^0 - c_i^{sol}}{c_i^{part} - c_i^{sol}} \sqrt{\frac{D_i}{\pi}} \frac{\exp\left(-\frac{k^2}{4D_i}\right)}{\operatorname{erfc}\left(\frac{k}{2\sqrt{D_i}}\right)}, \quad \forall i \in \{1, ..., n\} \\ \\ \Pi_{i=1}^n (c_i^{sol})^{m_i} = K \end{cases}$$

Using above solution we will present an approximate solution. We take the special case that

- $c_i^{part} >> c_i^{sol} > c_i^0 = 0, \forall i \in \{1, ..., n\}$.

The above case is common in metallurgical applications. Note that for this case a conserving exists in the sense of definition 3.1 (see proposition 3.1). For this case it can be proven using the first equation of system (S2) that the velocity of the interface $\frac{dS}{dt}$ can be approximated by:

$$\frac{dS(t)}{dt} = \frac{k}{2\sqrt{t}} \approx -\frac{c_i^{sol}}{c_i^{part}} \sqrt{\frac{\mathbb{D}_i}{\pi t}}. \tag{6}$$

From the above equation follows a recurrence relationship for the c_i^{sol}. After substitution of this recurrence relationship into equation 2 and defining $\mu := \Sigma_{i=1}^n m_i$, one obtains the following non-linear equation for c_1^{sol}:

$$\left(\frac{\sqrt{\mathbb{D}_1}}{c_1^{part}}\right)^{\mu} \cdot \Pi_{i=1}^n \left(\frac{c_i^{part}}{\sqrt{\mathbb{D}_i}}\right)^{m_i} (\tilde{c}_1^{sol})^{\mu} = K. \tag{7}$$

The solution to equation 7 is:

$$\tilde{c}_1^{sol} = \frac{c_1^{part}}{\sqrt{\mathbb{D}_1}} \cdot K^{\frac{1}{\mu}} \cdot \Pi_{i=1}^n \left(\frac{\sqrt{\mathbb{D}_i}}{c_i^{part}}\right)^{\frac{m_i}{\mu}} \tag{8}$$

Substitution of the real, positive solution of equation 8 into equation 6, yields:

$$\frac{dS(t)}{dt} \approx -\frac{c_{eff}^{sol}}{c_{eff}^{part}} \cdot \sqrt{\frac{\mathbb{D}_{eff}}{\pi t}}, \tag{9}$$

In which $c_{eff}^{sol} := K^{\frac{1}{\mu}}$, $c_{eff}^{part} := \Pi_{i=1}^n (c_i^{part})^{\frac{m_i}{\mu}}$ and $\mathbb{D}_{eff} := \Pi_{i=1}^n (\mathbb{D}_i)^{\frac{m_i}{\mu}}$ are referred to as the effective solid solubility, effective particle concentration and effective diffusion coefficient. The solution of the above equation is:

$$S(t) \approx S_0 - 2\frac{c_{eff}^{sol}}{c_{eff}^{sol}} \sqrt{\frac{\mathbb{D}_{eff} t}{\pi}}. \tag{10}$$

Here we approximate the vector valued Stefan problem by a scalar Stefan problem. This approach can be used easily for an estimate of the dissolution kinetics. Moreover, it can be used to test results from numerical calculations. We gave the above derivation in a more mathematically rigorous way in [6].

5 CONCLUSIONS

A self-similar solutions which is found for the dissolution of a particle in an unbounded one-dimensional geometry is extended to the dissolution of a multi-component particle. For the case of initial concentrations equal to zero, a simple expression is derived for the dissolution in terms of an effective diffusion coefficient. This effective diffusion coefficient is equal to a geometric diffusion coefficient of all components involved. The weight factors come from the stoichiometry of the compound of which the particle is constituted.

References

[1] S. Chen, B. Merriman, S. Osher, and P. Smereka. A simple level set method for solving Stefan problems. *J. Comp. Phys.*, 135:8–29, 1997.

[2] J. Crank. *Free and Moving Boundary Problems.* Clarendon Press, Oxford, 1984.

[3] Roger Hubert. Modelisation numerique de la croissance et de la dissolution des precipites dans l'acier. *ATB Metallurgie*, 34-35:5–14, 1995.

[4] J.S. Kirkaldy and D.J. Young. *Diffusion in the condensed state.* The institute of metals, London, 1987.

[5] M.H. Protter and H.F. Weinberger. *Maximum Principles in Differential Equations.* Prentice-Hall, Englewood Cliffs, 1967.

[6] F.J. Vermolen and C. Vuik. A mathematical model for the dissolution of particles in multi-component alloys. *CWI-report*, MAS-R9822, 1998.

[7] Fred Vermolen and Kees Vuik. A numerical method to compute the dissolution of second phases in ternary alloys. *Journal of Computational and Applied Mathematics*, 93:123–143, 1998.

[8] Fred Vermolen and Kees Vuik. A vector valued Stefan problem from aluminium industry. *CWI-report*, MAS-R9814, 1998.

[9] C. Vuik. *The solution of a one-dimensional Stefan problem.* CWI-tract 90. CWI, Amsterdam, 1993.

MODELLING AND RESULTS IN FLUIDYNAMICS OF CRYSTAL GROWTH FROM THE VAPOUR PHASE

A. Viviani, C. Golia
Seconda Università di Napoli, Dipartimento di Ingegneria Aerospaziale
via Roma 29, I-81031 Aversa, Italy. e-mail: viviani@unina.it

The fluid-dynamics of crystal growth from vapour has been recognized as playing an important role in technological processes employed to grow bulk crystals or epitaxial films by physical and chemical vapour transport; indeed the final properties of the crystal are strongly influenced by the thermodynamic conditions at the vapour-crystal interface and these, in turn, are the result of the complex physico-chemical mechanisms involved in the vapour transport.

In recent years a new impetus for studying vapour crystal growth fluid-dynamics has come from the utilization of space microgravity environment, where low-gravity conditions are expected to reduce gravity-driven disturbances and, therefore, to enhance the final properties of the crystals, resulting from the complex physico-chemical phenomena occurring in the vapour phase.

A large number of works, both numerical and experimental, have been performed on the subject, and different models have been proposed to investigate the role of natural convection and the interface kinetics in various geometrical configurations, for different gravity levels. In particular, double-diffusive vapour transport in idealized geometrical configurations (plane or cylindrical enclosures with differentially heated end walls) has been extensively investigated considering Navier-Stokes fluid-dynamics along with no-slip boundary conditions on the passive boundaries.

However, some "gas-kinetic" effects, usually masked by gravity on Earth, such as thermal and concentration stresses (volume-driving actions), thermal and concentration creep (surface-driving actions) may represent important sources of convection (described by Burnett equations and slip-boundary conditions) under the conditions encountered in low-gravity crystal growth but also,

depending on the size of the system and temperature/concentration differences, on earth.

The existence of new types of convective flows, induced in gases by stresses and creep, has been considered in the Soviet literature by Galkin et Al., who demonstrated that, in the absence of external forces, Burnett equations and slip-boundary conditions have to be considered, even in the first approximation, to describe a broad class of continuum flows.

The new transport mechanisms have been investigated by theoretical and numerical methods, demonstrating that these effects have an important role in processes of vapour crystal growth in space. In this lecture we deal with new possible sources of convection arising from non-linear irreversible thermodynamic effects (non-Navier-Stokes fluid-dynamics) and slip boundary conditions during typical processes of crystal growth from vapour phase. Attention is focused on the role played by Burnett stresses and side-wall creep in single component gases, as well as in the case of binary mixtures.

A rigourous non-dimensional order of magnitude analysis has been performed to compare these effects to the vapour transport mechanisms usually considered in vapour crystal growth fluid-dynamics, i.e. buoyancy and the so-called Stefan-Nusselt flow due to the evaporation at the source and condensation at the crystal; new characteristic velocities, lengths and corresponding new characteristic non-dimensional numbers are introduced and discussed for the characterization of the new phenomenologies, by identifying 15 classes of convection, and *a priori* conditions for the existence and characterization of all possible classes of convection and flow regimes, in terms of the problem's data, are formulated, by drawing the appropriate regime planes.

Then, we present numerical results obtained with the new set of field equations (Burnett equations with slip conditions) for geometrical configurations of interest in crystal growth by physical vapour transport. The results are presented for several combinations of the non-dimensional characteristic parameters, ranging from microgravity to earth environment conditionsand compared with the results of the corresponding solution of the Navier-Stokes approximation.

UNSTEADY THREE-DIMENSIONAL MELT FLOW COMPUTATION OF CZOCHRALSKI SINGLE CRYSTAL GROWTH OF SUPER-CONDUCTING MATERIAL

T. Yamauchi, G. Mika, J. Szmyd* and K. Suzuki

Department of Mechanical Engineering
Kyoto University, Kyoto 606-8501, Japan
**St. Staszic University of Mining and Metallurgy*
30 Mickievicz Ave., Krakow 30059, Poland

Summary Three-dimensional unsteady computation was made for the melt flow in the production process of super-conducting material Y123 with a modified Czochralski method. Results of the studied cases reveal the importance of three-dimensional computation in the determination of stability conditions and the unsteady behavior of the melt flow. How to suppress the melt flow instability and the patterns of melt flow in some typical unsteady conditions were also discussed.

INTRODUCTION

Czochralski method (hereafter called Cz method) is most popularly used in the single crystal growth of various materials. The present study pays attention to the production of a super-conducting material, $YBa_2Cu_3O_{7-x}$ (hereafter Y123 for convenience). In place of popular flux method which is not suitable for the production of large size single crystal of Y123[1,2], Yamada and Shiohara[3] made an effort to produce Y123 single crystal with a modified Cz method. In their method, Y123 single crystal was grown at the interface between the seed crystal and the 3BaO-5CuO melt produced in the crucible by electric heating. Yttrium (shortly just U in the following) was supplied from the bottom bed made of Y211. Its supply to the interface is controlled by the melt convection. Therefore, study of melt convection is very important as was actually studied by the same group [1,2]. These references assumed steadiness of the melt flow. However, this assumption cannot be validated because the rotation speed of the seed was rather high. Actually, Szmyd et al.[4-6] reported that melt flow can be unsteady in the conditions experimentally studied by Yamada and Shiohara. Since the previous studies were made under the two-dimensionality assumption, results of three-dimensional unsteady computation are reported in the present study.

This paper concentrates its attention to the unsteady behavior of the melt flow and related heat transfer in the crucible. This is because the melt flow governs the mass transfer of Y to the interface. Thermal field in the crucible varies in a complicated manner with the value of Prandtl number[7]. In this study, it is kept constant. In the previous studies[4-6], it was found that thermal boundary condition seriously affects the instability of the melt flow. The same issue will be discussed again in terms of the results obtained with the present three-dimensional computation.

NOMENCLATURES

□Gr Grashof number based on the temperature difference $(T_h - T_s)$
□Re_s crystal rotation Reynolds number $\Omega_s Re_s^2/\nu$
□t time, s
□T temperature, K
□U_i velocity component in x_i direction, m/s
□r, φ, z radial, azimuthal and axial coordinates in the cylindrical coordinate system

□ ν kinematic viscosity, m2/s
□ ρ density, kg/m3
□ Ψ stream function
□ Ω angular velocity, rad/s

Suffices
□s crystal
□f fluid
□* non-dimension

PROCEDURES AND CONDITIONS

Schematic diagram of the Cz furnace is illustrated in Fig.1 together with the used coordinate system and geometrical parameters. Melt flow and related heat transfer in the crucible are calculated by numerically solving the finite-difference equivalents of the momentum and energy equations. All the fluid properties were treated to be constant. Prandtl number of the melt was assumed to be 10.5. Pressure in the momentum equation was calculated by SIMPLER algorithm[8] in which pressure was adjusted so as to satisfy the continuity equation. For finite-differencing, the control volume method has been employed, and central finite-difference was used for the diffusion terms and QUICK[9] scheme for the convection terms. Staggered grid system was used and total number of grids points was $48 \times 25 \times 52$. In relaxation of the elliptic type finite-differenced equatoins, iterative procedure was adopted combining ADI (Alternative - Direction - Implicit) method[10] at each time step. Time step increment was set to be an order of 10^{-6} in the non-dimensional time scale $t^* \square \nu t / R_s^2$.

Rotating speed of crystal was changed in seven steps and corresponding values of the Reynolds number were Re_c=0,10,20,30,40,50 and 60. In every studied case, no rotation was given to the crucible. Free surface was treated to be completely flat and Marangoni effect was ignored. No slip condition was applied at wall surfaces and free boundary condition was adopted at the melt free surface. Melt-crystal interface and melt-Y211 solid-bed interface were assumed to be constant in temperature equal to T_s and T_h respectively. Temperature difference (T_h-T_s) was changed in three steps and the corresponding values of Grashof number were 0, 5,000 and 10,000. Radiative heat loss from the melt free surface to the surrounding of temperature T_e was calculated applying Stefan-Boltzmann equation. Side wall of the crucible was assumed to have a linear temperature distribution T_w=T_h-(z/H)$\Delta\theta$. $\Delta\theta$ was changed in two steps; namely $\Delta\theta$=0 and 12K.

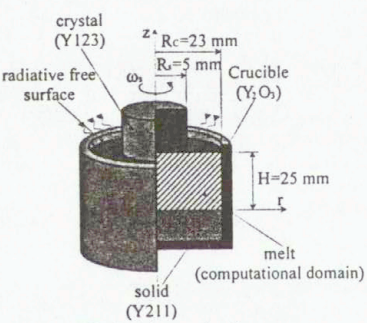

Fig.1 Schematic diagram

RESULTS AND DISCUSSIONS

First is discussed the case where $\Delta\theta$=0, namely where side wall temperature is uniform. A little different from the previous papers, melt flow obtained with the two-dimensional computation remained steady at any Reynolds number when Gr=0, 5,000 and 10,000. In the present three-dimensional computation, on the other hand, melt flow becomes unstable at Re=50 and 60 when Gr=0, and in the Reynolds number range Re=40-60 either when Gr is equal to 5,000 or 10,000. Therefore, melt flow is predicted to be more unstable in the three-dimensional computation than in two-dimensional computation. The melt flow is axi-symmetric as far as it remains steady. Figure 2 illustrates some examples of instantaneous isotherm contours calculated on the melt free surface for some cases where flow showed unsteadiness. It indicates that the melt flow and therefore the resulting thermal field are not axi-symmetric in the unsteady cases.

Melt temperature takes a minimum in the middle of free surface. Figure 3(a) shows an example of the melt flow isotherm contours and the contours of stream function in a vertical plane calculated in one case where flow remains steady. Two recirculating flow regions are observed to exist in the figure, one driven by the centrifugal force due to the crystal rotation and another resulting from the buoyant flow along the vertical side wall of the crucible. The low melt temperature region on the free surface is observed in the figure to coincide with the region where the two oppositely directed flows meet each other.

Appearance of the low melt temperature region deteriorates the quality of crystal but its effect is smaller if the region appears at a radial location of larger distance from the crystal. Figure 3(b) shows the radial position of the lowest melt temperature on the free surface obtained in all the studied conditions of $\Delta\theta$=0. The plotted position for unsteady melt flow conditions is its time mean value. As observed in the figure, larger Grashof number is not preferable in a sense that the lowest temperature position appears closer to the crystal but its location can be moved to a position more

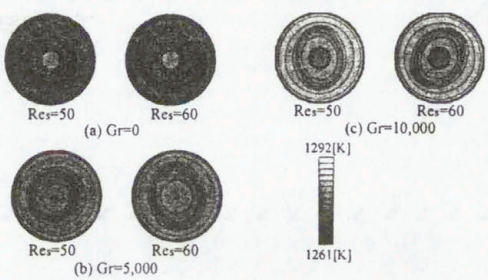

Fig.2 Instantaneous isotherms at the free surface

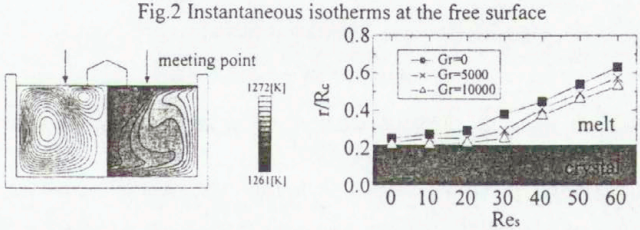

(a)Streamlines and isotherms (Gr=0.0, Res=40)

(b)Radial position of the lowest temperature on the free surface

Fig.3 Meeting point of forced and natural convection at the free surface

likely to occur. Unsteadiness of the melt flow can also produce the striation of the single crystal and is not desirable either. In this sense, three-dimensional computation is preferable with which the stability limit of melt flow can be assessed more accurately as discussed above.

As in the previous studies, computation was made for the cases of non-uniform side wall temperature, i.e. where $\Delta\theta$=12K. Calculated melt flow was found to become unsteady for all the cases of different values of Grashof number and of crystal rotation Reynolds number except for one trivial case where Gr=0 and Re_s=0. In addition to this, fluctuation pattern was found to be more complex in the cases $\Delta\theta$=12K than in the cases $\Delta\theta$=0. This is because the vertical distribution of side wall temperature may produce unstable fluid temperature stratification if the flow remains steady. Distribution pattern of the melt temperature on the free surface is illustrated in Figure 4 in the form of instantaneous isothermal contours for three cases of different Reynolds number at the Grashof number equal to 10,000. Thermal field in the crucible is far from axi-symmetry in the illustrated conditions. More pronounced, however, is the complicated pattern of temperature distribution than the results shown in Figure 2. One more noticeable feature of the temperature distribution on the free surface is that the peripheral non-uniformity is less pronounced in the case where Re_s=60 than in other cases of Re_s=0 and 10. Although not shown here to save space, the amplitude of temperature fluctuation sampled at a position close to the crystal surface indicates that temperature fluctuation is also weak in the case where Re_s=60. Thus, this is the most preferable case where good quality crystal can be produced.

CONCLUDING REMARKS

Necessity of unsteady three-dimensional computation has been confirmed for the melt flow of the Czochralski production process of super-conducting material. Three-dimensional computation gives narrower range of for melt flow stability. Unsteady behavior of melt flow is predicted more complicated with the three-dimensional computation than with the two-dimensional one. Low temperature region of the melt on the free surface comes to be located closer to the crystal surface with an increase of the Grashof number. However, this can be suppressed by the increase of crystal rotation Reynolds number and a condition for the production of better quality crystal can be established. At higher rotation speed of the crystal, melt flow becomes more unstable. However, at a certain level of the Grashof number, fluctuation of melt flow temperature near the crystal can be reduced in amplitude and production of better quality crystal can then be expected.

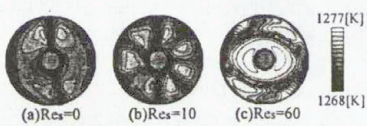

Fig.4 Instantaneous isotherms at the free surface

REFERENCES

[1] Y. Namikawa, M. Egami, Y. Shiohara, J. Japan Inst. Metals. Res. Vol. 59, No. 10, 1047 - 1054 (1995).
[2] Y. Namikawa, M. Egami, Y. Shiohara, J. Mater. Res. 11, 288 (1996).
[3] Y. Yamada, Y. Shiohara, Physica C 217, 182 (1993).
[4] J. S. Szmyd, T. Yamamoto, U. Bueckle and K. Suzuki, Proc. 1st JSPS-NUS Seminar on Integrated Engineering, 152-163 (1996).
[5] J. S. Szmyd, G. Mika and K. Suzuki, 1998, Advanced Computational Methods in Heat Transfer 5, pp.223-232.
[6] J. S. Szmyd, T. Yamamoto and K. Suzuki, 1998, Heat Transfer 98, Vol. 4, pp. 289-294.
[7] U. Bueckle, T. Yamamoto and K. Suzuki, to appear elsewhere.
[8] S.V. Patankar, D.B. Spalding, Int. J. Heat Transfer, 15, 1787 (1972).
[9] B.P. Leonard, Compt. Meths. Appl. Mech. Engng. 19, 59 (1979).
[10] P.J. Roache, Computational Fluid Dynamics, Hermosa, Publishers, 1976.